Thiol-Terminated Coatings using Low-Pressure Plasma and Vacuum Ultraviolet Radiation

EVELYNE KASPAREK

Department of Chemical Engineering
McGill University
Montréal, Québec, Canada
August 2018

A thesis submitted to McGill University in partial fulfillment of the requirements of

the degree of Doctor of Philosophy

Acknowledgements

First of all, I would like to thank my supervisors Prof. Pierre-Luc Girard-Lauriault, Prof. Jason R. Tavares and Prof. Michael R. Wertheimer for giving me the opportunity to conduct this research under their supervision. Thank you, Pierre-Luc, for always being available and open for discussions and for giving me freedom in executing my research. Thank you, Jason, for your continuous support, your prompt responses, for making me cross the mountain every two weeks and giving me a second wonderful research group. Thank you, Mike, for accompanying this work and for your scientific advice throughout this research.

I would also like to thank Prof. Rony Snyders and Dr. Damien Thiry for giving me the opportunity to work in their lab. Thank you, Damien, for offering to work with you. The two months abroad enriched my PhD experience by having the opportunity to not only work with an expert in the same research field but also a great and humble researcher.

Special thanks to Dr. Chris Corkery for offering the poster workshop at McGill and showing interest in our research leading to a strong collaboration with Sensoreal Inc. and a great opportunity for me to work on an industrial oriented MITACS project. Thank you also for reviewing this work in such detail.

I would like to thank all people who helped me every day during this PhD, especially my both lab groups, PPL and PhotoSEL. Special thanks to Faezeh, Donya, Felipe, Crisitina, Pablo, Elena, and Mitch for their constant support. Thank you, Pierre, for brining that positivity into the lab every single day, for all the laughter, coffees and lunches. Thank you, Larissa, for not only being a huge help in the lab, but also a great friend, writing and climbing partner; I wouldn't have been able to accomplish this work without your moral support. Thank you, Adya, for asking me once for help leading to

our motivating side project. Thanks for being such a good friend and an inspirational researcher. Special thanks to my summer/undergrad student Cedric. Thanks for always coming back and for helping me with whatever task you were asked to, thanks for always being just a text message away. Thanks to my new small Mexican family, especially to Norma and Mario.

I am very grateful to all technicians that helped me throughout this research. Thanks, Frank, for always being there for me, for all the coffees and tomato plants. Thanks to Gerald, Andrew and Lou for always being available for all my questions and concerns.

Thanks to my family and friends for all their support and love. Special thanks to my mum for being such a strong woman who taught me to never give up and fight for my dreams. Thanks for always being there for me, no matter the distance or time. Thanks also to my best friend Ilka, who was always just a text, or a Skype call away.

Last, but not least, I would like to thank the most important person in my life, Thomas, for accepting to go on this adventure with me and move to a new country. Thanks for all your love, support and encouragement throughout these past years and for being around even in my worst moments. Thanks for always pushing me to give my best and never give up. I would have never been able to do this without you; this work is yours as well.

Abstract

Thiol (SH)-terminated surfaces have a wide range of potential uses, including biomedical and catalytic applications. In the biomedical field, SH-terminated surfaces have shown great ability as anchoring sites for covalent immobilization of molecules representing an important criterion for diagnosis of different diseases or the formation of biosensors. For these applications, a target biomolecule holding a chemical group (e.g. maleimide, thiol or disulfide) reacts selectively with SH groups on the surface. Reproducible covalent attachment of bio-compounds is desired since the active sites of these compounds are generally more readily accessible, and a more even coverage of the surfaces can be achieved. The strong affinity between gold, Au, and SH groups also makes SH-terminated surfaces attractive as anchoring platforms for promoting Au adhesion or as a support for Au nanoparticles, crucial for low temperature catalysis applications.

The main goal of this research is to examine the synthesis of stable, SH-terminated organic coatings using chemical vapor deposition (CVD) methods. CVD is advantageous over wet-chemical alternatives because of its short reaction times, lack of toxic solvents, and more controllable outcomes through varying process parameters. Plasma-enhanced CVD (PECVD) is probably one of the most widely used CVD methods for the functionalization of surfaces. Photo-initiated CVD (PICVD) has proven to be a good alternative, and it involves exposure of the surfaces to UV radiation in a reactive gas or mixture of gases. The biggest advantage of PICVD over its plasma counterpart is a more "targeted" surface chemistry due to the use of mono-energetic photons rather than "hot" electrons that are characterized by a Maxwell-Boltzmann-like distribution of kinetic energies. The scalability of PICVD methods is however often limited, especially at low wavelengths (< 190 nm), due to the strong absorption of air

in this region, the need for expensive and sensitive materials which are transparent to those wavelengths, and slow rates of deposition.

The present research first probes the creation and full characterization of SH-terminated organic coatings from binary gas mixtures, hereafter "BGMs" (as opposed to single-molecule precursors) comprised of a hydrocarbon gas (either ethylene or butadiene) and a sulfur-rich functional gas (hydrogen sulfide, H_2S). The organic coatings were created using either a low-pressure (LP) radiofrequency plasma, or through vacuum ultraviolet (VUV, $\lambda<200$ nm) irradiation of the gas mixtures with a near-monochromatic krypton (Kr) lamp. Varying the gas mixture ratio, *R*, allowed control over the resulting films' properties, particularly the sulfur, [S], and thiol, [SH], concentrations. Surprisingly, coatings obtained from LP plasma treatments demonstrated higher [SH] values, up to 3%. All coatings showed high [S], up to 48 at. %, and stability in aqueous solution after immersion for 24 h.

Having learned that it is possible to obtain SH-terminated organic coatings from BGMs using two different CVD methods, extending this to a further BGM (acetylene / H_2S) represented the second objective of this research. For this, surface- and gas-phase phenomena were studied simultaneously as a function of applied power, $<P>$, and *R* in a special PECVD system that included mass-spectrometric diagnostics. The magnitude of $<P>$ greatly influenced the deposition rate, *r*, [S] and [SH]. Traditionally, single-molecule precursors that already contain the desired functionality are more often used in PECVD, and a range of earlier studies describe this deposition approach. Coatings from BGMs were compared with ones obtained in the same apparatus using propanethiol as a single-molecule precursor. Resulting [SH] values were found to be higher when using BGMs, rendering such coatings superior candidates for applications.

Studying VUV irradiation of a BGM comprising acetylene and H_2S in more detail has been the third objective of this work. A first-of-its-kind wavelength (λ)-dependent photo-deposition study was carried out in order to identify a specific photon energy, $h\nu$, leading to maximum [SH]. Results showed that different $h\nu$ values influence deposition kinetics and film composition, reflecting that photolytic reactions are governed by the gases' absorption coefficients, k. Coatings with the highest [SH] reported so far in the literature (~7.7 %) were obtained with a low-pressure xenon (Xe) VUV source (λ=147 nm).

To summarize, this thesis discusses the formation of SH-terminated organic coatings from BGMs using two different CVD methods. The results obtained throughout this study lay a foundation for understanding the mechanisms occurring during CVD-based formation of SH-terminated surfaces. It further demonstrates how process parameters can be adjusted to tune [SH] on the surfaces for specific applications. With this foundation, applications on the created SH-terminated organic coatings can now be tested, for example their influence on cell growth and -proliferation or the attachment of specific (bio)molecules to the surfaces.

Résumé

Les surfaces à terminaison thiol ont une large gamme d'utilisations potentielles, y compris des applications biomédicales et catalytiques. Dans le domaine biomédical, les surfaces terminées par des thiols ont montré une grande capacité en tant que sites d'ancrage pour l'immobilisation covalente de molécules, un critère important pour le diagnostic de différentes maladies ou la formation de biocapteurs. Pour ces applications, une biomolécule cible contenant un groupe chimique (par exemple le maléimide, le thiol ou le disulfure) réagit sélectivement avec les groupes thiols sur la surface. La fixation covalente reproductible des composés bio est importante car elle assure une couverture de surface homogène et l'accessibilité au site actif. La forte affinité entre l'or et les groupes thiol rend les surfaces à terminaison thiol aussi attrayantes comme couche intermédiaire pour favoriser l'adhérence de l'or ou comme support pour les nanoparticules d'or, cruciales pour les applications de catalyse à basse température.

L'objectif principal de cette recherche est d'examiner la synthèse de revêtements organiques stables à terminaison thiol, en utilisant des méthodes de dépôt chimique en phase vapeur (CVD pour l'anglais chemical vapor deposition). Les méthodes CVD sont avantageuses par rapport aux alternatives chimiques humides en raison de leurs temps de réaction courts, de l'absence de solvants toxiques et de résultats plus contrôlables grâce à des paramètres de procédé variables. Le CVD au plasma (PECVD) est la méthode CVD la plus utilisée pour la fonctionnalisation des surfaces. La déposition photochimique par CVD (PICVD) s'est avérée être une bonne alternative pour la fonctionnalisation de surface et implique l'exposition des surfaces et des gaz réactifs au rayonnement à basse pression. Le plus grand avantage de PICVD par rapport à son équivalent plasma est une chimie de surface plus «ciblée» due à l'utilisation de photons

monoénergétiques plutôt que d'électrons «chauds». La limitation principale du PICVD est le requis, lorsque la longueur d'onde retenue est faible (<190 nm), d'opérer à basse pression et d'utiliser des matériaux hautement spécialisés (et onéreux) pour assurer la transmission de la lumière.

Le principal but de cette recherche a d'abord été d'explorer la création et la caractérisation complète de revêtements organiques à terminaison thiol à partir de mélanges gazeux binaires (plutôt que de précurseurs moléculaires) constitués d'un gaz hydrocarboné (éthylène ou butadiène) et d'un gaz fonctionnel riche en soufre (sulfure d'hydrogène). Les revêtements organiques ont été créés en utilisant un plasma radiofréquentiel (r. f.) à basse pression ou des rayons ultraviolets énergétiques (VUV pour l'anglais vacuum ultraviolet, λ<200 nm) avec des mélanges gazeux avec une lampe au krypton quasi-monochromatique. La variation du rapport du mélange gazeux a permis de contrôler les propriétés des films résultants, en particulier les concentrations de soufre et de thiol. Étonnamment, les revêtements obtenus à partir de traitements au plasma à basse pression ont montré des concentrations de thiol plus élevées, allant jusqu'à 3%. Tous les revêtements ont montré une teneur élevée en soufre, allant jusqu'à 48 at. %, ainsi que de la stabilité en solution aqueuse après immersion pendant 24 h.

Ayant confirmé qu'il est possible d'obtenir des revêtements organiques terminés par un thiol à partir de mélanges gazeux binaires et par deux méthodes CVD différentes, le second objectif de cette recherche était donc d'acquérir une meilleure compréhension des mécanismes de la chimie et de la croissance à partir d'un autre mélange gazeux binaire (acétylène et sulfure d'hydrogène) dans un système plasma. Pour cela, les phénomènes de surface et en phase gazeuse ont été étudiés simultanément en fonction de la puissance appliquée et du rapport de mélange gazeux. La puissance appliquée influence grandement la vitesse de dépôt, la teneur en soufre et la concentration en thiol.

Traditionnellement, les précurseurs à molécule unique qui contiennent déjà la fonctionnalité désirée sont le plus souvent utilisés dans le PECVD et une gamme d'études existe pour cette approche de dépôt. Les revêtements de mélange de gaz binaires ont été comparés avec des revêtements obtenus dans une décharge similaire en utilisant du propanethiol en tant que précurseur de molécule unique. Les concentrations de thiol se sont avérées plus élevées lors de l'utilisation de mélanges de gaz binaires, rendant les revêtements à terminaison thiol obtenus à partir de cette approche des candidats supérieurs pour diverses applications.

Pour compléter cette étude sur les mécanismes en jeu à l'état plasma, le troisième objectif de ce travail est l'étude des processus se produisant au cours de l'irradiation VUV d'un mélange gazeux binaire d'acétylène et de sulfure d'hydrogène. Une étude des processus de déposition en fonction de la longueur d'onde a été réalisée afin de trouver une énergie photonique spécifique conduisant à une concentration maximale en thiol. Les résultats ont montré que différentes énergies de photons influencent la cinétique de dépôt et la composition du film, ce qui montre que les réactions photolytiques sont régies par les coefficients d'absorption des gaz. Les revêtements avec les concentrations de thiol les plus élevées rapportées jusqu'ici dans la littérature (~ 7,7%) ont été obtenus par rayonnement VUV avec une source résonnante au xénon (λ = 147 nm).

Cette thèse présente l'étude de la formation de revêtements organiques à terminaison thiol à partir de mélanges de gaz binaires en utilisant deux méthodes CVD différentes. Les résultats obtenus dans cette étude constituent une base pour la compréhension des mécanismes se produisant au cours des méthodes CVD conduisant à des surfaces terminées par un thiol. Il est d'ailleurs démontré comment les paramètres du procédé peuvent être ajustés pour contrôler les concentrations de thiol sur les

surfaces pour d'éventuelles applications spécifiques. Avec cette base, des applications sur les revêtements organiques à terminaison thiol peuvent maintenant être testées, par exemple leur influence sur la croissance et la prolifération cellulaire ou la fixation de (bio) molécules spécifiques aux surfaces.

Table of contents

List of Tables

List of Figures

List of Abbreviations

AFM	Atomic Force Microscopy
AM	Allylmercaptan
ATR-FTIR	Attenuated Total Reflectance – Fourier Transform Infrared Spectroscopy
Au	Gold
BE	Binding Energy
BGM	Binary Gas Mixture
CVD	Chemical Vapor Deposition
DMSO	Dimethyl sulfoxide
EI	Electron Impact
FTIR	Fourier Transform Infrared Spectroscopy
FWHM	Full Width Half Maximum
GDMS	Glow Discharge Mass Spectrometry
GFTIR	Gas-phase Fourier Transform Infrared Spectroscopy
GL	Gaussian-Lorentzian
Hg	Mercury
HMDSO	Hexamethyldisiloxane
HR	High Resolution
IR	Infrared
Kr	Krypton
LMW	Low Molecular Weight
LP	Low-Pressure
L-PPA:S	Low-Pressure Plasma-Polymerized Sulfurized Acetylene

L-PPB:S	Low-Pressure Plasma-Polymerized Sulfurized Butadiene
L-PPE:S	Low-Pressure Plasma-Polymerized Sulfurized Ethylene
MPTMS	3-Mercaptopropyl Trimethyloxysilane
MS	Mass Spectrometry
OES	Optical Emission Spectroscopy
PECVD	Plasma-Enhanced Chemical Vapor Deposition
PICVD	Photo-Initiated Chemical Vapor Deposition
PP	Plasma Polymer
PPF	Plasma Polymer Film
Pr	Propanethiol
r.f.	radiofrequency
RGA	Residual Gas Analysis, RGA, mode
S	Sulfur
SH	Thiol
UV	Ultraviolet
UV-PA:S	Ultraviolet-Polymerized Sulfurized Acetylene
UV-PB:S	Ultraviolet-Polymerized Sulfurized Butadiene
UV-PE:S	Ultraviolet-Polymerized Sulfurized Ethylene
VUV	Vacuum ultraviolet
VTM	Vacuum Transfer Module
Xe	Xenon
XPS	X-ray Photoelectron Spectroscopy
DBD	Dielectric Barrier Discharge

Chapter 1 Introduction

1.1 Motivation

Biomaterials are non-living materials intended to be used in medical devices while interacting with a biological system.[1, 2] Over the years, the demand and the need for more sophisticated and readily available materials has increased. Ideally, a biomaterial would be a single material which is compatible with the studied biological system, disintegrates over time (if for the application required), possess good mechanical properties, and simultaneously promotes cell adhesion, growth, and differentiation.

Ceramics, metals, alloys, glass, and polymers are common materials used for the fabrication of biomaterials.[3] Synthetic polymers are broadly used as implants, bio-sensors, prostheses, antimicrobial surfaces, and engineered tissues. The popularity of these materials can be explained by their excellent bulk properties, high mechanical stability and elasticity, non-toxicity, and low degradation rate in the human body.[4-6] A major difficulty when using synthetic polymers is that interactions between their surfaces and the biological environment are restricted or undesirable, since their surfaces are generally chemically inert, minimizing their performance.

One approach to improve the performance of polymeric biomaterials consists of enhancing interactions between their surfaces and the biological system through surface modification. Several surface modification techniques have been developed to improve biocompatibility by introducing a variety of functional groups. This enables subsequent immobilization of biological compounds, directly influencing cell adhesion and differentiation. The main methods for immobilizing biomolecules

to a surface, as well-discussed by Gorddard et al., are: "(i) adsorption via electrostatic interactions, (ii) ligand-receptor pairing, and (iii) covalent attachment".[6] Nitrogen- and oxygen-containing functional groups, more specifically primary amines (NH_2), carboxylic acids (COOH), or hydroxyl (OH) functionalities, have shown to promote protein and cell adhesion through immobilization method (i).[7-12] Immobilization through adsorption can be advantageous in some applications (i.e. drug release), however, covalent attachment implies the formation of a firm and stable bond between a (functionalized) surface and a biomolecule, offering some benefits compared to the other two immobilization methods. Advantages include the specific attachment of the biomolecules while making its active side available, greater stability and durability, and better bioactivity.[6, 13] In this context, sulfur-containing functional groups, more specifically thiol (SH) groups, have recently shown great potential for covalent immobilization of biomolecules via thiol-ene click chemistry.[14] Through the creation of covalent bonds between SH-terminated surfaces and biomolecules, a well-defined system is created with good control over the biomolecule conformation.[4, 15, 16] A detailed description of the importance of sulfur-based surfaces is given in section 2.1.

Although SH-terminated surfaces offer several advantages for biomedical applications, their fabrication through surface modification methods, either through wet-chemical or chemical vapor deposition (CVD) approaches, has not been fully exploited. While wet-chemical methods can be useful and do not require specialized equipment, they have demonstrated several disadvantages, namely: non-specificity, moderate reproducibility, and surface etching. Furthermore, they often require the use of an expensive, corrosive, and/or toxic solvent to dissolve the desired

monomer. Due to these disadvantages, alternative methods should be considered for large-scale, industrial applications.[2, 6]

In contrast to wet-chemical approaches, CVD methods are considered to be cleaner and simpler. Many of those are based on non-equilibrium or "cold" plasma treatments at low or atmospheric pressure (plasma enhanced CVD or PECVD) and are used for the simple functionalization of surfaces. During plasma treatments, radicals are created in the gas phase through collisions of electrons with (precursor) molecules, as well as ions, allowing for the incorporation of new functionalities onto the surfaces. A detailed description behind the functionalization mechanism by aid of a low-pressure (LP) plasma is presented in section 2.3.

Photo-initiated CVD (PICVD) methods have proven to be effective alternative methods for the functionalization of polymer surfaces.[17, 18] These methods involve exposure of surfaces to radiation in reactive gases. The biggest advantage of photo-induced methods over their plasma counterparts is a more "targeted" surface chemistry due to the use of mono-energetic photons rather than "hot" electrons, as further described in section 2.4.[19, 20] Photo-initiated approaches appear to be superior to plasma chemistry by producing nearly "mono-functional" films, often with reduced infrastructure requirements. The creation of nearly "mono-functional" surfaces is specifically desired to better understand the biochemical immobilization processes. This motivates to further study LP plasma and photo-based surface functionalization methods in more detail.[21]

1.2 Objectives

There is increasing interest in the literature in SH-terminated surfaces, as anchors for further immobilization of biomolecules. Nevertheless, those specific surfaces

are mainly obtained through tedious and complicated wet-chemical approaches. CVD methods, especially plasma-based ones, have been studied as an alternative method to obtain nitrogen- and oxygen-rich surfaces, demonstrating great potential for a simple and versatile modification technique. However, those methods have not been fully exploited in the context of sulfur-rich surfaces.

Based on the limited amount of studies found in the literature, the main objective of the present research is to create SH-terminated surfaces for further applications using CVD methods. Two methods are explored: plasma-enhanced CVD (PECVD) and photo-initiated CVD (PICVD). As the surfaces could be of interest for biomedical applications, they have to be optimized in a sense that they have a high density of SH-groups and are simultaneously stable in air and aqueous solutions. To obtain SH-terminated surfaces with either of the two above-mentioned methods, binary gas mixtures, BGMs, comprising a hydrocarbon backbone and hydrogen sulfide, H_2S, as the functional gas, are used as precursors.

The following specific objectives are addressed in this thesis:

i. Create SH-terminated films from ethylene / H_2S, butadiene / H_2S, and acetylene / H_2S BGMs through PECVD and PICVD methods at similar conditions, and examine the influence of process parameters on the surface properties, such as chemical composition, morphology and stability;
ii. Compare SH-terminated films obtained from BGMs and single-molecule precursors in terms of SH concentrations and stability;
iii. Investigate the wavelength (λ)-dependency of the surfaces by using different types (different energies) of vacuum ultraviolet (VUV, $\lambda<200$ nm) lamps in terms of deposition kinetics, chemistry, and morphology.

1.3 Organization of the thesis

This manuscript-based thesis consists of seven chapters. Following this introduction (Chapter 1), Chapter 2 gives an overview of the existing literature and is subdivided into six sections introducing the relevance of sulfur-containing surfaces, different surface modification techniques, more detailed descriptions of plasma-enhanced chemical vapor deposition (PECVD) and photo-initiated (PICVD) techniques, and the importance of the stability as well as the growth of the created surfaces.

The first part of Chapter 3 describes the experimental setups used to synthesize SH-terminated surfaces, namely the PECVD and PICVD experimental setups. For the case of the PICVD setup, where different sources were used, the experimental determination of the relationship of photon flux as a function of distance is further described. The second part of Chapter 3 gives an overview of surface characterization and plasma diagnostic techniques used in this work.

Experimental results are presented and discussed in Chapter 4 to Chapter 6 and are manuscripts published in scientific peer-reviewed journals. Chapter 4 presents the first ever reported fabrication and characterization of sulfur-rich films obtained through plasma- and vacuum-ultraviolet photo-polymerization from binary gas mixtures, BGMs, of a hydrocarbon (either ethylene or butadiene) and H_2S.

Chapter 5 describes the influence of process parameters, especially the radiofrequency (r.f.) power, on the properties of SH-terminated surfaces obtained from BGMs of acetylene and H_2S using PECVD. Data obtained from

complete surface characterizations are compared with those obtained in a similar discharge when using propanethiol as single-molecule precursor. Additional plasma diagnostic experiments are performed to gain better understanding on the growth mechanisms.

A first-of-its-kind wavelength (λ)-dependent study is presented in Chapter 6 aiming to identify a specific photon energy leading to maximum thiol concentrations, [SH]. BGMs of acetylene and H_2S are irradiated with four different VUV lamps to create SH-terminated films.

Conclusions derived from this work and recommendations for future works are summarized in Chapter 7. The appendices (Chapter 8) include supplementary information associated with the presented manuscripts. A list of references cited in this work follows the appendices.

Chapter 2 Background

2.1 Sulfur-rich organic coatings

Sulfur (S)-containing groups, especially sulfites ($-SO_3$), sulfates ($-SO_4$), disulfides (-S-S), and thiols (-SH) occur in a variety of biomolecules, particularly proteins, antioxidants and glycosaminoglycans.[22, 23] Thiol and disulfide groups facilitate the organization of secondary structure in proteins and have shown to be involved in cell physiology.[22] Due to the importance of those S-containing groups, there is interest to study interactions of material surfaces bearing such functionalities with biological proteins and their contribution to defining bio-interfacial interactions.[22] Sulfonated surfaces have shown improved cell adhesion,[24, 25] delayed onset of thrombus formation, and improved hemocompatibility,[26-28] desirable characteristics of suitable biomaterials.

SH-terminated surfaces demonstrate potential for selective and specific bio-interfacial interactions through thiol-ene click reactions. The rising interest in thiol-ene click chemistry[14, 29-34] plays an important role in potential applications and significance of SH-terminated surfaces. This specific click reaction between SH groups and ene moieties leads to the formation of stable thioether bonds (Figure 2-1) and has demonstrated a high degree of specificity and reactivity. Based on these benefits, this coupling reaction has been widely exploited for covalent immobilization of antibodies, enzymes, peptides and DNA.[35-40]

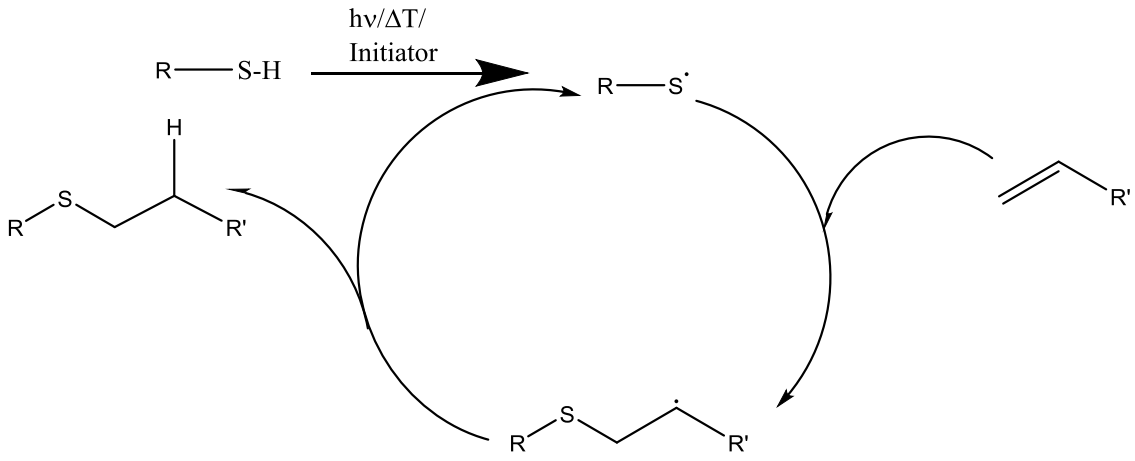

Figure 2-1: Mechanism of thiol-ene click reaction. [14]

Besides biomaterials, S-rich organic surfaces have demonstrated potential applications in conducting films,[41-44] proton exchange membranes in fuel cell applications,[45, 46] catalysts in acetalization reactions,[47-49] biodiesel production,[50] and water purification.[51-53] Depending on the specific application, the thiol concentration on the surfaces can be crucial for a successful use of such surfaces. For the specific example of water purification, SH and $SO_x(H)$ functionalized materials, more specifically silica particles and mesoporous carbon, have shown great potential as electrostatic adsorbents. These materials can remove (soft) metal ions effectively over a wide pH range and it was shown that the degree of functionalization greatly influences the heavy metal removal efficiency. It is therefore evident, that for this specific application high functional group concentrations are required in order to obtain an efficient removal of heavy metals from water. This wide field of applications makes the development of S-containing surfaces important and techniques to simplify their creation are becoming more significant.

2.2 Surface modification techniques to create S-rich surfaces

2.2.1 Wet-chemical approaches

The most common approach for producing surfaces containing sulfur has been through wet-chemical techniques,[22] including bulk-polymerization,[54-56] electrochemical polymerization,[57] and self-assembled monolayers.[22, 58-60] S-containing functionalities can also be incorporated onto silica surfaces through a coupling reaction between a silane sulfur-containing coupling agent, such as 3-mercaptopropyl trimethyloxysilane (MPTMS), and sinalol groups on the substrate surface.[61, 62] These approaches can be complex and complicated, substrate dependent, non-environmentally friendly, highly time consuming, and can suffer from low efficiency, inhomogeneous distribution of S-containing functionalities, stability, and reduction of the substrate's mechanical integrity.[63-66]

2.2.2 Chemical vapor deposition (CVD)

Suitable alternatives to wet-chemical approaches for the creation of S-containing surfaces are chemical vapor deposition (CVD) techniques. These techniques are recognized to be cleaner, substrate-independent, room-temperature, one-step, solvent-free processes producing reduced amounts of waste.[67, 68] This approach is often referred to as a green approach since chemical reactions are driven and maintained using electricity, therefore making it possible to take advantage of renewable resources while reducing the environmental impact.

During CVD a solid product, or organic coating, is created through dissociation and/or chemical reactions of volatile precursors. The deposition occurs either through homogeneous reactions between species in the gas phase, in which gaseous species polymerize and then adsorb onto the surface, and/or heterogeneous chemical reactions,

in which gaseous species first absorb to the surface and then polymerize on the surface.[69] Depending on the activating environment (heat, light, plasma) to initiate a polymerization reaction (i.e. creation of radicals) different variations of the CVD techniques exist, two of which will be discussed in detail in sections 2.3 and 2.4.[67, 69, 70]

CVD processes have shown to be appropriate for the deposition of S-rich materials,[22, 44, 71-73] however there has only been a limited amount of work reported to date compared to oxygen- and nitrogen-rich materials.[11, 74-83] Among the different CVD techniques, plasma-enhanced CVD (PECVD) is the most frequently reported CVD technique for the production of S-rich surfaces.

2.3 Plasma-enhanced chemical vapor deposition (PECVD)

So far, the production of S-rich organic coatings through PECVD has mainly involved the use of single-molecule precursors. However, such studies have been hindered by a marked shortage of suitable monomers, as they do not vaporize easily, and are not stable in the plasma, thus showing low retention of sulfur functionalities on the resulting organic coatings.[22] When using benzene sulfonic acid as a precursor for example,[84] the resulting organic coatings did not contain sulfonic groups since these groups were unstable in the plasma. Plasma polymerization of vinyl sulfone derivates, such as methyl vinyl sulfone, ethyl vinyl sulfone, and vinyl sulfone, demonstrated the presence of a variety of S-containing groups (R-S-R, R-SO-R, R-SO_2-R).[85] The resulting organic coatings are also often referred to as plasma polymers and should not be mixed up with conventional polymers as they are significantly different from each other; this will be discussed in more detail in the following section. Alternatively, plasma "co-polymerization" of SO_2 with unsaturated hydrocarbon monomers (C_2H_2 and C_2H_4),[26,

45] or hexamethyldisiloxane (HMDSO),[28] dimethyl sulfoxide (DMSO) and 1,7-octadiene, gave more promising results; a greater amount of sulfur groups at higher oxidation states were found in the coatings.[86]

The desire to obtain SH-terminated organic coatings for specific applications keeps driving the search for further S-containing precursors to help improve the incorporation of SH functionalities.[87] More recently allylmercaptan,[71, 88, 89] thiophene,[44, 51, 73, 90] and propanethiol[72, 91-94] have been used as precursors to create SH-terminated surfaces via PECVD. These precursors were promising choices since the desired SH functionality is already incorporated in the molecule and they can be easily transferred into the gas phase. Nevertheless, only Thiry et al. have reported a complete study combining plasma diagnostics and plasma polymer synthesis, connecting the influence of different plasma parameters on the chemical properties of propanethiol plasma polymers.[72, 91-93] The same group also developed a derivatization method allowing specific identification of SH groups and their concentrations on the surfaces.[94]

Since PECVD is one of the most common CVD techniques used for the creation of S-rich films, its fundamentals, mechanisms, and relevant process parameters will be discussed in detail in the next section.

2.3.1 Plasma polymerization: Fundamentals and mechanisms

Plasma refers to the state of an ionized gas, which can be completely or only partially ionized. Plasma contains electrons, ions, and other reactive (but neutral) particles such as excited atoms and molecules, radicals, and photons (from infrared to vacuum ultraviolet).[84, 95-98] Low-temperature or non-equilibrium plasma is used to initiate polymerization reactions through collisions of the precursor gases with electrons, which

acquire their kinetic energy directly from the applied electromagnetic field.[70, 99-102] As a result, precursor molecules dissociate and consequently the growth of a film on the substrate occurs from the absorption of free radicals and molecules, neutralization of impacted ions, and chemical reactions of the mentioned species with simultaneous desorption of by-products.[100, 103] Overall, plasma can be considered an "energy soup" in which reaction pathways are difficult to control.

Ideally, PECVD is used to deposit thin (from few nanometers to micrometers), well-adhering, and highly-functionalized polymer-like films on substrate surfaces. In reality however, these films do not resemble the precursor's structure, but rather an oligomer structure, and often even lose its functionalities (Figure 2-2).[95] Compared to conventional polymers, plasma polymers do not show regularly repeating units, are branched, and show a high degree of cross-linking.[104]

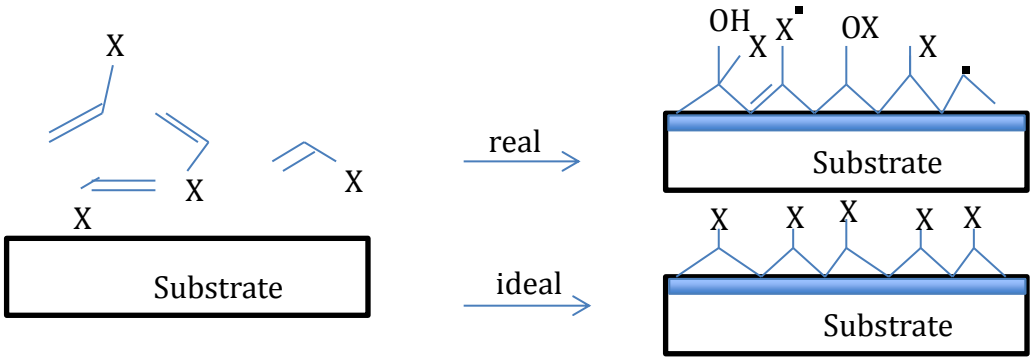

Figure 2-2:Scheme of ideally and realistically structured plasma polymers. [95]

The challenge of obtaining better control during PECVD lies in the variety of process parameters available for tuning. Over the past years, detailed studies have been undertaken to understand the relationships between different process parameters and the chemical and/or physical properties of plasma polymer films, aiming to optimize process parameters to obtain films with desired properties for specific applications.[98]

Through careful tuning of the process parameters, organic coatings with a great variety of properties can be obtained.

2.3.2 Influence of process parameters on film chemistry and deposition rate

Process parameters controlling plasma polymerization can be divided into two major categories:

1. Reactor-specific parameters, which can be altered but in most cases are not variable, such as reactor geometry, distance between the electrodes and frequency of the electric power; and
2. Operation-specific parameters, such as discharge power, system pressure, precursor flow rate, and precursor type.[103]

Only operation-specific parameters will be discussed in more detail in the following sections since these were mainly varied during this research.

Discharge power

In general, increasing the discharge power leads to an increased number of electrons in the plasma phase, which can consequently collide with molecules resulting in their dissociation and fragmentation.[105] Precursor activation, fragmentation and dehydrogenation processes increase with the applied discharge power and thus the rate of polymerization generally increases.[102, 106] Low power conditions usually yield reduced fragmentation of the precursor(s) resulting in polymer-like films with high concentrations of functional groups (if already present in the precursor). High power conditions yield substantial fragmentation of the precursor(s), resulting in a high amount of low-molecular weight active species. These active species usually lose great

parts of the precursor's original structure, therefore also reducing the incorporation of functional groups in the resulting polymer-like films, and can recombine to form more cross-linked structures.[107] At very high power conditions, high-energy conditions are enhanced, leading to ablation processes and therefore a decrease in the rate of polymerization.[108]

Pulsed PECVD represents an alternative PECVD mode (compared to continuous-wave PECVD) where the applied electric field is pulsed during plasma polymerization, thus reducing the energy input into the system.[109] During the short plasma pulses, precursors are exposed to the glow discharge leading to their activation and initiation of plasma polymerization reactions. During the "off" times, only long-lived radicals are present in the gas phase initiating purely chemical chain reactions (Figure 2-3).[98, 110] The resulting plasma polymers are expected to consist of more well-defined repeating units, to exhibit higher concentrations of the desired functional groups, to be more dense, and to demonstrate an increased stability.

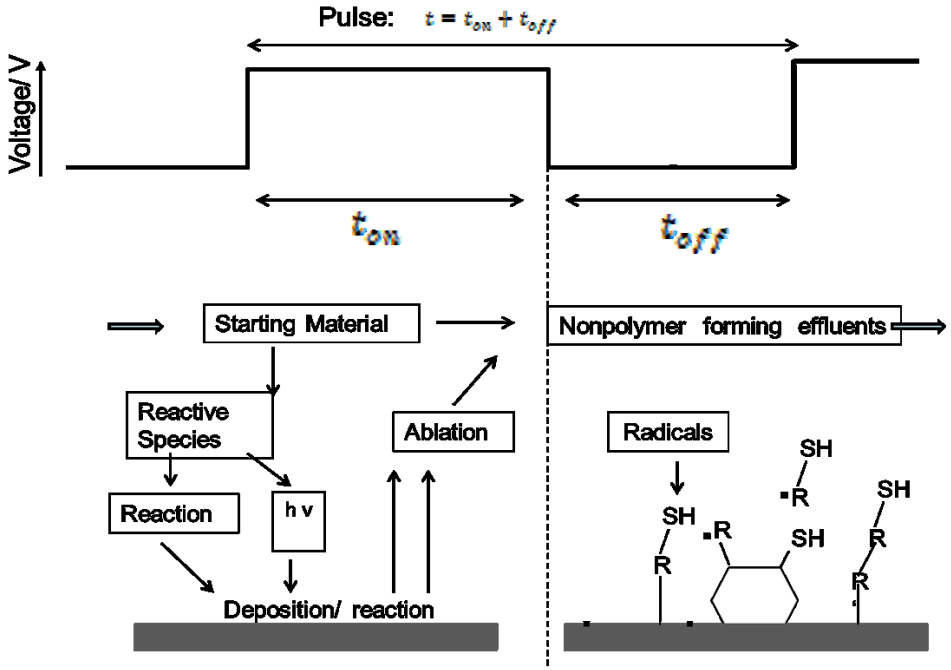

Figure 2-3: Possible mechanisms taking place during the "on" and "off" times of the pulsed plasma polymerization. [109]

Precursor flow

The precursor(s) flow rate(s) greatly influence the deposition kinetics. At very low flow rates, the residence time of the precursor(s) is high and polymerization reactions will consume all precursor(s) supplied to the system. As the flow rate increases, the supply of the precursor(s) also increases, resulting in an increased rate of polymerization. With further increase of the flow rate, a point will be reached at which the residence time of the precursor(s) is so small that all active species are removed from the system before initiating a polymerization reaction, resulting in a decrease of the deposition rate.[111] In a specific example of plasma polymerization of pure acetylene, using low flow rates results in a challenge to maintain a stable system pressure, as all acetylene is immediately consumed and polymerized.

System pressure

Similar to the precursor flow, the system pressure has a significant influence on the deposition rate. Most gases under vacuum can be treated as ideal gases and, in a fixed volume, the pressure can be considered proportional to the gas molecules in the closed system. Furthermore, the system pressure determines the mean free path, *l*, of gas molecules and therefore the frequency of collisions between them and the walls of the reactor. Generally, with rising pressure the collision frequency between gas molecules and the reaction probability of active species increases leading to an increase in deposition rate.[76, 99] The dependence of deposition rate on pressure has been reported to follow a p^2 dependence, which however saturates at high pressure values.[110, 112] At low pressures, *l* is long (see equation 2-2) and electrons in the plasma can acquire more energy from the r.f. field. Therefore, their impact with molecules results in greater fragmentation and ionization leading to an increase in electron density and therefore deposition rate. Increasing the pressure results in a decrease in *l* as well as a decrease in average electron energy acquired from the r.f. field.[112]

The system pressure can be used to determine the nature of gases via the Knudsen number, K_n:

$$K_{\mathrm{n}} = \frac{l}{d} \tag{2-1}$$

With the mean free path *l* and the characteristic length of a given system *d*. As mentioned before, the mean free path describes the average distance between collisions for gas molecules and is inversely proportional to the system pressure *p*:

$$l = \frac{k_b T}{\sqrt{2}\sigma p} \tag{2-2}$$

Where k_b is the Boltzmann constant, *T* the temperature, σ the effective area for collisions, and *p* the pressure. Viscous gases are characterized by K_n<0.01 (high *p* and

short *l*) and the gas flow is dominated by molecule-molecule collisions. When K_n>1 (low *p* and long *l*), gases are characterized through molecular flow and molecule-wall collisions are predominant. K_n values between 0.01 and 1 describe a transition or slip flow.[113] Determining K_n for different gases (or mixtures), pressures and temperatures can be helpful for explaining different phenomena observed in plasma polymer films, as for example varying composition trends with pressure.

For plasma polymerization processes it should be considered that not only high energy electrons and photons are responsible for providing energy to create active sites, but also ions play a significant role. Ions can either yield direct deposition or can use their energy to create active sites on the substrate facilitating the reactions of active species from the plasma. The energy provided by ions is orders of magnitude higher than that of electrons or photons, therefore dominating and should not be neglected.[112] At low pressures, ions originating from the plasma might cross the plasma sheath almost non-collisional and the flux of ions is comparable with that of neutrals. As the pressure increases, collisions within the sheath increase and at high pressures the sheath becomes collisional. At this point, the increased probability of collisions between ions and neutral species results in loss of the ions' kinetic energy resulting in loss of radical species with pressure leading to decreased deposition rates.[110, 112, 114]

Precursor

The selection of the appropriate precursor is crucial for obtaining thin films with desired chemical and physical properties. The structure of the precursor has a large effect on the types of active species that are formed in the plasma, and therefore the composition of the resulting plasma polymer. Many of the precursors that have been used to obtain plasma polymers can be considered "polymerizable", as they contain sites of

unsaturation, such as a carbon-carbon double bond; a prerequisite for conventional polymerization reactions.[109] Sulfur-containing precursors falling into this category are allylmercaptan or thiophene. However, some precursors that have been used to produce plasma polymers can be considered "non-polymerizable", as they are saturated. This demonstrates the exclusivity of plasma phase reactions and highlights that multiple simultaneous polymerization pathways might be taking place during plasma polymerization reactions.[115] An example of a "non-polymerizable" precursor for the creation of S-rich films is the well-studied propanethiol.

To optimize the deposition kinetics of the polymerization reaction, the structure of the precursor(s) should be considered. At otherwise comparable reaction conditions, precursors containing sites of unsaturation yield faster polymerization reactions (faster deposition rates), and the more sites of unsaturation in the precursor molecule the faster the polymerization.[102, 111] Acetylene, for example, which contains a triple bond, polymerizes more than an order of magnitude faster than ethylene, which contains a double bond. In another example, 1,3-butadiene polymerizes faster than ethylene, due to its more unsaturated structure.

The selection of an appropriate precursor is also crucial when the stability of the resulting polymer-like films is of importance. Nitrogen-rich films obtained from ethylene and ammonia gas mixtures, for example, demonstrated a significant lack of stability after immersion in water for 24 h.[9] By choosing a more unsaturated hydrocarbon precursor (i.e. butadiene) more stable films could be obtained, since a higher cross-link density in the films is expected. Acetylene is a good precursor to increase the stability of the coatings.[83] In this case, the stability is increased by a more densely cross-linked structure (compared to ethylene films) due to the present triple bond in the acetylene molecule.

Overall, two precursor selection approaches are recognized to create plasma polymer films with desired functionalities:

(i) Use of a single-molecule precursor that already contains the desired functional group. In the case of SH-terminated films, allylmercaptan, thiophene, and propanethiol have been used as single-molecule precursors.

(ii) Use of binary precursor gas mixtures, consisting of a functional precursor and a hydrocarbon precursor that is responsible for building the polymer backbone. This approach has been used in the past to produce nitrogen- and oxygen-rich films,[11, 76, 78, 80, 81, 83, 116, 117] however no such methods have been used to create sulfur-rich films.

While the first method allows for direct incorporation of the desired functionality into the films, the second approach allows to adjust the gas mixture ratio *R* enabling better fine-tuning of the films' properties:

$$R = \frac{F(X)}{F(C_x H_y)} \tag{2-3}$$

Despite the advantages and great progress achieved with the creation of S-rich surfaces through PECVD several drawbacks of this approach should be kept in mind. As mentioned above, plasma resembles an "energy soup" and the reactions occurring in a plasma are difficult to control. The electrons, the main originators of chemical reactions in non-equilibrium plasmas, possess a broad, Maxwell-Boltzmann-like energy distribution,[10, 78, 115, 118] thereby making the reactions non-specific and non-selective. Furthermore, the plasma itself can damage the substrate and/or pre-deposit devices. Moreover, since this technique is usually performed under vacuum the required equipment and its maintenance can be very costly making its scale-up

challenging. Photo-initiated CVD (PICVD), which will be introduced in detail in the next sections, demonstrates great potential for a more selective and controllable process.[109]

2.4 Photo-initiated chemical vapor deposition (PICVD)

Photo-initiated CVD (PICVD) is very close to PECVD since they share common basics. One can imagine selecting a single plasma component, namely the photons, to carry out (photo-)chemistry. By isolating one component with a known energy content of the rather complex plasma, the reactions are expected to be more selective and easier to control. The selective and specific nature of PICVD treatments compared to PECVD has been shown in the past for nitrogen and oxygen-rich organic coatings.[10, 77, 119] Another big advantage of using radiation, in this work specifically vacuum ultraviolet (VUV, λ<200 nm), is that most hydrocarbons and organic molecules strongly absorb at the given spectral range and the energy of the photons exceeds most covalent chemical bond energies, eliminating the necessity of an initiator required for other photochemical reactions.[70] Furthermore, some of the VUV lamps used in this work are based on an electrodeless radiofrequency (r.f.) electrical discharge in the corresponding gas at low pressure.

2.4.1 Photochemistry of gases: Fundamentals and mechanisms

Photochemistry is the study of chemical reactions induced in a system through radiation. These reactions follow a series of steps:[120]

1. Absorption of a photon ($h\nu$) by a molecule (M) and consequent formation of an electronically excited state (M*);

2. Consequent reactions of M*, including dissociation, pre-dissociation, fluorescence, phosphorescence or collisional deactivation to the ground state;
3. Possible molecular rearrangements (isomerization) of the electronically excited state.[121, 122]

All steps involving M* are part of primary photochemical processes. For some molecules, M* neither dissociates nor fluoresces immediately and the reactions of excited states become significant (e. g. acetylene, carbon dioxide). Secondary processes include all processes which the products of dissociation or the excited molecules either undergo or initiate.

If photons are energetic enough to break chemical bonds, molecules dissociate directly into several fragments, including radicals.[121, 123] Some important bond dissociation energy values, *D*, are summarized in Table 2-1. In the present work, VUV radiation is used to initiate photochemical reactions. In this region, the energy of the photons (up to 10 eV or 124 nm, $E(eV) = \frac{hc}{\lambda(nm)} = \frac{1240}{\lambda(nm)}$) is sufficient for the rupture of most chemical bonds. Therefore, the dissociation energy of a chemical bond is usually not the limiting factor in the photo-dissociation process. Apart from bond dissociation energies, the most important data for photo-dissociation is the absorption, *k*, of molecules as a function of wavelength, λ, since almost all observed absorption continua correspond to a dissociation process.

Table 2-1: Bond dissociation energies, D, and the corresponding wavelengths, λ, of common chemical bonds in organic molecules (in case that the molecule absorbs at the specific λ). [124, 125]

Bond	Bond dissociation energy, *D* (kJ/mol)	Bond dissociation energy, *D* (eV)	Corresponding wavelength, λ (nm)
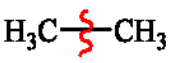	377	3.9	318
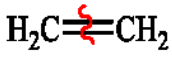	602	6.2	200
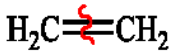	743	7.7	161
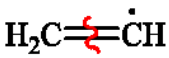	690	7.2	172
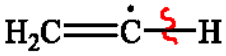	347	3.6	344
	670	6.9	180
	965	10.0	124
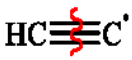	745	7.7	161
	596	6.2	200
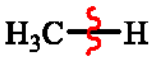	439	4.6	270
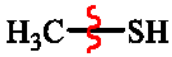	313	4.2	295
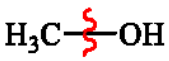	389	4.0	310

Baxamusa et al. suggested a reaction mechanism for PICVD, in which polymerization reactions are initiated by radicals.[67, 126] Incident light decomposes the molecules into radicals by homolytic or heterolytic fission of covalent bonds. Chain growth and termination occurs through a reaction of the created radicals with reactive species in

the gas phase, on the surface, or with each other, forming new functional groups, C=C bonds, or a cross-linked network.[120, 127] Similar to PECVD treatments, precursor(s) are exposed to a light source inducing a reaction which leads to deposition of thin films on substrates.

2.4.2 Common light sources used in PICVD

In photo-induced methods, light is used to initiate photo-reactions and is highly important. Therefore, different kinds of light sources have been used and studied.[123] The electromagnetic spectrum of light with respective photon energies and wavelengths is represented in Figure 2-4. For the direct photolysis of organic molecules, vacuum ultraviolet (VUV, λ<200 nm) or ultraviolet (UV, λ<400 nm) sources are required to achieve photo-dissociation. The definition of VUV varies but can be explained by the fact that air strongly absorbs radiation at λ<190 nm and therefore it can be only used effectively in a vacuum. In some cases, the cutoff of quartz (λ=180 nm) is used to define the boundary between VUV and UVC radiation, however throughout this research the above-mentioned definition will be applied. The selection of a proper light source is critical for PICVD. From a practical point of view, output wavelength should ideally match an absorption band of the precursor(s) used for deposition. In addition, other factors to consider are intensity, coherence, lifetime, economic, and maintenance factors.

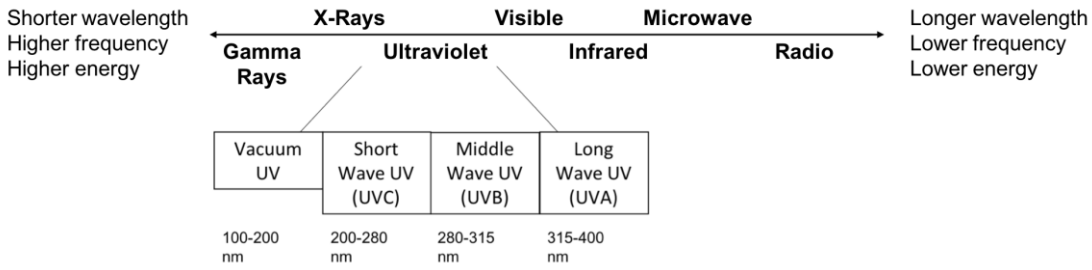

Figure 2-4: Electromagnetic spectrum of light from gamma rays to radio waves and a more detailed illustration of the ultraviolet range relevant to this research.

Low-pressure mercury lamps are commonly used as a photon source. These lamps generate UV light at 184.9 and 253.7 nm, matching absorption bands of many gases used for thin film deposition. These lamps have been successfully used in the past to deposit a-Si:H films from disilane, silicon nitride films from SiH_4 and NH_3, iron films from pentacarbonyl iron, and tantalum oxide films from $Ta(OCH_3)$, to name a few.[123] Further commercial lamps available are arc lamps with continuous emission spectra above 190 nm, D_2 lamps with continuous emission spectra between 120 and 400 nm, as well as rare-gas resonance VUV lamps.[121] Although the latter lamps generate light at low intensities only, they are becoming more popular, since most organic molecules strongly absorb light at their short emission wavelengths, making them attractive for PICVD. Besides coherent (V)UV light sources, excimer sources are also commonly available.[19, 128, 129] Excimers are short-lived excited molecules which can be formed in a dielectric barrier discharge (DBD) and can occur heterodimeric or dimeric:

$$e^- + Xe + Xe \rightarrow e^- + Xe + Xe^* \rightarrow Xe_2^* + e^-$$

Excimers are unstable and decompose typically within less than a microsecond giving off their excitation energy in the form of (V)UV radiation.[129-131]

$$Xe_2^* \rightarrow 2Xe + hv(172\ nm)$$

The main emission lines of some of the above-mentioned light sources with their respective peak wavelengths are shown in Figure 2-5.

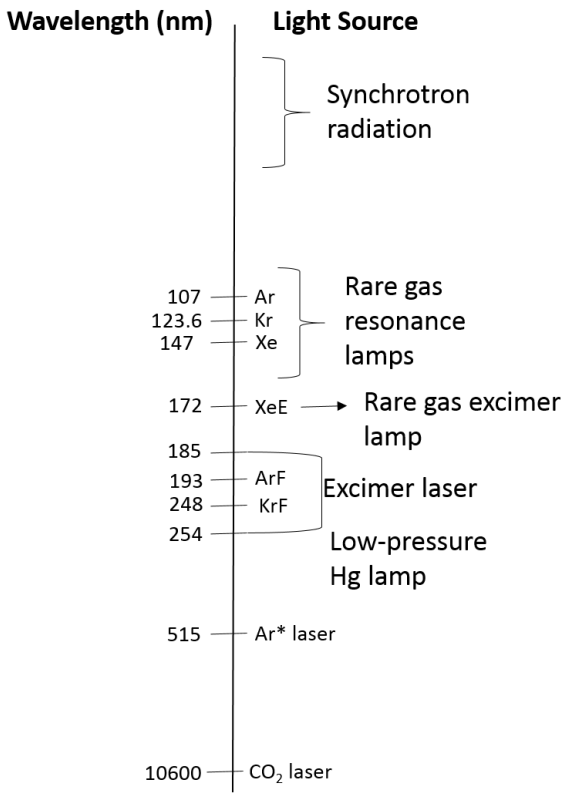

Figure 2-5: Main emission lines of some common light sources with their respective peak wavelengths. [123]

2.4.3 PICVD reactor design

PICVD reactors can differ substantially from each other making the comparison between reported results challenging. Nevertheless, all apparatuses share some common components: (i) a reaction cell with the substrate of interest, (ii) a light source, (iii) a pumping and exhaust system, and (iv) a gas (precursor) delivering system. An example of a home-made reactor which was used in this work is presented in Figure 6-2. In order to introduce the desired radiation to the reaction cell an optical window (often attached to the light source) is required. Depending on the radiation wavelength, different window materials can be used as shown in Figure 2-6.[123, 132]

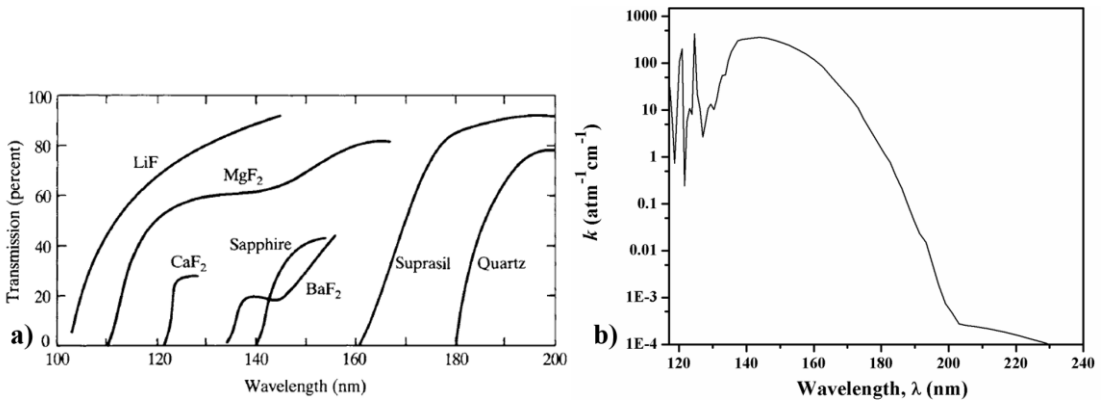

Figure 2-6: a) Transmission curves of readily available window materials (from [132]), and b) absorption spectrum of oxygen in the region 120 to 240 nm (k is given in units of atm^{-1} cm^{-1}, base e).[133]

If the reactor uses a light source with λ>200 nm more readily available and cost-effective quartz windows can be used, as the light beam can travel efficiently through air without being absorbed. In addition, expensive pumping systems are not required. In this research most of the PICVD experiments were carried out at λ<170 nm and therefore specialized window materials, as well as good isolation from air is required. The need for such materials (in our case MgF_2 windows) results in high costs of the light sources and small window areas which in turn results in small deposition areas (~1 cm^2). St-Georges-Robillard et al.[134] developed a "conveyor" device in order to by-pass this limitation enabling the continuous treatment of a moving strip and therefore increasing the effective coated substrate area.

Another important consideration when designing a PICVD reactor is the reactor's geometry and irradiation path relative to the substrate, namely parallel or perpendicular to it. Truica-Marasescu et al.[135] demonstrated that photochemical nitriding of various polymer surfaces strongly depends on the substrate orientation. When the polymer sample was placed perpendicular to the irradiation path, the sample was subjected to photons and free radicals in the gas phase, resulting in high nitrogen

incorporation (up to 25 at.%) on the surfaces. In contrast, when the polymer sample was placed parallel to the irradiation path, it was only subjected to free radicals in the gas phase, resulting in low nitrogen incorporation on the surfaces (≤10 at. %). If selective-area deposition is desired, the radiation beam can be further focused on a specific point of interest.

The resulting properties of the photo-polymer-like films, such as deposition rate, chemical composition, stability, and morphology, strongly depend on the choice of different arrangements discussed above.

2.4.4 Process parameters

Similar to PECVD, process parameters can be adjusted in PICVD to optimize the deposition kinetics and resulting properties of organic coatings. Parameters found in PECVD processes, such as precursor(s) flow rate(s), have comparable effects in PICVD.

System pressure

In contrast to PECVD, in PICVD the pressure only influences the concentration of gas molecules in the fixed volume and therefore the molecular collision frequency and creation probability of active species. Increasing the pressure entails a higher concentration of potential reactive species, which results in more intense photodissociation and an increase in deposition rate through increased rate of gas phase collisions and more efficient gas phase nucleation reactions. As the pressure further increases, light is more strongly absorbed and photodissociation reactions are more intense in close vicinity to the light source. As a consequence, an important amount of reactive species might not reach the substrate and will be conducted directly to the

exhaust system resulting in a reduction in deposition rate. As mentioned in the PECVD section, the deposition rate in PICVD experiments can also be increased by increasing the residence time of the gas molecules in the reactor.[136] The longer the precursor molecules interact with the specific radiation the more active species can be created resulting in higher deposition rates. Longer residence times can be achieved by lowering the precursor(s) flow rates and system pressure.[137]

Precursor

Photon absorption by the desired precursor(s) is crucial for a successful photo-reaction. The absorptivity of each individual precursor(s) and the subsequent initiation of photochemical reactions depends on their absorption spectrum. The photochemistry of different precursors, relevant to this study, will be discussed in the following sub-sections.

Ethylene (C_2H_4)

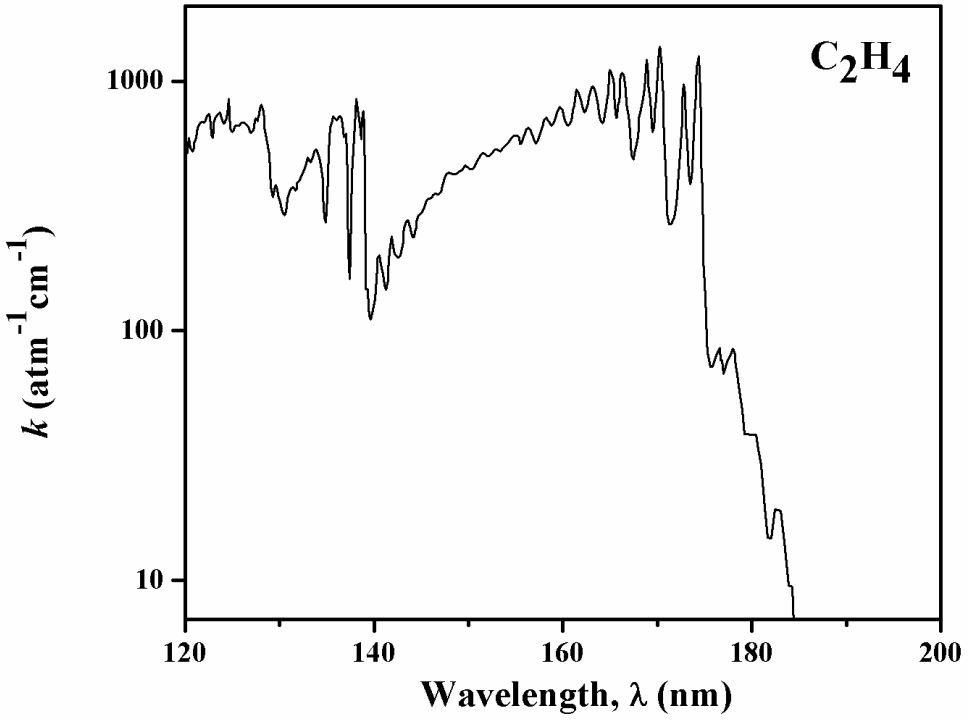

Figure 2-7: Absorption spectrum of ethylene in the region 120 to 200 nm (k is given in units of atm^{-1} cm^{-1}, base e). [138, 139]

The absorption spectrum of ethylene (Figure 2-7) consists of diffuse bands between λ=165-185 nm which become a continuum at shorter wavelengths.[140-142] At λ>200 nm, ethylene is basically transparent to UV radiation.

Three primary processes of similar importance have been identified upon irradiation of ethylene over its absorption range, leading to the formation of acetylene, hydrogen, and excited vinyl radicals:[138, 143-145]

$$C_2H_4 + h\nu \rightarrow C_2H_2 + H_2 \quad (2\text{-}4)$$

$$C_2H_4 + h\nu \rightarrow C_2H_2 + 2H \quad (2\text{-}5)$$

$$C_2H_4 + h\nu \rightarrow \cdot C_2H_3^* + H \quad (2\text{-}6)$$

The excited vinyl radical, [$\cdot C_2H_3$*], can be stabilized by collisions at high pressures and its creation drastically decreases with decreasing photon energy, as reported by Back et

al.[143, 146] Secondary processes include the formation of ethyl radicals, $\cdot C_2H_5$, and further reactions of the latter to create high molecular species, such as C_2H_6, and C_4H_{10}. Photolysis of ethylene at different wavelengths yields the same products.[147, 148]

Butadiene (C_4H_6)

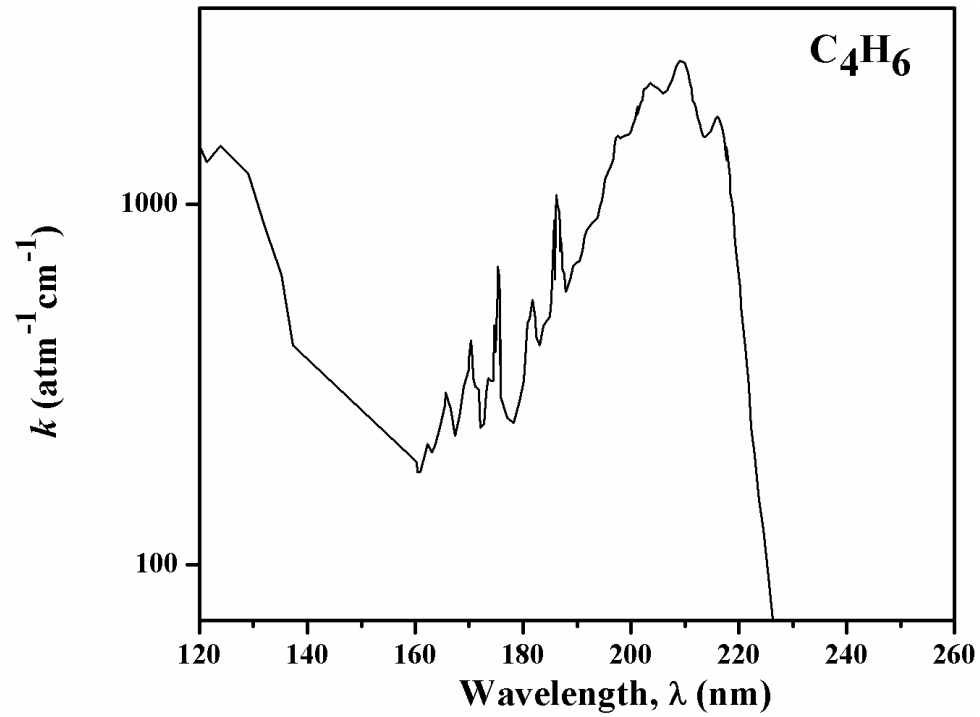

Figure 2-8: Absorption spectrum of butadiene in the region 120 to 260 nm (k is given in units of atm^{-1} cm^{-1}, base e). [149, 150]

The absorption spectrum of butadiene (Figure 2-8) shows a first strong absorption at about λ=225nm and continues with diffuse bands at shorter wavelengths.[151] Diverse primary processes have been reported at different spectral regions and only the ones relevant to this study will be discussed below.

λ=220-260 nm

Primary processes of the photolysis of 1,3-butadiene in the far-UV region include the formation of acetylene, ethylene, hydrogen, and vinylacetylene:[152, 153]

$$1{,}3-C_4H_6+h\nu \rightarrow 1{,}3-C_4H_6^* \quad (2\text{-}7)$$

$$1{,}3-C_4H_6^* \rightarrow C_2H_2+C_2H_4 \quad (2\text{-}8)$$

$$1{,}3-C_4H_6^* \rightarrow H_2+C_4H_4 \quad (2\text{-}9)$$

Furthermore, isomerization to excited 1,2-butadiene has been observed, which can decompose subsequently in several radical or molecular channels:

$$1{,}3-C_4H_6+h\nu \rightarrow 1{,}3-C_4H_6^* \rightarrow 1{,}2-C_4H_6^* \quad (2\text{-}10)$$

$$1{,}2-C_4H_6^* \rightarrow C_2H_2+C_2H_4 \quad (2\text{-}11)$$

$$1{,}2-C_4H_6^* \rightarrow H_2+C_4H_4 \quad (2\text{-}12)$$

$$1{,}2-C_4H_6^* \rightarrow \cdot CH_3+\cdot C_3H_3 \quad (2\text{-}13)$$

At increased pressures, a decrease in the quantum yields of the products has been observed due to increased collisional deactivation of the excited molecules:

$$1{,}3-C_4H_6^*+M \rightarrow 1{,}3-C_4H_6 \quad (2\text{-}14)$$

$$1{,}2-C_4H_6^*+M \rightarrow 1{,}2-C_4H_6 \quad (2\text{-}15)$$

λ=147 nm

An additional primary process observed during the photolysis of 1,3-butadiene at λ=147 nm is the direct dissociation of the central carbon-carbon bond resulting in two vinyl radicals: [152]

$$1{,}3-C_4H_6+h\nu \rightarrow 1{,}3-C_4H_6^* \rightarrow 2\cdot C_2H_3 \quad (2\text{-}16)$$

This process is not possible in the far-ultraviolet region, since not sufficient energy is available to break this bond. Apart from reaction (2-16), the same primary processes ((2-8) and (2-9)) are reported in the vacuum-ultraviolet region.

λ=123.6 nm

The increased photon energy from 8.4 eV to 10 eV has shown to have very little effect on the product distribution during the photolysis of 1,3-butadiene.[152] A possible additional reaction in this high-energy region is the formation of the (parent) ion of 1,3-butadiene since its ionization potential of 9.1 eV lies well below the photon energy.

Acetylene (C_2H_2)

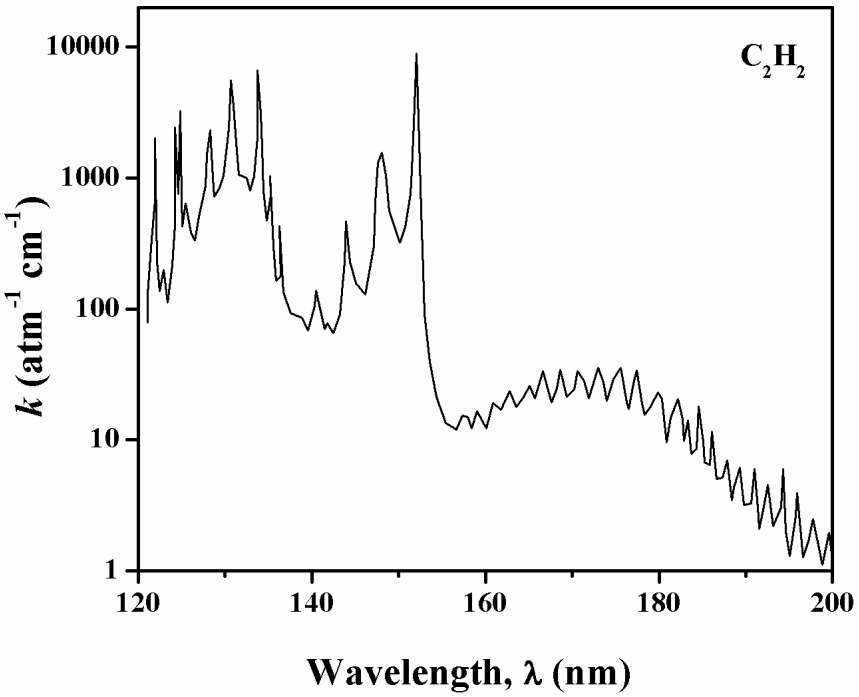

Figure 2-9:Absorption spectrum of acetylene in the region 120 to 200 nm (k is given in units of atm^{-1} cm^{-1}, base e). [121]

The absorption spectrum of acetylene (Figure 2-9) contains a system of weak, diffuse bands superimposed in a continuum in the 155-200 nm region. The vibrational structure below 155 nm suggests the formation of an electronically excited acetylene. At all wavelengths of interest, two primary processes have been identified:[121, 154-157]

(i) Direct dissociation

$$C_2H_2 + h\upsilon\ (> 5.8\ eV) \rightarrow C_2H\cdot + H\cdot \qquad (2\text{-}17)$$

And

(ii) The formation of an excited, metastable acetylene molecule

$$C_2H_2 + h\upsilon\ (> 5.8\ eV) \rightarrow C_2H_2^* \qquad (2\text{-}18)$$

Polymer formation can occur through recombination of the created radicals in reaction (2-17) or through collisions of the metastable acetylene molecule with ground state acetylene.

Although the same primary processes have been identified for all wavelengths of interest, differences in quantum yield of reactions (2-17) and (2-18) are wavelength- and pressure-dependent.[158, 159]

λ=123.6 and 147 nm

At low pressures (p<0.8 Torr) the quantum yield of reaction (2-17) is higher compared to reaction (2-18) and direct dissociation is the most important primary photochemical process. As the pressure increases (p>0.8 Torr), reaction (2-18) becomes more likely and an increased formation of (stable) molecules, such as diacetylene, benzene, and ethylene, are observed. Besides the creation of stable molecules, deactivation of the metastable acetylene molecule through collisions with the reactor walls or other molecules becomes more important and less polymer formation is observed.[157, 160]

λ=172 and 185 nm

At low pressures the quantum yield of reaction (2-18) is higher than of (2-17) and the deactivation of the excited, metastable acetylene molecule has been reported to be more probable than polymer formation. As pressure increases, reaction (2-17) becomes more significant and deactivation less relevant through higher probability of radical creation, increasing polymer formation.[157, 158, 161]

Hydrogen Sulfide (H_2S)

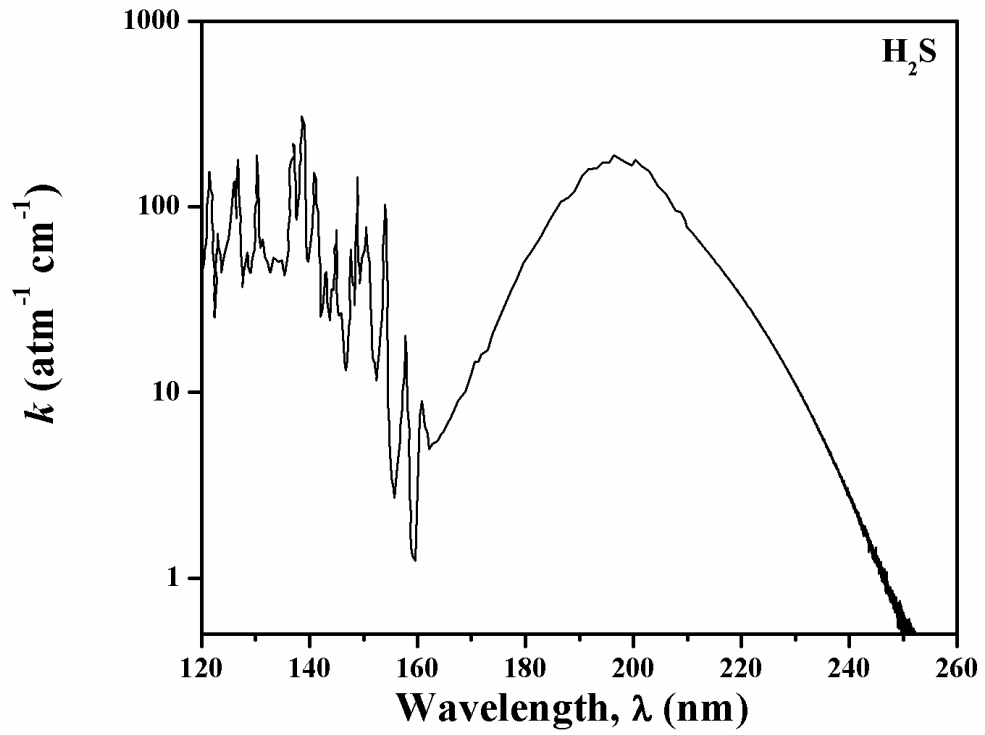

Figure 2-10: Absorption spectrum of hydrogen sulfide in the region 120 to 260 nm (k is given in units of atm^{-1} cm^{-1}, base e). [121]

The absorption spectrum of hydrogen sulfide (Figure 2-10) shows a broad absorption in the 160-250 nm region. The direct photolysis of hydrogen sulfide has been identified as primary process for all λ<309 nm:[162-165]

$$H_2S + h\upsilon\ (> 4.0\ eV) \rightarrow SH\cdot + H\cdot \tag{2-19}$$

Secondary reactions can be initiated through the created radicals and main products include hydrogen and sulfur.

Radiation wavelength

As seen above, each precursor responds differently to different radiation wavelengths based on their absorption properties. In order to optimize the deposition and incorporation of functionalities in a coating, absorption of photons must be significant. Through judicious selection of a proper light source, the absorption of photons by the precursors can be maximized.

Ideally, in PICVD reaction pathways should be controllable through selective excitation However, an observed complication is the occurrence of uncontrolled secondary reactions, therefore reducing the asset of selective excitation. This limitation can be mitigated by using monochromatic light sources. Once a truly selective excitation is achieved, differences in photo-reactions and in the properties of the resulting organic coatings as a function of radiation wavelength can be obtained.[123] Selective excitation has not been studied in detail so far, mainly due to the lack of suitable light sources. With more suitable and readily available light sources, a truly controllable deposition technique could be achieved.

Photon flux and radiation intensity

The number of photons emitted by a source can be characterized by its flux, Φ, which is defined as the number of photons passing through a unit area per unit time and is related to the radiation intensity:[166]

$$\Phi = \frac{I}{E_p} = \frac{I \cdot \lambda}{h \cdot c} \tag{2-20}$$

Where I is the radiation intensity (W/m^2), E_p the photon energy (eV), λ (m) the peak wavelength of the lamp, h ($6.626 \cdot 10^{-34}$ m^2·kg/s) the Planck's constant, and c ($2.998 \cdot 10^8$ m/s) the speed of light in vacuum.

The photon flux represents an important process parameter in PICVD because it allows us to understand how many photons are actually interacting with the precursor gases and therefore how many active species can be generated to initiate deposition reactions. Generally, by increasing the intensity of a source (and therefore the number of photons) the rate of polymerization can be increased.[167] The more photons are present, the more active species can be created, leading to an increase in film-forming species and therefore deposition rate. Thus, the concentration of created radicals is proportional to the photon flux.[135] At very high fluxes, however, the reaction rate saturates due to very fast polymerization and the diffusion of the precursor(s) becomes the rate-limiting factor.[167]

From a technical point of view, the biggest disadvantage of PICVD, specifically when dealing with VUV radiation, is the absorption of air in this spectral region. All experiments must be performed under vacuum to avoid absorption of λ<190 nm through air and a good isolation during irradiation is unavoidable. Additionally, only specialized materials transparent to those wavelengths can be used during such experiments, as discussed in detail in section 2.4.3.

2.5 Stability of S-rich organic coatings

An important requirement of new created surfaces for (biomedical) applications is their stability in air, commonly referred as ageing, or in aqueous media. In general, (chemical) stability can be defined as a surface's ability to withstand changes when in contact with different environments (or chemicals). Possible post-treatment reactions when exposed to air include oxidation of dangling bonds or (unstable) functional groups, and reorganization of near-surface regions.[118, 168, 169]

The main factors affecting the stability of plasma- or photo-polymer-like coatings include:[9, 10]

- High reactivity of certain functional groups; this can change the desired functionality and affect the material's physico-chemical properties.
- Presence of free radicals, mainly tertiary carbon radicals, in the (cross-linked) organic coatings; those radicals represent reactive sites where oxygen incorporation can occur when the surface is exposed to air, as shown in the reactions below.

$$C\cdot + O_2 \rightarrow C - O - O\cdot \tag{2-21}$$

$$C - O - O\cdot + R - H \rightarrow C - O - OH + R\cdot \tag{2-22}$$

$$C - O - O\cdot + C - O - O\cdot \rightarrow C - O - O - C + O_2 \tag{2-23}$$

$$C-O-OH\ or\ C-O-O-C \tag{2-24}$$

$$\rightarrow Ketones, aldehydes, alcohols, esters$$

The reactivity of functional groups upon exposure to the atmosphere needs to be considered. Thiols are susceptible to oxidation by molecular oxygen and it is best to eliminate as much oxygen as possible in order to preserve the desired functionalities.[170] For the specific case of sulfur-rich films, drastic reduction in sulfur content (up to 75%) upon ageing in air has been reported in the past.[93] During plasma polymerization of sulfur-rich precursors, stable molecules are created in the plasma (i.e. H_2S, CS_2), which do not contribute to film growth but remain unbound and can be trapped in the polymer-like network. Upon exposure to atmosphere or in solution, the trapped sulfur molecules in the organic coatings are released, leading to a decrease in overall sulfur content.[72, 87, 92, 93, 171] Other than the release of stable sulfur-based molecules upon exposure to air, the ageing behavior of sulfur-rich films was found to be similar in process to oxidation of nitrogen-rich films, where oxidation of carbon-centered radicals dominates the reaction pathways. Interestingly, the extent of oxidation was found to be much smaller than with nitrogen-rich films.[86]

If the newly engineered surfaces are meant to be used for biomedical applications, their behavior in aqueous solutions is of specific importance. In this work, a coating was considered to be stable in aqueous solution, if a change in film thickness after immersion is <20 %. Three distinctive phenomena have been observed when plasma- and photo-polymer-like coatings are subjected to aqueous solutions, and their extent depends on the precursor(s) and process parameters employed to create them:

(i) Hydrolysis reactions,

(ii) Dissolution of non-covalently bonded, soluble, low molecular weight fractions (oligomers), observed as a decrease in thickness, and

(iii) Swelling, observed as an increase in thickness, dictated by the cross-link degree and chemical properties of the organic coatings.[9, 172]

For nitrogen- and oxygen-rich organic coatings it has been reported that the solubility of the coatings increases with initial concentration of functional groups. This can be explained by a higher concentration of polar groups and their strong affinity for polar solvents.[9, 83] Furthermore, Rupper et al.[173] reported low-density polymer-like films with increasing oxygen concentration due to a decreased mass deposition rate. Therefore, a balance between high density of functional groups and high stability of the films in aqueous media has to be found for each newly engineered surface.

A special note concerning the stability of photo-polymer-like coatings should be addressed. These coatings have shown to possess great physical and chemical stability due to a high cross-linking degree, originating from the photo-polymerization process. The high cross-linking degree caused through (V)UV irradiation has been already observed in early experiments during irradiation of (conventional) polymers and was explained to be caused through recombination reactions between the carbon-centered radicals and resulting bond scissions.[18, 174, 175] Due to this cross-linking near the surface, (V)UV treated samples are believed to have a higher resistance towards ageing than their low-pressure plasma counterparts.[18, 135, 168, 175]

Since the stability of plasma- and photo-polymer-like coatings plays such an important role for further applications, different strategies are currently applied to reduce ageing on those surfaces. A common strategy includes the enhancement of stability by increasing the cross-link density in the films. The higher the cross-link

density in the polymer-like coating the lower the probability of water molecules to enter into the polymer-like structure. However, this is mostly achieved at the expense of the degree of functionalization in the films, which might be relevant for applications.[9, 176] Alternatively, the formation of vertical gradient structures, consisting of a highly cross-linked base structure followed by the growth of a (highly-)functional, thin top-layer has shown promising results. This new architecture of polymer-like organic coatings allows to obtain a highly-functionalized, yet stable organic coating.[169, 177] Besides changes in the synthesis approach of the coatings, storage can also greatly help to reduce the ageing behavior of the polymer-like coatings. Storage at -20°C showed almost undistinguishable results from freshly prepared nitrogen-rich coatings.[178] A further approach to reduce the ageing of the samples prior to analysis, done throughout this work, is to build the experimental set up inside a nitrogen-filled glovebox. This system makes it possible to precisely study the native properties of the new-engineered films without considering the changes introduced through ageing.

2.6 Thin film growth

When designing new (biomaterial) thin films, it is important not only to consider the films' deposition kinetics and chemical composition, but also growth and topological features. These can affect the performance of the films because they determine the mechanical properties, stability, solubility, and interactions with bio-compounds.[179] The growth of thin films on planar surfaces depends on the interactions between adparticles and the underlying substrate. During plasma- or photo-polymerization, reactive species are generated in the gas phase and adhere to the surface forming adparticles. These adparticles can then stick to other adparticles forming islands or stick

to the underlying substrate forming a layer-by-layer film. Three basic growth modes are used to describe how thin films are formed (Figure 2-11):[180, 181]

1. Island growth (Volmer-Weber): small stable aggregates of adparticles stick to the substrate and grow in three dimensions to form islands. This is the case when homogeneous interaction forces between adparticles are stronger than heterogeneous interaction forces between the adparticles and the underlying substrate. These islands can continue to grow and coalesce on the surface, resulting in chemically homogeneous but roughened surfaces, which might become smooth after sufficient thickness is reached.
2. Layer-by-layer growth (Frank-van der Merwe): small stable clusters diffuse fast in two dimensions, resulting in the formation of a layer-by-layer film. In this growth mode heterogeneous interaction forces between the adparticles and the underlying substrate are stronger. The resulting layers are smooth and generally strongly adhered to the substrate.
3. Mixed growth (Stranski-Krastanov): combination of the two other modes. After forming one or more layers, subsequent layer growth becomes unfavorable and islands start to form.

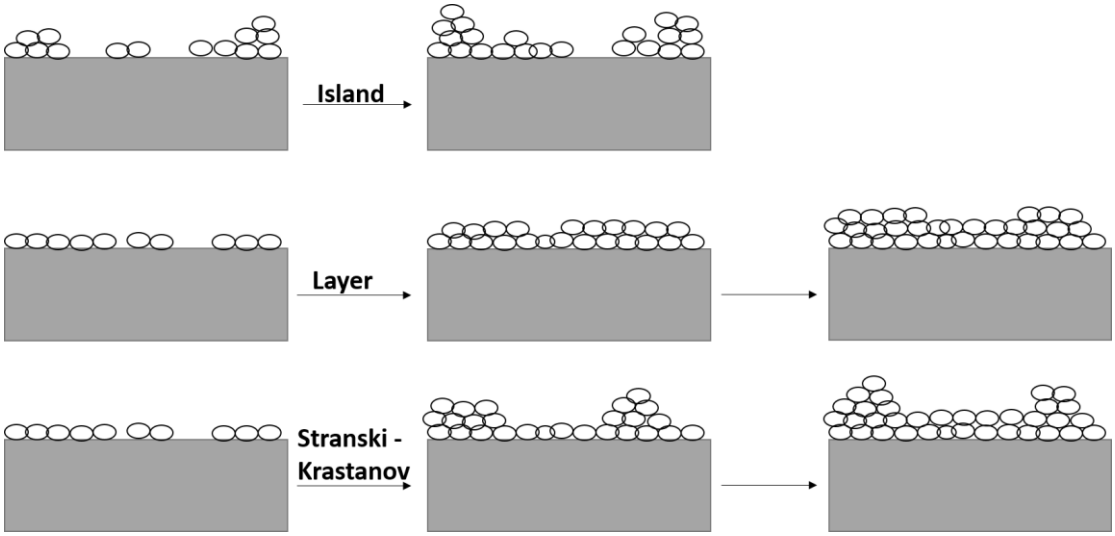

Figure 2-11: Basic modes of thin film growth. [180]

Different growth modes have been reported for nitrogen-rich plasma polymers, which are observed to be dependent on the precursor used. Michelmore et al. were able to show that, while films obtained from n-heptylamine showed Volmer-Weber growth, films from allylamine demonstrated smooth surface morphologies resembling the Frank-van der Merwe growth mechanism.[182] Sulfur-rich films obtained through plasma polymerization of thiophene demonstrated island-like growth for the first seconds of deposition, and continued to grow and coalesce with increasing deposition time.[183] While the growth kinetics of metal or oxide thin films are well-known, there are only few examples reporting the growth kinetics of polymer(-like) thin films. Their lack of information remains an issue leading to a restriction in the application of these films.

In summary, it became evident from the reviewed literature that even though there is an increasing interest in SH-terminated surfaces for different applications (i.e. biomedical), their fabrication is still in the early development stages. So far, these surfaces have been mostly obtained through wet-chemical approaches and there is a drive to continue finding simpler, faster, and more reliable methods to obtain high SH group concentrations on material surfaces. Plasma-based CVD methods are becoming more popular for the fabrication of sulfur-rich surfaces; however, such studies are still very limited and in no means comparable to the body of work existing for nitrogen- and oxygen-rich organic coatings. Moreover, such studies focused on the use of single-molecule precursors only. Based on the limited amount of studies found in the literature, the main objective of this research is to create stable SH-terminated surfaces, which can be of potential use for biomedical applications. We aim to expand the available studies on SH-terminates organic coatings by introducing the "co-

polymerization" of gas mixtures comprising a hydrocarbon backbone and hydrogen sulfide, acting as the functional gas. This method has shown to be advantageous in the possibility to fine-tune the properties of the obtained coatings compared to the traditional single-molecule precursor approach. Furthermore, photo-initiated CVD methods will also be examined. These methods have proven to be a good alternative to PECVD methods as their reactions have shown to be more selective and specific, creating nearly "mono-functional" organic coatings for the case of nitrogen- and oxygen-rich films. Nonetheless, such methods have not been studied for sulfur-rich films. Therefore, it is of major interest to study the fabrication of SH-terminated surfaces through such methods and to investigate the influence of different process parameters, especially the photon energy and system pressure, on the properties of the resulting organic coatings. As these surfaces might be of interest for biomedical applications, they have to be optimized in a sense that they have a high density of SH-groups and are simultaneously stable in air and aqueous solution.

Chapter 3 Experimental Methodology

In the following two sub-sections additional information, which is not provided in Chapter 4 to Chapter 6, on the experimental setups (PECVD and PICVD) is presented, followed by the determination of the photon flux as a function of distance of the VUV sources. In the following sections, surface characterization as well as plasma diagnostic techniques are presented.

3.1 Deposition of sulfur-rich coatings

3.1.1 PECVD experimental setup

Low-temperature plasmas can be created in an AC or DC discharge using different coupling methods (capacitive or inductive), frequencies (r.f. or m.w.), and electrode configurations. In an AC discharge, the excitation source is either a continuous wave or in a pulsed mode. In a typical capacitively coupled PECVD setup (Figure 3-1), the sample to be treated is placed on either the grounded or hot electrode within an enclosed vacuum chamber, while in an inductively coupled PECVD setup (Figure 5-1) the sample is placed on a sample holder close to the coil. In the case of the capacitively coupled reactor, the developed negative self-bias on the surface connected to an RF power supply can be significant and influences the processes happening at the surface (e.g. deposition). The negative self-bias on the surface is created as a result of different thermal velocities between electrons and ions. As a consequence, positive ions are accelerated towards the surface and can participate in deposition and/or etching processes. The influence of ions on the deposition of thin films is less pronounced in inductively coupled PECVD setups, usually yielding lower deposition rates. Before starting a deposition run, the vacuum chamber is evacuated to low base pressures,

followed by the introduction of the precursor(s) at desired flow rates. Using different valves, the working pressure is maintained constant during depositions.

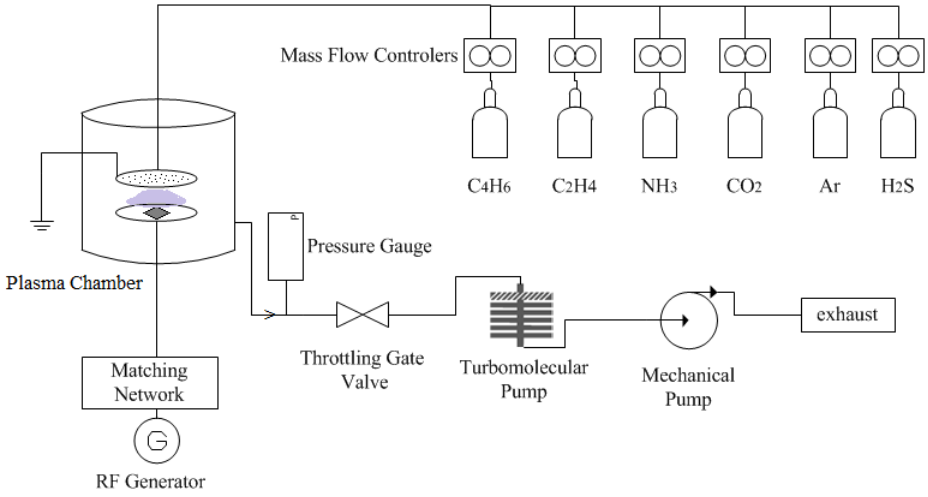

Figure 3-1: Schematic of a parallel plate, capacitively coupled system for PECVD treatment.

3.1.2 PICVD experimental setup

General considerations when designing a PICVD setup were discussed in section 2.4.3. The "home-made" experimental setup used in this research to obtain photo-polymer-like films consisted of a stainless steel "cross chamber" (Figure 6-2), in which the substrates can be mounted on a stainless-steel sample holder that can move axially within the treatment chamber. By varying the distance, *d*, between the sample and the VUV source, the photon flux, Φ, arriving at the substrate surface can be varied. Before starting a deposition run, the chamber is evacuated to low base pressures, followed by the introduction of the precursor(s) at desired flow rates. Using different valves, the working pressure is maintained constant during depositions. On account of the available VUV lamps' small MgF_2 windows and the substrate holder, photo-polymer-like films

can be deposited only on a small area (~1 cm^2) per deposition run. The different VUV sources used in this research are described in the next section.

3.2 VUV sources

Four VUV sources were used to deposit sulfur-rich polymer-like organic coatings. Three of these sources are non-coherent, commercially available lamps (Resonance Ltd., Barrie, ON, Canada), based on an electrodeless radio-frequency (r.f., 100 MHz)-powered discharge plasma. Depending on the wavelength of the VUV source, a noble gas, such as Krypton, Kr, or Xenon, Xe, is contained in a high-grade Pyrex ampoule sealed with a MgF_2 window (cut-off wavelength, λ=112 nm, Figure 3-2).[20, 119, 135, 184]

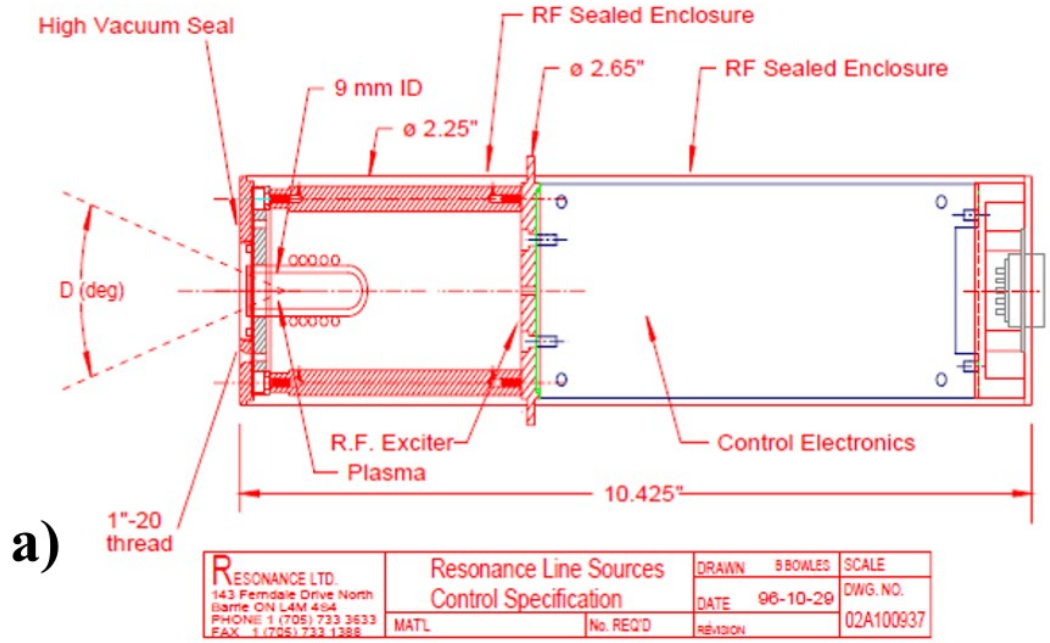

b)

Figure 3-2: a) Schematic illustration of a resonant VUV source; b) Photograph of the front of a resonant VUV source.

The discharge inside the source is initiated by an inductively coupled, power source (up to 5 W of r.f. power). All parts are enclosed within a sealed aluminum tube preventing r.f. leakage.[184] The lamps are directly incorporated into the VUV setup through an adaptor flange designed for the current setup.

Spectral intensity distributions, $I(\lambda)$, of the three VUV sources were obtained by Truica-Marasescu[184] through calibration using a VUV spectrophotometer. The results obtained at d=6 cm (Figure 6-3) show that the Kr resonant lamp (KrL, Figure 6-3a)) is nearly monochromatic, with 90% of its irradiance at λ=123.6 nm and about 10% at λ=116.5 nm. The Xe resonant lamp (XeL, Figure 6-3b)) is also observed to be nearly monochromatic, with a narrow emission line at λ=147 nm. The Xe_2^* excimer lamp (XeE, Figure 6-3c)) shows an emission line centred at λ=172 nm.

The fourth lamp used in this work is an ozone producing, short-wave, low-pressure, mercury (Hg) lamp (STER-L-RAY®, Hauppauge, NY, USA). This lamp is operated by a preheat start circuit that employs a relatively compact ballast. In order to integrate this lamp into the PICVD setup, it was mounted in front of a flanged fused silica window (Figure 3-3). The Hg lamp shows several emission lines, the most pronounced being at λ=253.7 nm. However, due to the absorption profiles of the precursors of interest (see section 2.4.4), the important emission line for the experiments presented in this research is at λ=184.9 nm, representing about 7% of the lamp's total output (Figure 6-3d)).

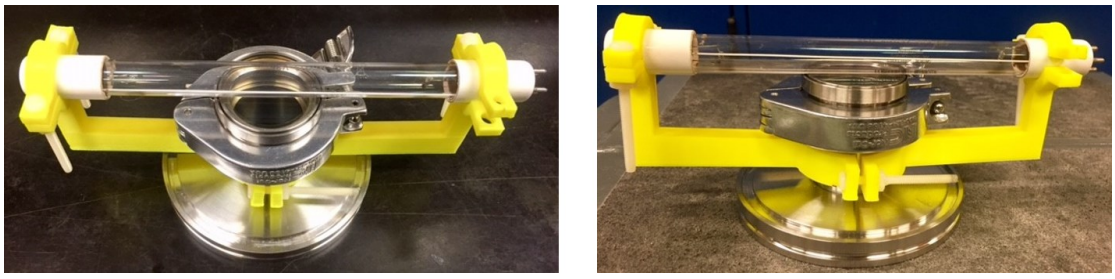

Figure 3-3: Photograph showing Hg source mounted on a flanged silica window.

3.2.1 Variation of photon flux, Φ, with frontal distance, *d*

The number of photons emitted by a source can be characterized by its flux, Φ, which is generally defined as the number of photons passing through a unit area per unit time.[166] The determination of Φ as a function of the distance, *d*, was of great importance to determine the decay of Φ for each source. To do so, the photocurrent, *i*, of each source at different *d*, using two different photodiodes, CsI and CsTe (NIST calibrated, Resonance Ltd., Barrie, ON, Canada) was measured; their response curves are shown in Figure 3-4.

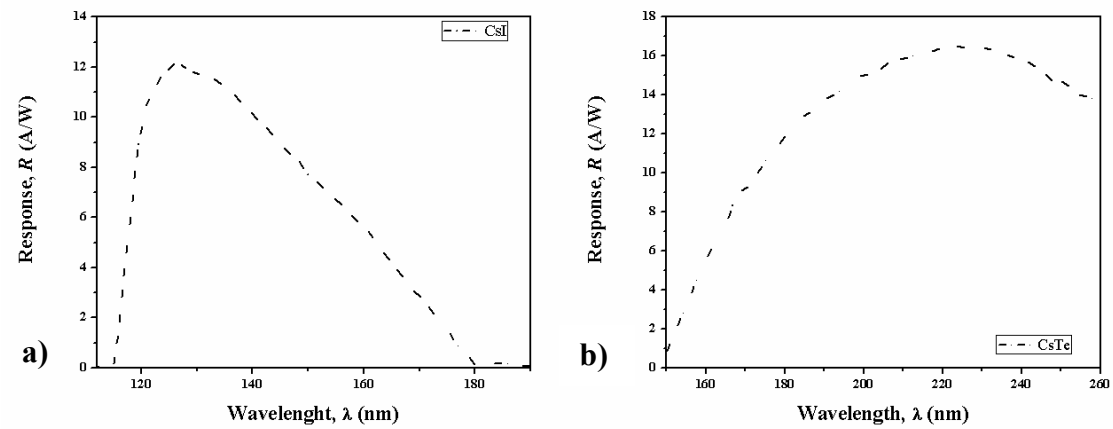

Figure 3-4: Spectral response, R, of the a) CsI and b) CsTe photodiodes. [185]

The photocurrent generated by the different VUV sources was measured under high vacuum in the PICVD experimental chamber by placing the respective photodiode at different *d* with respect to the source's window. Depending on the spectral response, the photocurrent, *i*, of the KrL and XeL sources was measured using the CsI photodiode, while the CsTe photodiode was used to measure *i* of the XeE and Hg sources. Using the measured photocurrent, the intensity, *I* (W/cm^2), of the VUV sources was calculated using following equation:

$$I = \frac{i}{R * S} \tag{3-1}$$

With the photocurrent, i (A), the photodiode's response, R (A/W), and the photodiode's active surface area, S (cm^2). By measuring i at different distances, I as a function of d could be obtained.

Since we are interested in knowing how many photons actually interact at the surface at a specific distance, the following equation was used to calculate Φ ($ph/cm^2/s$) from the previously obtained intensity:

$$\Phi = \frac{I}{E_p} = \frac{I \cdot \lambda}{h \cdot c} \tag{3-2}$$

Where E_p is the photon energy (eV), λ (m) is the peak wavelength of the lamp, h ($6.626 \cdot 10^{-34}\ m^2 \cdot kg/s$) is Planck's constant, and c ($2.998 \cdot 10^8$ m/s) is the speed of light in vacuum.

The obtained Φ as a function of d for the four different sources are plotted in Figure 3-5. The presented Φ values are the average of six measurements and the error bars represent the standard deviation of these measurements. The $\Phi=\Phi(d)$ curves were fitted with an allometric function $\Phi(d) = a \cdot d^b$; a and b are constants determined by the fitting procedure.

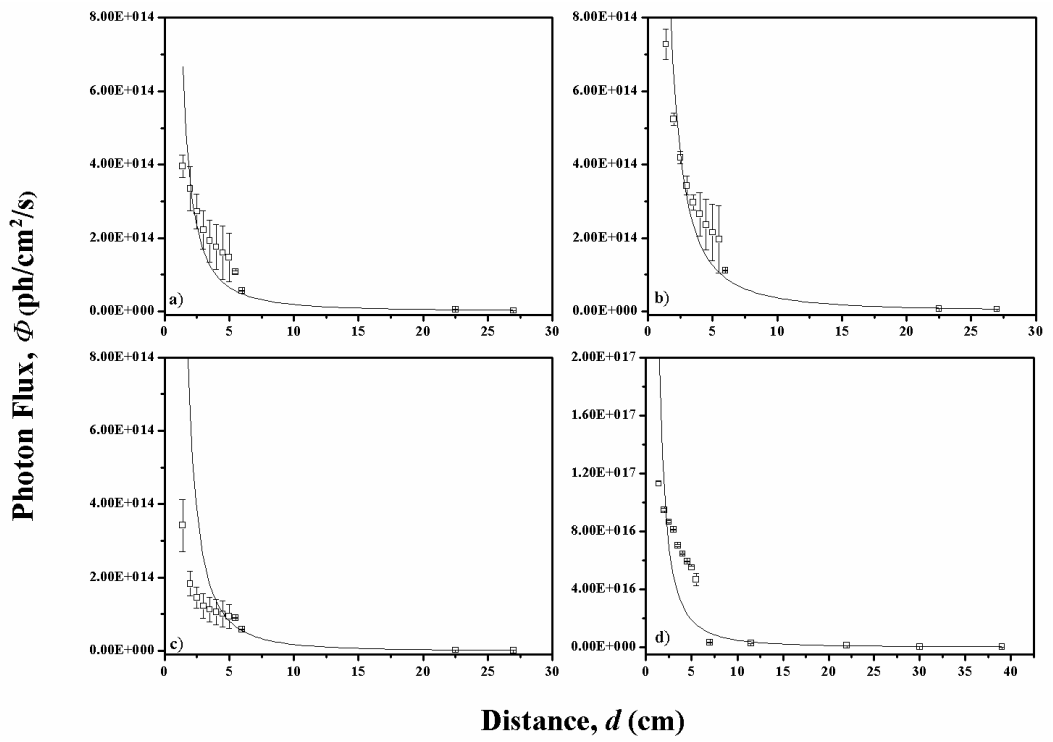

Figure 3-5: Photon flux, Φ, as a function of distance, d, for a) KrL; b) XeL; c) XeE and d) Hg lamps. The photon flux was calculated from the measured photocurrents, i, using two different photodiodes CsI and CsTe.

The empirically obtained photon flux decay functions for each lamp are summarized in Table 3-1.

Table 3-1: Φ(d) for different VUV sources. Functions were obtained from a fitting procedure.

Lamp	Empirical photon flux decay functions
KrL	$\Phi(d)=1.2\cdot10^{15}\cdot d^{-1.8}$
XeL	$\Phi(d)=2.2\cdot10^{15}\cdot d^{-1.8}$
XeE	$\Phi(d)=2.9\cdot10^{14}\cdot d^{-2.2}$

UVC	$\Phi(d)=3.9\cdot10^{17}\cdot d^{-1.9}$

It is well established that regardless of the type of source, its flux decreases with increasing distance travelled. However, the decrease in flux depends on the type of source and radiation.[166] Theoretically, if light is emitted from a non-coherent point source, the flux decreases with d from the source following an inverse square relationship:

$$\Phi \propto \frac{1}{d^2} \tag{3-3}$$

Where d is the distance between the point source and the receiver where the flux is calculated.

Truica-Marasescu[184] had already reported that the $\Phi \sim d^{-2}$ relationship quite closely applies to the "Resonance" lamps , even though these are far from being point sources. In the present work (Table 3-1), we also observe values of $b \approx -2$ and we can conclude that the photon flux of our sources, even of the Hg one, which deviates the most from being a point source, indeed decreases according to the theoretically predicted inverse square law.

3.3 Surface Characterization

The main techniques used to characterize the created sulfur-rich films in this work are briefly described in the following sections.

3.3.1 Profilometry

The estimation of film thickness is usually one of the first characterization methods used.[186] If a mask or a scratch down to the substrate is used during deposition to define a step to the film, thickness can be determined directly with a surface profiler, an easy and fast analytical tool for measuring thickness. This instrument drags a needle with a constant tracking force across the film and differences in height are converted in electric signals.[187] Disadvantages of this technique are that (1) very thin films cannot be measured (minimum thickness is around ~10 nm), (2) soft films can be destroyed if a high force is used, and (3) only surfaces with low roughness can be measured reliably.

3.3.2 X-Ray photoelectron spectroscopy (XPS)

X-ray photoelectron spectroscopy (XPS) is an analytical tool to study the chemical composition and state of ~10 nm depth of material surfaces. XPS is based on the photoelectric effect. The surface is irradiated with X-rays ($h\nu$) which interact with core-level electrons in the material and eject photoelectrons (Figure 3-6). The kinetic energy of the ejected photoelectrons, which is characteristic of each core-level/element combination, is measured by an electron analyzer and can be converted to electron binding energy:[101, 109]

$$E_B = h\nu - E_K - \phi \tag{3-4}$$

Where E_B is the binding energy, E_K is the measured kinetic energy of the photoelectron, $h\nu$ is the X-ray energy, and ϕ is the work function of the spectrometer.

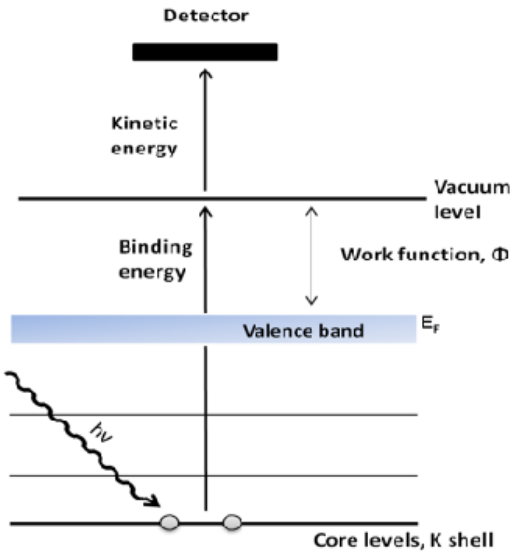

Figure 3-6: Basic principle of XPS measurements. [188]

Since photoemission peaks arise from different energy levels of different elements, the obtained data reveals the target chemical element and information regarding the quantity of this element. Small shifts in the binding energy values can additionally be used to determine chemical environment of the atoms in the sample, identifying functional groups. These shifts arise from changes in electronegativity of the bonded atom(s).

For the specific case of sulfur-rich films, especially for quantification of thiol groups on the surface, a main disadvantage of XPS has to be considered. Functional groups with similar electronegativities give rise to overlapping peaks, making the analysis of the spectra and assessment of the chemical environment challenging. In general, as pointed out by Siow et al., the high-resolution S2p peak can include three categories of components with different oxidation states:[22, 86]

1. Unoxidized sulfur-containing groups (S-H, S-C, S-S) at binding energies of 163-165 eV,

2. Oxidized sulfur-containing groups in low oxidation states (SO, SO_2) at binding energies of 165-167 eV, and
3. Oxidized sulfur-containing groups in high oxidation states (SO_3H, SO_3, SO_4) at binding energies 167-169 eV.

Specific functionalities within these three groups are difficult to distinguish and identify with certainty. This is also due to large discrepancies in the reported binding energy values recorded on numerous S-containing surfaces, as reviewed by Siow et al. (Figure 3-7).[87]

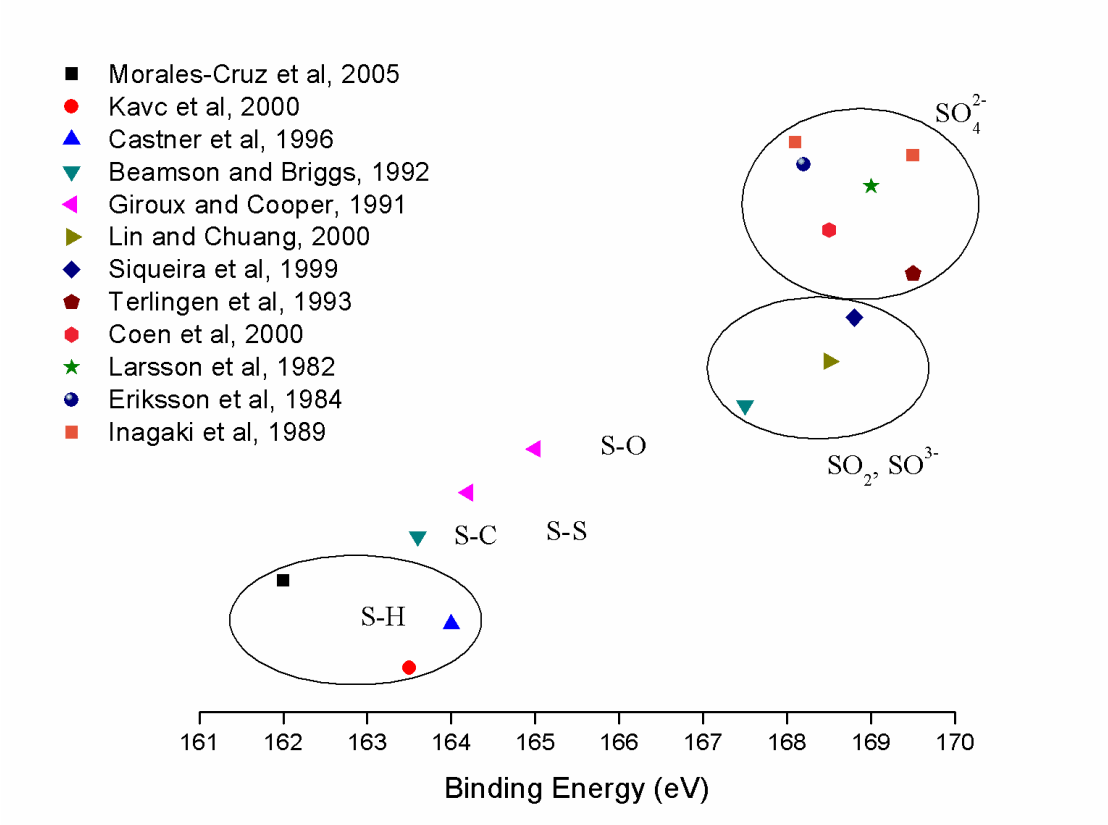

Figure 3-7: XPS S2p binding energies of various organo-sulfur compounds.[87]

The chemical shift of the C1s peak associated with different carbon-sulfur-based chemical functionalities (e.g. C-SH, C-S-C, C=S, C-S-S) is too low compared to the XPS resolution to allow for a truthful analysis.[94] In order to determine specific groups

with more certainty, derivatization reactions in combination with XPS measurements are commonly used.

3.3.3 Derivatization reaction with *N*-ethylmaleimide

Derivatization reactions consist of a chemical reaction between a functional group of interest and a labeling compound holding a specific function which can be easily detected by an analytical technique. This approach is already used for the quantification of several nitrogen- and oxygen-containing functional groups, such as primary amines ($C\text{-}NH_2$),[9, 178, 189, 190] carboxylic acids (C-COOH),[74] alcohols (C-OH),[189, 191] and ketones (C=O).[192]

Thiry et al. developed a derivatization technique to quantify thiol functionalities on surfaces, which involves the selective and quantitative reaction between *N*-ethylmaleimide (as labeling compound) and SH groups (as functional groups of interest).[94] *N*-ethylmaleimide reacts with SH groups on the surface via an addition reaction across the double bond to form a stable thioether bond and is an example of the earlier described thiol-ene click reaction (Figure 3-8).[170, 193, 194] Maleimide reactions are specific and selective for SH groups in the pH range 6.5-7.5. Even though the reaction between a thiol group and a maleimide moiety is known to be quantitative, Thiry et al. demonstrated that only a maximum thiol concentration of 40 % can be reached using this derivatization method due to steric effects of the *N*-ethylmaleimide molecule.

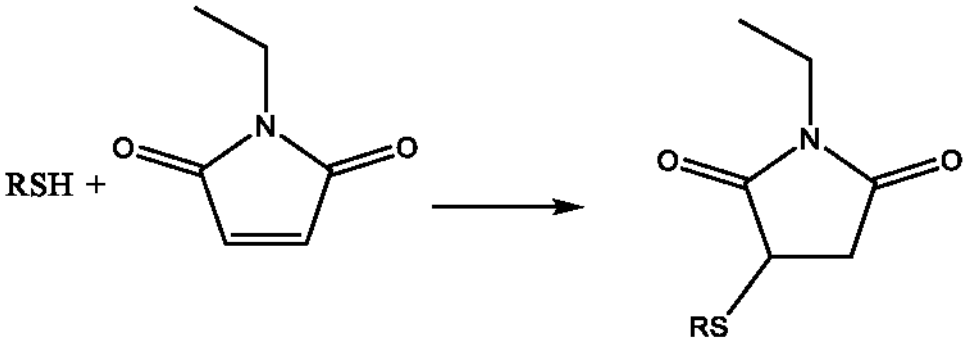

Figure 3-8: Derivatization reaction between a thiol group and N-ethylmaleimide.

Following the derivatization reaction, new elements (N, OCN, RCN) that can be detected by XPS are incorporated on the surface. Therefore, a successful derivatization reaction should reveal the presence of nitrogen and new carbon-based functionalities (C-N and O=C-N) in the XPS spectra. Assuming a selective reaction between *N*-ethylmaleimide and the available SH groups, the concentration of carbon bearing SH groups, [SH], can be calculated as follows:

$$[SH] = \frac{[N]}{[C] - 6[N]} \cdot 100\ (\%) \tag{3-5}$$

Where [N] and [C] represent the atomic nitrogen and carbon concentration measured by XPS. The term 6[N] is related to the amount of carbon introduced through the derivatization reaction.[94]

3.3.4 Infrared spectroscopy

Infrared (IR) spectroscopy is a further important experimental tool used to obtain the chemical composition of (rather thick) films. In attenuated total reflection infrared spectroscopy (ATR-IR) an optically dense crystal with a high refractive index is irradiated with IR light (typically between 1000 and 4000 cm^{-1}). The IR light enters the crystal at such an angle that total internal reflection occurs. This internal reflection

creates an evanescent wave, which probes a few micrometers beyond the crystal surface into the sample. The beam is reduced at frequencies corresponding to the vibrational modes of the sample structure.[195] IR spectroscopy is mainly used for qualitative and sometimes quantitative characterization. Quantitative characterization can be challenging since the bands of interest should have a high molar absorptivity and should not overlap with other bands. Ideally, a known band is used to create a calibration curve from which a quantitative analysis can be performed for other desired functionalities.[196] Since the depth of analysis of this technique is >1 μm, the polymer-like films need to be thick enough or the bulk rather than the surface properties of the films may be determined.[181, 197]

Compared to conventional polymers, the IR spectra of a plasma- and photo-polymer-like films generally become less resolved, show broader bands, and have some peaks that are significantly reduced in intensity.[103] The observed broader bands are caused by variable bond angles, characteristic of bond angle strain in a highly cross-linked polymer.[22] Unfortunately, the C-S-H stretching vibration gives rise to very weak absorptions in the IR spectrum, and the SH band (2600-2550 cm^{-1}) is considered to be useful for general characterization only.[198]

3.3.5 Atomic force microscopy (AFM)

Atomic force microscopy (AFM), a method belonging to the scanning probe microscopy family, is a high-resolution imaging technique capable of measuring topographical features to less than 1 nm in different media and atmospheres.[181] To image surfaces beyond the resolution of optical microscopy, a flexible cantilever with a sharp probe tip is scanned across the sample collecting information about the sample surface and its structure. Deflection of the cantilever is proportional to the forces acting

between the tip and the surface and is measured by reflecting a laser beam off the back of the cantilever onto a position sensitive photodiode. Resolution of this imaging technique is limited by the sharpness of the tip, which is usually less than 10 nm radius. [188, 199] AFM can be used to image topographical features on plasma- and photo-polymer-like surfaces, but also to follow their growth over time.

3.4 Plasma diagnostic techniques

Surface characterization techniques alone are usually not sufficient to completely understand the complex processes taking place during plasma- (or photo-) polymerization. Investigating the composition of the plasma (or photoactive gas) is necessary for identifying reactive species participating in the polymer-like formation. Insight can be gained by combining surface characterization techniques with those analyzing the chemical composition of a plasma (or photoactive gas) such as mass spectrometry (MS), optical emission spectroscopy (OES), as well as gas-phase Fourier Transform Infrared Spectroscopy (GFTIR). From the techniques mentioned above, only MS was used in the present work and will be discussed in the following section.

3.4.1 Mass spectrometry (MS) measurements to elucidate plasma polymerization processes

Mass spectrometry (MS) has emerged as a practical diagnostic technique for investigating plasma polymerization processes. Among many advantages, MS is able to measure ions, radicals, and stable (neutral) species from the plasma without showing limitations characteristic to optical techniques.[200]

In general, MS is an analytical technique used to detect gas-phase ions generated from a gas, liquid, or solid sample allowing to determine its composition. Depending on the analysis mode, MS enables the detection of neutral (residual gas analysis, RGA, mode) and charged (glow discharge mass spectrometry, GDMS, mode) species present in the gas phase. In RGA mode, ionization of neutral particles has to occur first. The most common approach to create ions is by heating up a filament generating an electron beam which results in ionization of the neutral species through electron impact leading to formation of cations. For both analysis modes, ions are transferred through an energy analyzer and separated according to their mass-to-charge (m/z) ratio. Once the ions have been separated, they are converted to a measurable signal using a secondary electron multiplier detector, following the conversion to a mass spectrum. Since the measurements are based on precise manipulation of ion trajectories by electric and magnetic fields, the collisions with other species must be avoided. Therefore, any mass spectrometer must be operated under high vacuum ($<5 \cdot 10^{-6}$ Torr) to ensure long mean free paths of the ions.[107, 115, 200]

A drawback of the RGA analysis mode comes with the required ionization process. As mentioned before, in order to analyze neutral species, ionization needs to take place, bringing those species to an excited state. Due to the high energies required, further fragmentation of the molecular ions can take place, resulting in additional peaks in the mass spectra. These additional peaks are not directly related to the species formed during plasma polymerization and can lead to misinterpretation of the obtained mass spectra.[107]

Chapter 4 Sulfur-rich Organic Films deposited by Plasma- and Vacuum-ultraviolet (VUV) Photo-polymerization

4.1 Preface

This chapter presents an article published in the journal of "*Plasma Processes and Polymers*". The complete citation of the published manuscript is:

> E. Kaparek, J. R. Tavares, M. R. Wertheimer and P.-L. Girard-Lauriault (2016), *Sulfur-rich Organic Films Deposited by Plasma- and Vacuum-ultraviolet (VUV) Photo-polymerization*, Plasma Processes and Polymers 13(9): 888.

The research was planned, analyzed and written by E. Kasparek (Ph.D. candidate). Dr. Girard-Lauriault, Dr. Tavares and Dr. Wertheimer were responsible for supervision and review of the work.

With interest in obtaining sulfur-rich materials, especially for biomedical applications, it became evident that new, simple, and fast methods need to be developed to obtain nearly "mono-functional", stable materials. In this article we report two different methods for creating sulfur-rich, thiol-terminated, organic coatings. The first method involves the use of a low-pressure plasma, while the second uses monochromatic radiation; a method that had not been used for the creation of any sulfur-rich organic coatings in the past. For the first time, SH-terminated organic coatings were obtained from binary gas mixtures of a hydrocarbon (either ethylene or butadiene) and hydrogen sulfide.

Sulfur-rich Organic Films deposited by Plasma- and Vacuum-ultraviolet (VUV) Photo-polymerization

Evelyne Kasparek[a], Jason R. Tavares[b], Michael R. Wertheimer[c], Pierre-Luc Girard-Lauriault[a]

[a]Plasma Processing Laboratory, Department of Chemical Engineering, McGill University, Montreal, QC H3A 2B2, Canada; [b]Photochemical Surface Engineering Laboratory, Department of Chemical Engineering, École Polytechnique de Montréal, Montréal, QC H3C 3A7, Canada; [c]Groupe des couches minces (GCM) and Department of Engineering Physics, École Polytechnique de Montréal, Montréal, QC H3C 3A7, Canada.

Abstract

Thiol (SH)-terminated surfaces have been progressively gaining interest over the past years as a consequence of their widespread potential applications. Here, SH-terminated thin films have been prepared by "co-polymerizing" gas mixtures comprising ethylene (C_2H_4) or butadiene (C_4H_6) with hydrogen sulfide (H_2S). This has been accomplished by either vacuum-ultraviolet (VUV) irradiation of the flowing gas mixtures with near-monochromatic radiation from a Kr lamp, or by low-pressure r.f. plasma-enhanced chemical vapor deposition (PECVD). Varying the gas mixture ratio, *R*, allows one to control the films' sulfur content as well as the thiol concentration [-SH]. The deposits were characterized by X-ray photoelectron spectroscopy (XPS), before and after chemical derivatization with *N*-ethylmaleimide, and by ATR FTIR. VUV- and plasma-prepared coatings were found to possess very similar structures and characteristics, showing chemically bonded sulfur concentrations, [S], up to 48 at. % and [-SH] up to 3%. All coatings remained essentially unchanged in thickness after immersion in water for 24 h.

4.2 Introduction

4.2.1 General introduction

Thiol (SH)-terminated surfaces have been gaining interest over the past years, to promote adhesion of gold layers[201-204] and nanoparticles,[205-208] and for immobilization of biomolecules like DNA,[71, 89, 209] carbohydrates,[88] and proteins.[40] In particular, protein immobilization can be accomplished by covalently attaching them to the surface through thiol-ene click chemistry. Such covalent attachment is important because it ensures homogeneous surface coverage and accessibility to the active site(s) of the protein;[39, 40, 210] it therefore appears superior to electrostatic attachment, the presumed surface interaction for amine (NH_2)-rich organic thin films.[9, 10, 119, 211]

So far, SH-terminated surfaces have been synthesized using wet-chemical approaches comprising several different steps,[39, 40] with different solvents and long reaction times. An alternative solvent-free, single-step process is low-pressure (LP) plasma deposition of thin coatings, something that has been accomplished using single volatile organic precursors with the desired functionality.[71, 91, 92, 94] Additionally, binary gas mixtures if SO_2 and hydrogen have recently shown to be able to create thiol containing surfaces,[87, 212, 213] but no complete characterization of these surfaces was performed. In this study, *binary* gas mixtures comprising a hydrocarbon, here ethylene (C_2H_4) or 1,3-butadiene (C_4H_6), and hydrogen sulfide (H_2S) are used to create SH-terminated surfaces. This approach of using feed-gas with controllable gas mixture ratios, *R*, has been demonstrated to be at least equal, if not superior,[9, 10, 20, 83, 119] to the single-molecule precursor for nitrogen-containing coatings (amongst others),[17-19,23-25] as *R* allows for increased versatility to achieve coatings with tailored properties. Although binary-mixture feeds have been already used by Yasuda[103] and more

recently by Hegemann and coworkers,[80, 81, 214, 215] neither they, nor any other group, have so far reported using H_2S as a co-reagent, to the best of our knowledge.

For a number of years, nitrogen (N)- [or better, amine (NH_2)]-rich polymer surfaces have been created using low-pressure plasma polymerization of C_2H_4-ammonia (NH_3) mixtures.[9, 77, 119] More recently, vacuum-ultraviolet (VUV, $\lambda \leq 200$ nm)-assisted photo-polymerization of such mixtures using quasi-monochromatic sources[20, 119] has also been demonstrated. In essence, VUV-assisted processing retains only one energy-source component of the plasma, the VUV photons, to carry out (photo-) chemistry, thus potentially allowing for better control of the overall process. Indeed, VUV-based deposits tend to possess higher amine concentrations, [-NH_2], likely due to more specific and selective reactions occurring via mono-energetic photons; "hot" electrons, the main originators of chemical reactions in low-pressure plasmas, necessarily possess a broad, Maxwell-Boltzmann-like energy distribution.[10, 78, 119] In addition, VUV radiation can more readily promote intermolecular cross-linking, leading to more stable films compared with their low-pressure plasma counterparts.[10]

The purpose of the present research is to compare S-containing organic thin films created by photo- and plasma-assisted polymerization of C_2H_4 or C_4H_6 with H_2S, and to gain insight into the reaction pathways that favor high thiol concentrations and coating stability. It is useful, however, to first present some introduction into the photochemistry of small molecules,[121] particularly those relating to the above-listed gaseous reagents.

4.2.2 VUV photolysis of C_2H_4, C_4H_6 and H_2S

In order to achieve appreciable sulfur (S) incorporation into the organic thin films, absorption of photons in the precursor gas mixtures (and thus, their photo-dissociation) must be significant. Absorption coefficients, *k*, should ideally be high at the VUV emission wavelength of the KrL lamp used here (see Section 4.3), λ_{Kr} = 123.6 nm. Figure 4-1 shows plots of *k* for the three precursor gases as a function of the wavelength, λ, as well as λ_{Kr}, where all three *k* values are seen to be very high, favoring bond scissions and formation of reactive radicals for film-forming reactions.

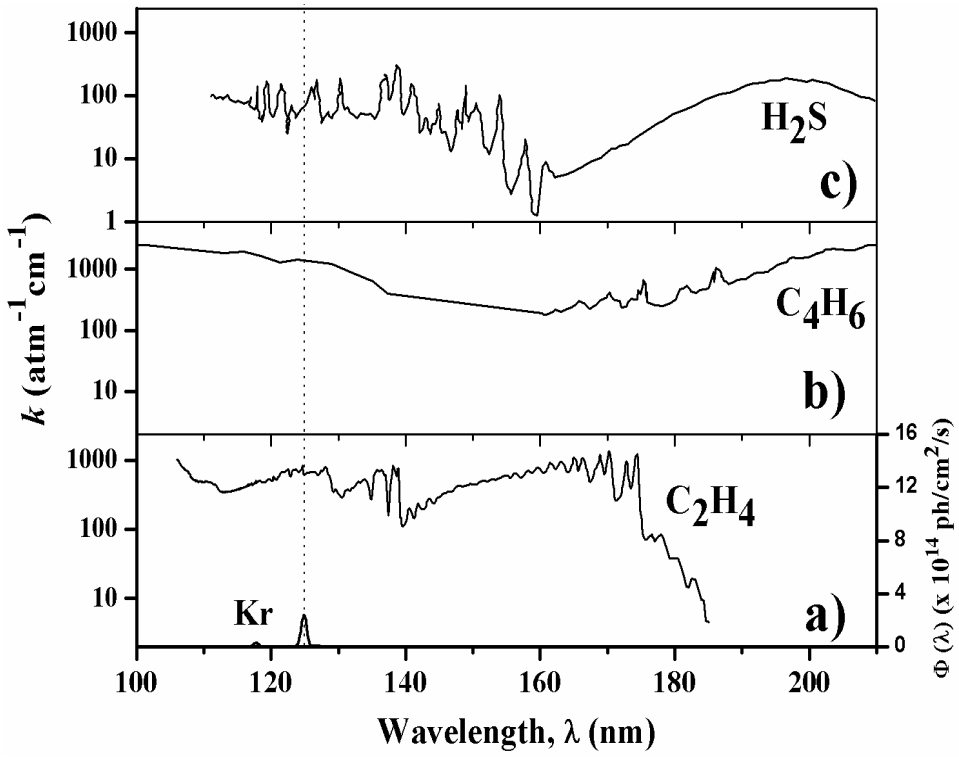

Figure 4-1: VUV absorption coefficients, k ($atm^{-1}cm^{-1}$, base e), of gaseous a) C_2H_4, [138, 139] b) C_4H_6 [149, 150] and c) H_2S [121]; the wavelength of the Kr (λ_{Kr}= 123.6 nm) resonant VUV lamp is also shown.

Two primary dissociative processes of similar importance have been reported for ethylene, C_2H_4, both leading to the formation of acetylene:[10, 77, 78, 119],[138]

$$C_2H_4 + h\nu \rightarrow C_2H_2 + H_2 \quad (4\text{-}1)$$

$$C_2H_4 + h\nu \rightarrow [C_2H_3^* + H] \rightarrow C_2H_2 + H_2 \quad (4\text{-}2)$$

Secondary reactions include those of H to form ethyl radicals, $C_2H_5\cdot$, and reaction of the latter to form higher species, such as C_4H_{10}, C_2H_4 and C_2H_6.

Photolytic reactions of butadiene, C_4H_6, include the formation of hydrogen, radicals and other unsaturated molecules. Additionally, low structural isomers of 1,3-butadiene can be formed, namely 1,2-butadiene, cyclobutadiene and bicyclobutadiene. Five primary reaction channels have been reported for the dissociation of 1,3-butadiene, including three radical (4-3 to 4-5) and two molecular (4-6 to 4-7) channels:[153]

$$C_4H_6 + h\nu \rightarrow C_3H_3\cdot + \cdot CH_3 \quad (4\text{-}3)$$

$$C_4H_6 + h\nu \rightarrow C_4H_5\cdot + \cdot H \quad (4\text{-}4)$$

$$C_4H_6 + h\nu \rightarrow C_2H_3\cdot + C_2H_3\cdot \quad (4\text{-}5)$$

$$C_4H_6 + h\nu \rightarrow C_2H_4 + C_2H_2 \quad (4\text{-}6)$$

$$C_4H_6 + h\nu \rightarrow C_4H_4 + H_2 \quad (4\text{-}7)$$

The primary photo-reaction of H_2S at short wavelengths ($\lambda < 317$ nm) is predominantly the production of hydrogen atoms and SH· radicals:[121]

$$H_2S + h\nu \rightarrow H\cdot + HS\cdot \tag{4-8}$$

Secondary reactions include:

$$H\cdot + H_2S \rightarrow H_2 + HS\cdot \tag{4-9}$$

$$2HS\cdot \rightarrow H_2S + S \tag{4-10}$$

$$2HS\cdot \rightarrow HS_2\cdot + H\cdot \tag{4-11}$$

$$2HS\cdot \rightarrow S_2 + H_2 \tag{4-12}$$

$$2HS\cdot \rightarrow H_2S_2 \tag{4-13}$$

Recombination of radicals from the photolysis of C_2H_4-H_2S or C_4H_6-H_2S mixtures then clearly leads to reaction pathways that form the polymer-like thin films.

4.3 Experimental Section

4.3.1 VUV photo-polymerization

The experimental set-ups shown in Figure 4-2 are housed in a glovebox (see photograph in Figure 4-2a), on account of the highly toxic nature of H_2S; the reactor used for VUV

photo-chemical experiments, shown in Figure 4-2c), is very similar to that of Truica-Marasescu et al.[20, 119, 127, 135, 168]

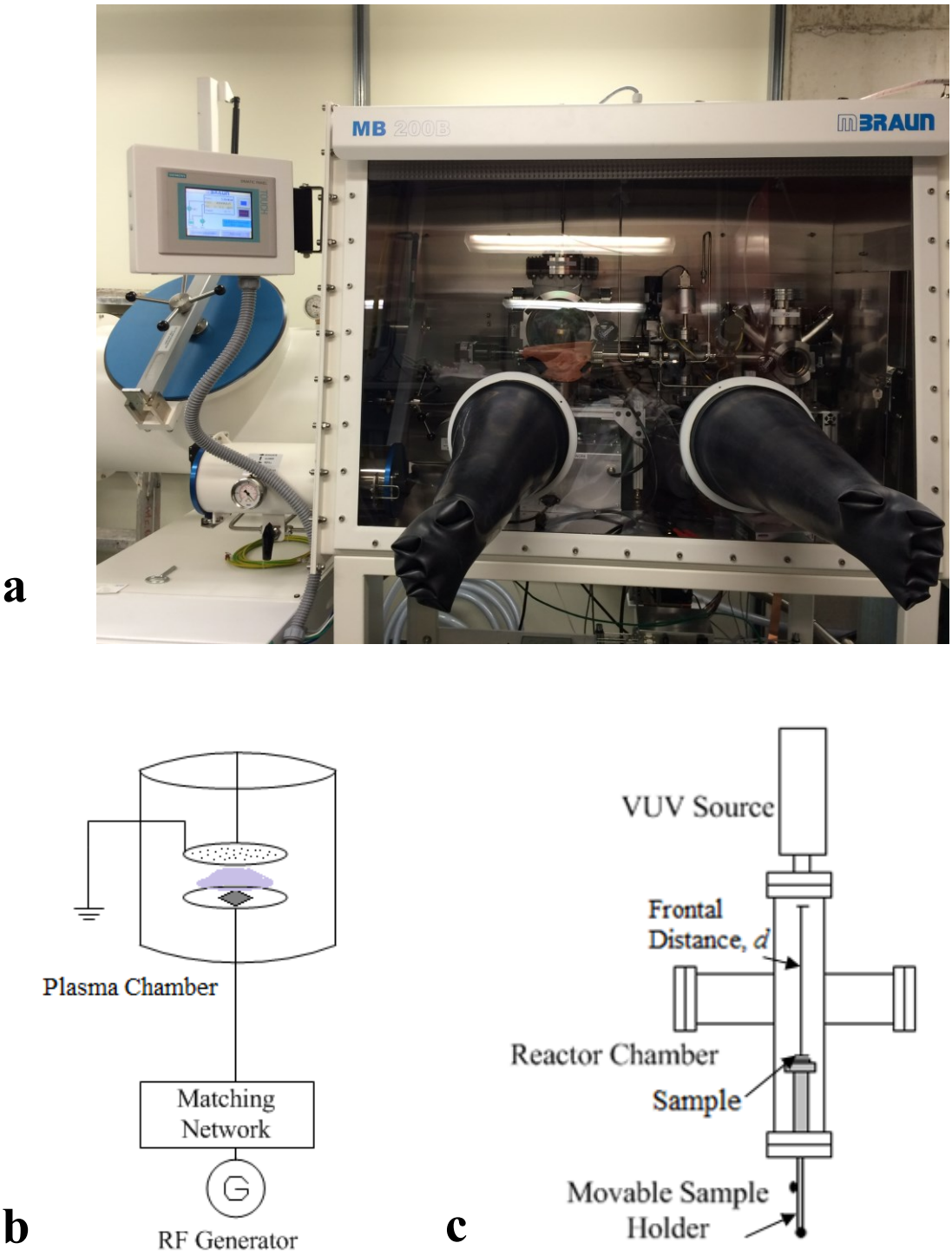

Figure 4-2: (a) Photograph showing the experimental setups inside a glovebox (top) and schematic views (bottom) of (b) the low-pressure r.f. reactor; and (c) the vacuum

ultra-violet (VUV) photo-chemical reactor, used for depositing sulfur-rich thin organic thin films, L-PPE:S, L-PPB:S and UV-PE:S, UV-PB:S, respectively.

Briefly, it consists of a stainless steel ‘‘cross’’ chamber, evacuated to high vacuum using a turbo-molecular pump supported by a two-stage rotary vane pump (base pressure $p = 10^{-5}$ Pa). As in previous experiments,[9, 10, 77, 78, 83, 119] the operating pressure during deposition was maintained near p = 13 Pa (100 mTorr). The flow rate of the high-purity hydrocarbon source gases C_2H_4 (99.999%, Megs Inc., Montreal, QC, Canada), F_{C2H4}, or C_4H_6 (99.8%, Megs Inc., Montreal), F_{C4H6}, was kept constant at 10 sccm using mass flow controllers (Brooks Instruments, Hatfield, PA), while the flow rate of H_2S (99.5%, Megs Inc., Montreal), F_{H2S}, was varied between 0 and 15 sccm, also using a mass flow controller; this yielded values of R (e.g. F_{H2S}/F_{C4H6}) ranging from 0 to 1.5. The polymer-like[216] coatings resulting from the photo-chemical reactions, henceforth designated ‘‘UV-PE:S’’ (for ‘‘ultraviolet- polymerized sulfurized ethylene’’) and “UV-PB:S” (for “ultraviolet- polymerized sulfurized butadiene”), were deposited on 500 μm-thick (100) p-type silicon wafers (University Wafer, Boston, MA, USA), or on glass slides with a thin (ca. 100 nm) Au coating, substrates being placed at a frontal distance, d, of 10 mm facing the VUV source. The exact value of d is important, because radiation intensity decreases as d^{-2}.[135] We used a non-coherent commercial VUV (“KrL”) lamp (Resonance Ltd., Barrie, ON, Canada), based on an electrodeless radio-frequency (r.f., 100 MHz)-powered discharge plasma in krypton (Kr) gas at low pressure: the Kr is contained in a Pyrex ampoule sealed with a MgF_2 window (cut-off wavelength, λ = 112 nm), as described in further detail elsewhere[20, 119, 135]; as already mentioned in the section on VUV photolysis, its (resonant) emission wavelength is λ_{Kr} = 123.6 nm (photon energy ca. 10 eV).

Finally, it is appropriate to mention that plasma and VUV effective power values at the substrate during deposition are of comparable magnitude, ca. 0.1 W cm^{-2}.

4.3.2 Plasma polymerization

For comparison, we have also used low-pressure r.f. plasma to deposit thin plasma polymer (PP) films with the same gas mixtures and the same *R* values, henceforth-designated ‘‘low-pressure plasma-polymerized, sulfurized ethylene’’, L-PPE:S, or “low-pressure plasma-polymerized, sulfurized butadiene”, L-PPB:S. Depositions were performed in a cylindrical stainless steel vacuum chamber (20 cm in diameter and 50 cm in height), with a disc-shaped powered electrode (10 cm in diameter) onto which substrates were placed (Figure 4-2b). A showerhead gas distributor and the metallic chamber walls served as the grounded electrode. L-PPE:S and L-PPB:S films were deposited under mild plasma conditions (r.f. power, P =20 W, resulting in a bias voltage of -40 V, gas pressure, p = 80 Pa = 600 mTorr).

4.3.3 Characterization studies

All deposits were characterized by X-ray photoelectron spectroscopy (XPS), performed in a ThermoScientific K-Alpha™ instrument (Waltham, MA, USA), using a monochromatic AlKα radiation source (hv = 1486.6 eV). The elemental composition (in atomic %, at. %) and the chemical environment of the elements in the deposits were obtained by XPS analyses (survey- and high-resolution, HR, spectra). Survey spectra were acquired at a pass energy of 160 eV, a dwell time of 200 ms and energy steps of 1 eV. HR spectra were acquired at a pass energy of 20 eV, a dwell time of 200 ms and energy steps of 0.1 eV. No evidence of X-ray induced damage was ever observed, based on observation of the C1s spectra before and after analyses. Spectra were acquired at

0° emission angles, normal to the sample surface; possible charging was corrected by referencing all peaks to the C1s peak at binding energy (BE) = 285.0 eV. The constituent elements were quantified from broad-scan spectra using 2.3.16 PR 1.6 Casa XPS software, by integrating the areas under relevant peaks after a Shirley-type background subtraction, and by using sensitivity factors from the Wagner table. C1s spectra were peak-fitted according to BEs of the different possible chemical bonds, before and after derivatization reactions (Table 4-1).

Table 4-1: Assignment of expected chemical bonds to binding energies (BE) of peaks labelled C1-C4 for sulfur-rich thin films (a) as-deposited, and after (b) derivatization with N-ethylmaleimide.

C1s peak assignments				
Peak label	**a) As-deposited**		**b) After derivatization**	
	Possible Chemical Bond	Peak BE (eV)	Possible Chemical Bond	Peak BE (eV)
C1	C-C, C-H	284.8±0.2[217]	C-C, C-H	284.8±0.2[217]
C2	C-S	285.3±0.2[217]	C-S	285.3±0.2[217]
C3			C-OR	286.5±0.2[217]
C4			N-C=O	288.1±0.2[217]

Fourier-transform infrared (FTIR) spectroscopy (Digilab FTS7000-UMA600 instrument, equipped with a mercury cadmium telluride (MCT) detector) in ATR mode was used for further chemical characterization.

4.3.4 Chemical derivatization with *N*-ethylmaleimide

To quantify thiol concentrations, [SH], we used the chemical derivatization reaction with *N*-ethylmaleimide (98%, BioShop Canada, Inc., Burlington, ON, Canada), as recently described by Thiry et al.[94] The reaction mechanism is shown in Scheme 4-1, wherein *N*-ethylmaleimide reacts selectively with SH-groups via a nucleophilic addition between the S atom and the double bond in the maleimide structure (thiol-ene click reaction), forming a stable thio-ether.

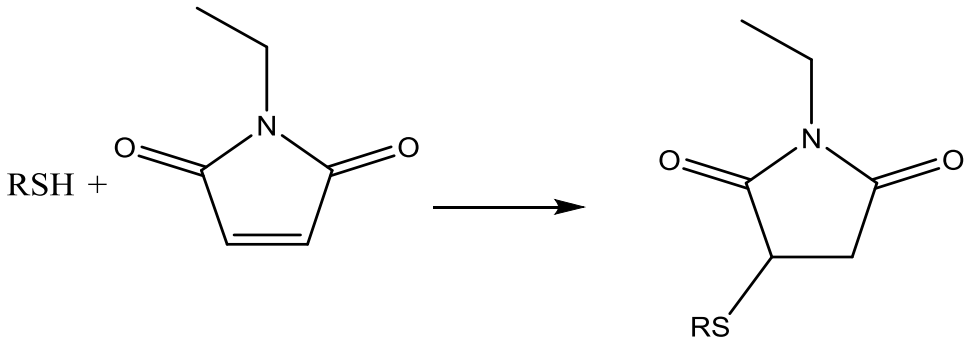

Scheme 4-1: Derivatization reaction between a thiol and N-ethylmaleimide.

In a typical experiment, the derivatization reaction was carried out in a phosphate buffer solution at pH = 7, where the *N*-ethylmaleimide concentration was fixed at 0.1 M. The samples were immersed in this solution for 40 h, following which they were rinsed in simple buffer solution for 5 min to eliminate any unreacted molecules, then dried under a flow of dry nitrogen.

XPS survey spectra were obtained before and after performing the derivatization reaction, allowing nitrogen, [N], and carbon, [C], concentrations to be quantified; the concentration of thiol groups, [SH], is then calculated as follows:

$$[SH] = \frac{[N]}{[C] - 6[N]} \times 100\ (\%) \tag{4-14}$$

4.3.5 Deposition rates

The deposition rates, r (in nm min^{-1}), were determined from the thickness, T, measurements as a function of the duration of deposition by evaluating the depth of a "scratch" produced by a sharp needle using a surface profilometer (Veeco Dektak^{3}ST-Surface Profile Measuring System, Plainview, NY, USA).

4.3.6 Stability studies

The stability against dissolution of all coatings was examined after immersion in Milli-Q water or toluene for 24 h. Profilometry was used to measure possible changes in film thickness, T, (before and after immersion on three different points, ΔT, in %) due to partial dissolution. The rationale for using these two solvents will be presented later in this text.

4.4 Results and Discussion

4.4.1 Deposition kinetics

Figure 4-3 shows plots of deposition rates, r (in nm/min) of the all coatings, as a function of the gas mixture ratio, R.

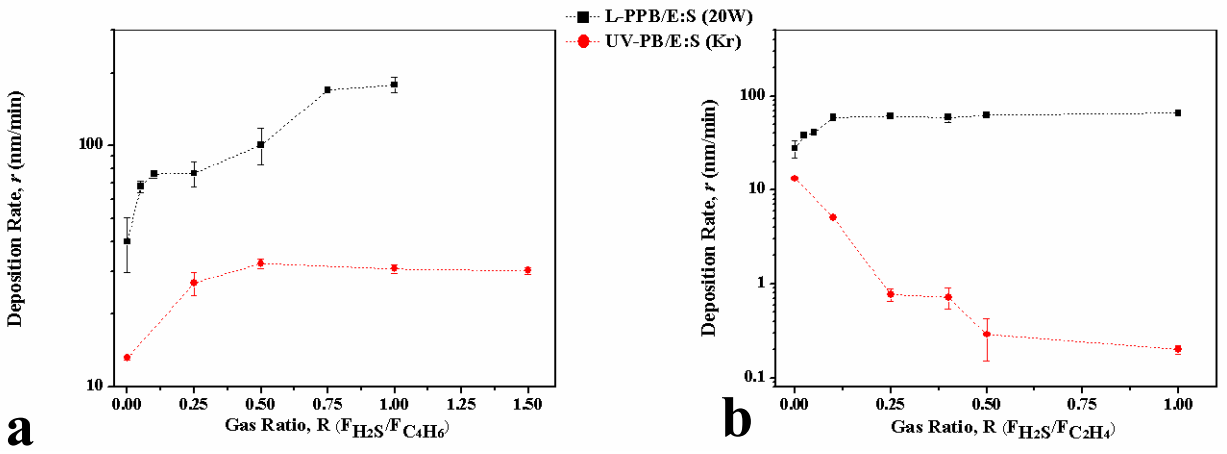

Figure 4-3: Deposition rates, r, of (a) L-PPB:S (squares, 20 W) and UV-PB:S (circles, KrL) and (b) L-PPE:S (squares, 20 W and, UV-PE:S (circles, KrL) as a function of gas mixture ratio, R. Error bars show standard deviation of three measurements. The lines are to guide the reader's eye.

The most striking features noted are as follows:

(i) When comparing photo- and plasma-polymerized films for both source gases, it can be observed that values of *r* for the VUV-deposited films are significantly lower than those from plasma polymerization. This may be due to higher efficiency of radical creation by plasma compared with VUV irradiation, as first pointed out by Truica et al.[119]

(ii) Comparing the two different source gases, it can be noted that butadiene-based *r* values are much higher than those with ethylene, likely due to *two* double bonds and twice as many C atoms in the former molecule. These features render the butadiene molecule more reactive than ethylene, which is also understandable when looking at Equation (4-3 – 4-7). A related finding occurred when acetylene, C_2H_2, was used as source gas.[83] In addition, when using C_4H_6, no drop in *r* was observed, even at higher *R* values; this is somewhat surprising, because *r* decreased substantially in

previous experiments with C_2H_4 and N- or O-containing gas mixtures.[10, 77, 78, 119] In those previous works it has been shown that NH_3, for example, acts as an etchant for organic materials, because with increasing *R* values atomic H is released during fragmentation, leading to a decrease in *r*.[83] Of course, the relative concentration of C_xH_y radicals decreases with rising *R* when *p* and F_{CxHy} are kept constant. Therefore, the decrease in *r* with increasing *R* when using C_2H_4, as observed in previous experiments, comes as no surprise.[20, 119] The near-constant *r* value when using H_2S (except for UV:PE:S films) shows that deposition (not etching) dominates, even at higher *R*.

4.4.2 Compositions of deposited films

Figure 4-4 shows surface-near sulfur concentrations, [S], from broad-scan XPS, as a function of *R*, for the four different types of coatings.

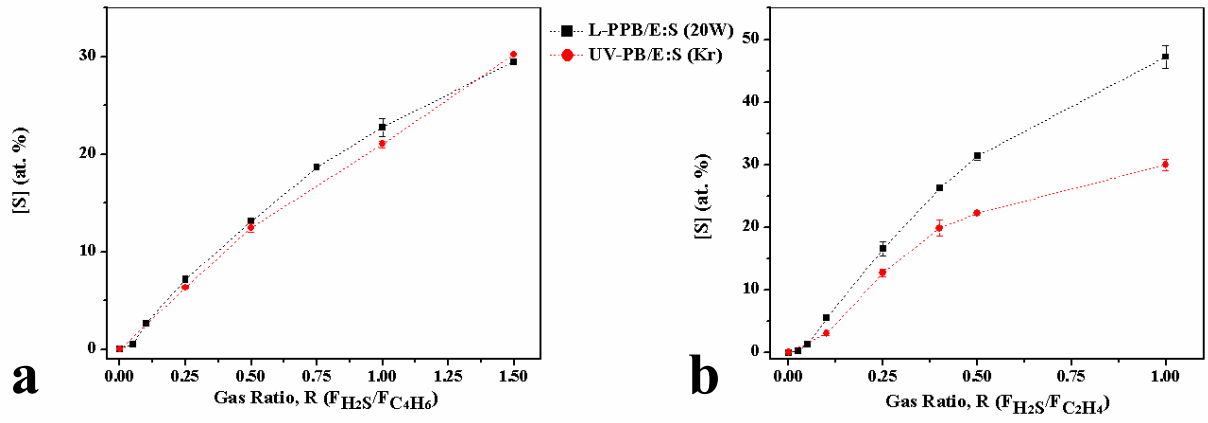

Figure 4-4: Surface-near sulfur concentrations, [S] (in at.- %), as measured by XPS of (a) L-PPB:S (squares, 20 W) and UV-PB:S (circles, KrL) and (b) L-PPE:S (squares, 20 W) and UV-PE:S (circles, KrL) as a function of gas mixture ratio, R. The lines are to guide the reader's eye.

[S] is seen to increase monotonically with rising *R*; for the case of C_4H_6 (Figure 4-4a), no apparent distinction can be made between the photo- and plasma-polymerized films, and [S] values up to 30 at.% could be obtained. The similarity between the photo- and plasma-polymerized films had previously been observed for N-containing films based on C_2H_4.[119] In contrast, here, when using the latter hydrocarbon, PP films yield higher [S] values, up to 48 at.% (Figure 4-4b). Similar results were also reported for O-containing films,[78] a clear indication that the plasma- and VUV-based chemistries are quite different and complex. Further, surface oxygen concentrations were always below 5 at.% (results not shown), which could be an indication that these films are more stable toward aging compared to nitrogen containing films.

Figure 4-5 presents [SH] values obtained from derivatization experiments, as a function of *R* for the four different types of films. While the evolution of [S] as a function of *R* (Figure 4-4) is very similar between the photo- and plasma-polymerized films, this is not the case for [SH].

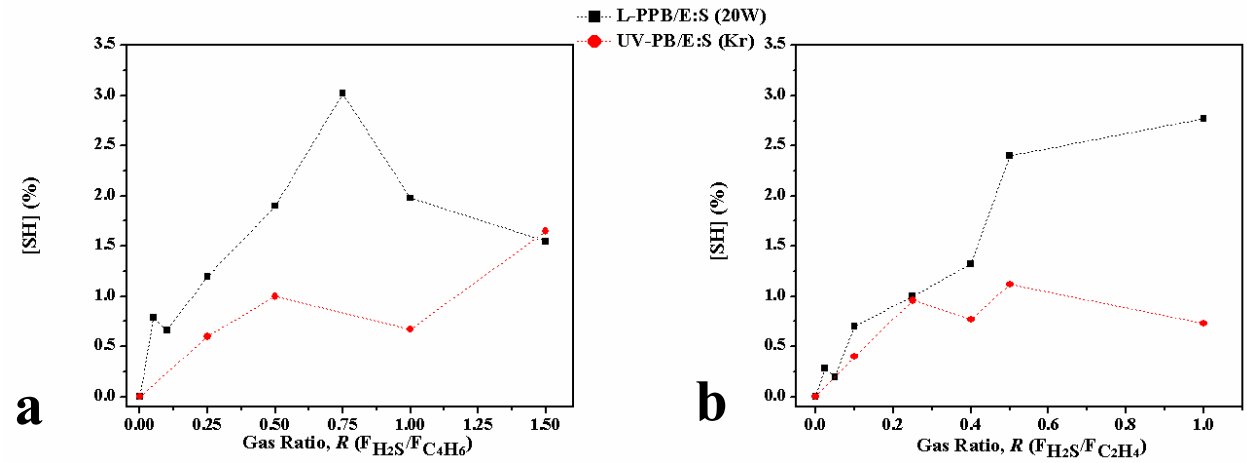

Figure 4-5: Thiol concentrations, [SH] (in %), determined using chemical derivatization XPS: (a) L-PPB:S (squares, 20 W) and UV-PB:S (circles, KrL) and (b) L-PPE:S (squares, 20 W) and UV-PE:S (circles, KrL) as a function of gas mixture ratio, R. The lines are to guide the reader's eye.

Contrary to expectations and to results for N-containing films,[10, 119] L-PPB/E:S coatings are seen to be richer in thiols (up to 3%) than their UV-PB/E:S counterparts (only 1.6 %). This is surprising since the retention of functional groups is believed to be limited in plasma polymerization due to heterogeneous reactions of gas phase species competing at the growing surface. The reason of this opposed result is under current investigation. For comparison, Thiry et al.[94] reported [SH] values up to 5 %, using the SH-containing precursor molecule, propanethiol.

4.4.3 Infrared spectra

Figure 4-6 shows selected ATR FTIR reflection spectra of L-PPB:S (Figure 4-6a) and UV-PB:S (Figure 4-6b) films at two different *R* values, *R* = 0 and *R* = 1.

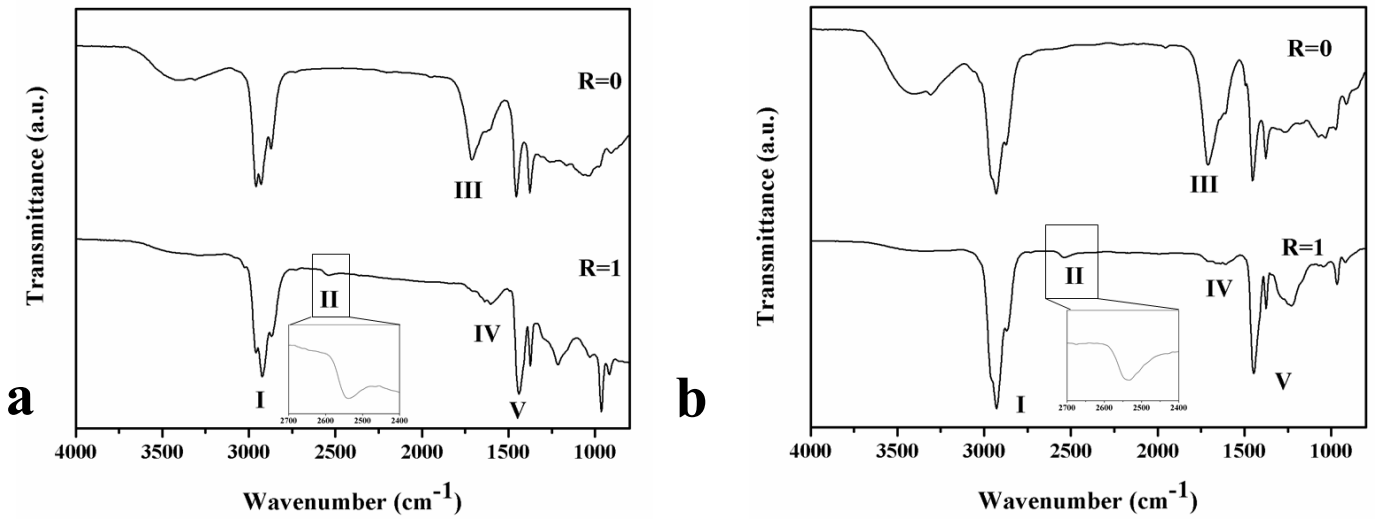

Figure 4-6: ATR FTIR spectra of (a) L-PPB:S and (b) UV-PB :S films. Comparison between L:PPB:S (20W) and UV-PB:S (KrL) deposited with R values (R= 0 and R=1, [S]~22 at. %). See Table 4-2 for assignments of bands "I", "II", "III", "IV" and "V".

Peak assignments in the principal absorption regions, labeled "I - V", are listed in Table 4-2.

Table 4-2: Infrared peak assignments of sulfur-containing thin films.[218]

Bands	Peak (cm^{-1})	Peak assignment
I	2969-2965	Antisymmetric CH_3 stretch
	2929-2912	Antisymmetric CH_2 stretch
	2884-2883	Symmetric CH_3 stretch
	2861-2849	Symmetric CH_2 stretch
II	2590-2560	SH stretch
III	1725-1700	C=O stretch
IV	1648-1638	C=C stretch
V	1473-1443	CH_3, CH_2 deformations
	1466-1465	CH_3 deformation
	1385-1368	CH_3 symmetric deformation

Unfortunately, C-S and C-S-H stretching vibrations tend to give rise to very weak absorptions in the infrared spectrum,[198] but the thiol S-H band can be considered to be of use for general characterization. Therefore, most noteworthy is the appearance of band "II" for $R = 1$, assigned to SH stretch vibrations (shown amplified in Figure 4-6 insets). This reconfirms the presence of S bound in the form of thiol groups, as also identified via *N*-ethylmaleimide derivatization. The bands appearing in region "V"

(around 1300 cm^{-1}) could also arise from sulfur-oxy compounds. Since the sulfur containing films were found to have very little (if any) oxygen, this region can be rather attributed to CHx deformation as stated in Table 4-2.

Additionally, we note structural differences between the plasma- and VUV films, as also confirmed XPS data in the next sub-section.

4.4.4 High-resolution (HR-) XPS spectra

HR-XPS can help one to assess the nature of chemical bonding in the different films, before and after chemical derivatization. Possible bond types and their corresponding binding energies are shown in part (a) of Table 4-1. Typical C1s HR-XPS spectra for different films at R = 0.5 reveals two components: (i) aliphatic C-C and C-H bonds (C1); and (ii) carbon-sulfur bonds (C2) (Figure 4-7). For all films, the sub-peaks were placed and fixed at binding energy positions relative to the C1s peak, following a procedure described by Girard-Lauriault et al.[178] To obtain the best overall fits, the Gaussian-Lorentzian product peak shape parameter was set at 30. Different types of S-bonding do not result in appreciable chemical shifts in the S2p HR-XPS spectrum, as the 2p electron of S in C-S, S-S and S-H bonds has a similar binding energy.[219-221]

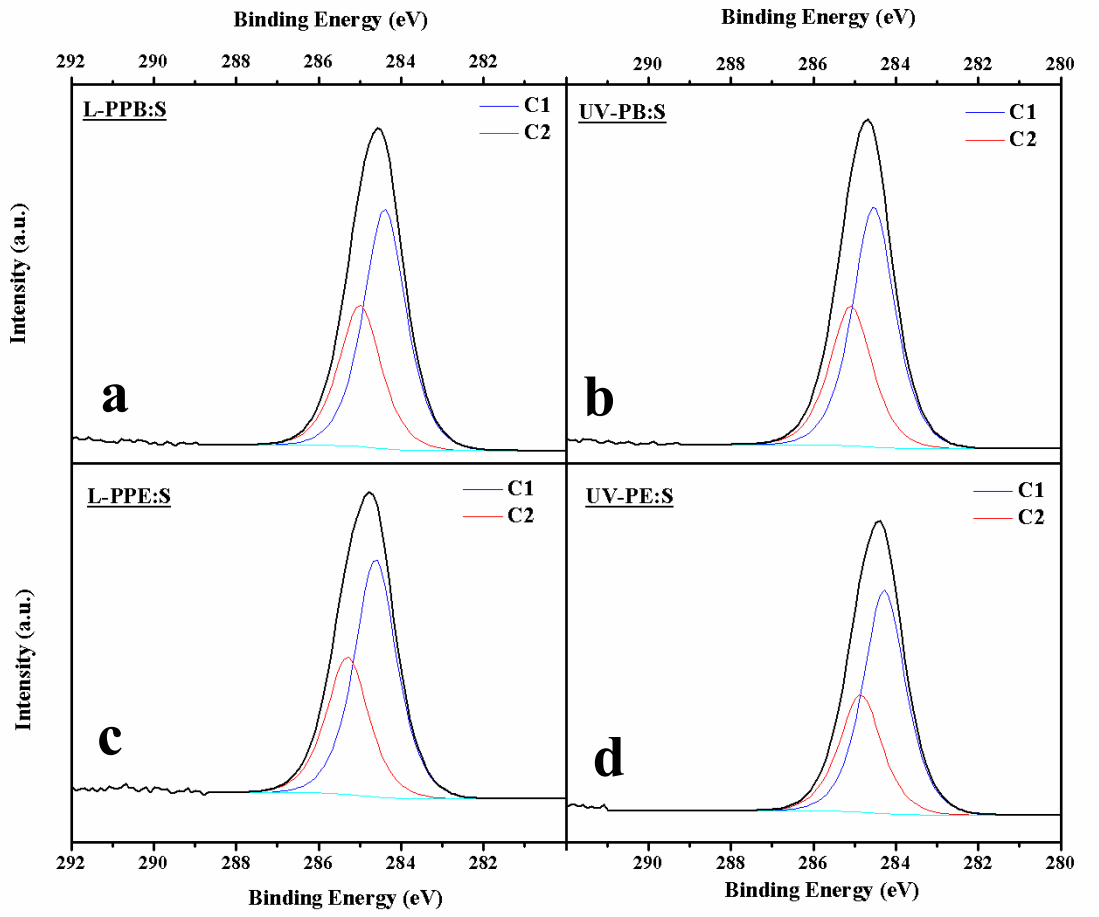

Figure 4-7: Typical high-resolution C1s XPS spectra of sulfur-containing deposits (R=0.5): (a) L-PPB:S, (b) UV-PB:S, (c) L-PPE:S, (d) UV-PE:S fitted with two component-peaks (FWHM 1.2 eV, peak shape GL(30)).

In Figure 4-8, relative C1s peak fit component areas (in %) in four different films are shown plotted versus *R*.

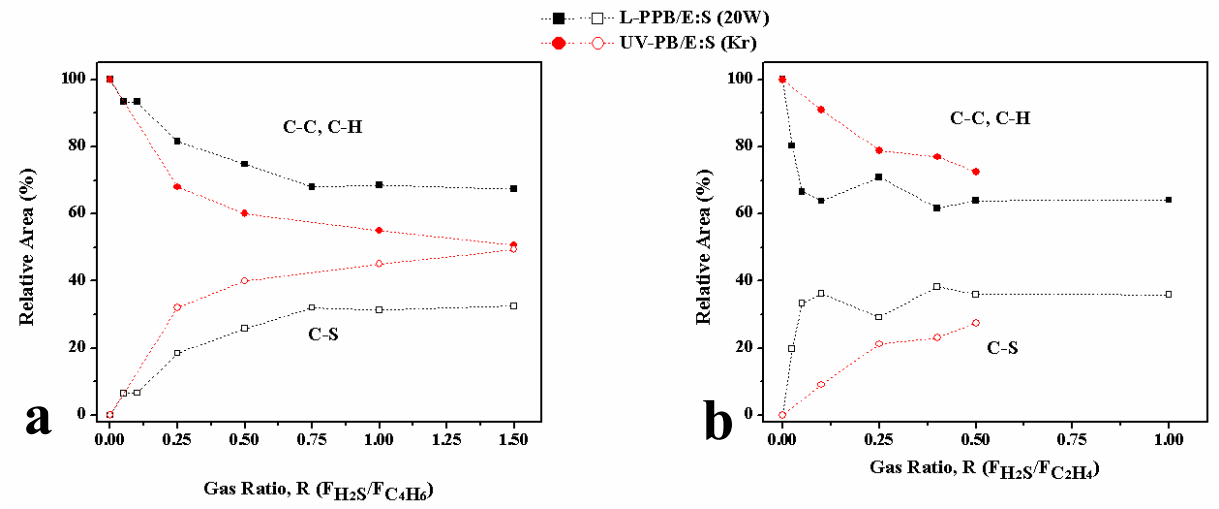

Figure 4-8: Evolution of HR-XPS C1s peak fit components for (a) L-PPB:S (squares, 20 W) and UV-PB:S (circles, KrL) and (b) L-PPE:S (squares, 20 W) and UV-PE:S (circles, KrL) deposits as a function of gas mixture ratio, R. The lines are to guide the reader's eye.

As before, the plasma- and VUV data for the C_4H_6- and C_2H_4-based films show similar behavior. Figure 4-8a is consistent with the XPS survey spectra, in that C-S peak intensity increases monotonically with rising *R*. Figure 4-8b, although less straightforward to interpret (especially for the plasma C_2H_4-based films), also shows an increase of the C-S peak intensity with rising *R*. The C1s peaks offer very few distinguishing features making it difficult to obtain information from these peaks. Therefore, the peak fitting procedure is very sensitive to noise in the signal.

Assignments of likely chemical bonds after derivatization with *N*-ethylmaleimide are shown in part (b) of Table 4-1, while typical high-resolution C1s spectra are presented in Figure 4-9.

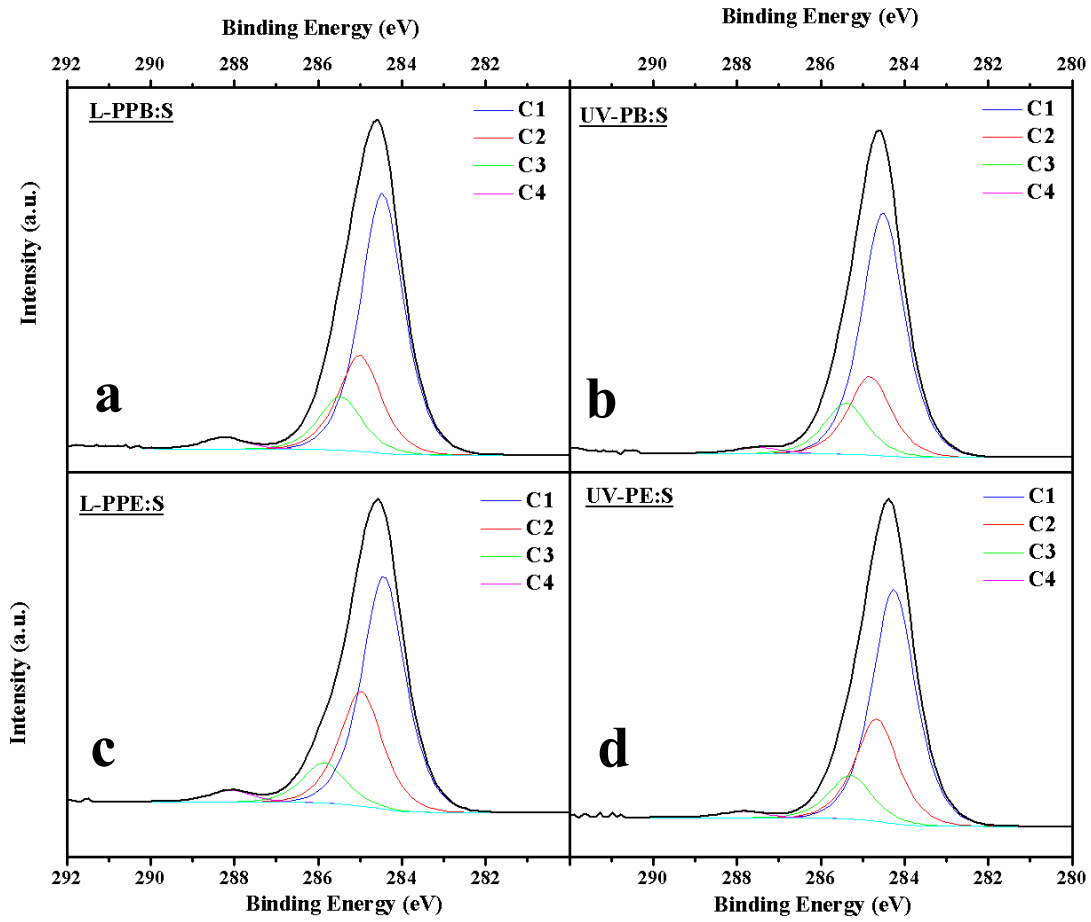

Figure 4-9: High-resolution C1s XPS spectra of sulfur-containing deposits (R=0.5) after derivatization with N-ethylmaleimide: (a) L-PPB:S, (b) UV-PB:S, (c) L-PPE:S, (d) UV-PE:S fitted with four component-peaks (FWHM 1.2 eV, peak shape GL(30)).

Unlike those in Figure 4-7, these now show additional components (C3 and C4, attributed to C-OR and C-N=O) corresponding to new functionalities after derivatization (see Scheme 4-1).

4.4.5 Physico-chemical stability in water and toluene

The stability of plasma- and VUV-deposited coatings in aqueous media is of crucial importance if they are to be used in biomedical applications. Indeed, the stability of NH_2-containing coatings has been extensively discussed, and it was pointed out that

primary amines in those films oxidize to form other functional groups, such as amides, in the presence of water and atmospheric oxygen.[9, 10, 78] Moreover, high concentrations of bonded heteroatoms (N and/or O) increase the solubility of coatings in polar solvents (e.g. water). This is attributed to the presence of highly soluble, low molecular weight fractions formed during the deposition process, which are extractable in polar solvents.[172, 222] In this context, it was also reported that VUV films tend to be less soluble than their plasma counterparts of comparable compositions, due to a higher cross-link density in the former that result from the photo-polymerization process.[9]

All C_4H_6-based coatings (plasma- and VUV alike) showed limited solubility in Milli-Q water, for $0 \leq R \leq 1.5$, although data did show some scatter, and in one case ($R = 0.5$) a 20% loss in thickness (ΔT). A possible explanation of the high stability of these coatings might be a particularly high cross-link density resulting from the molecule's two double bonds. This seems to be supported by the slightly higher observed solubility of the C_2H_4-based (plasma- and VUV-) coatings, although the latter also manifested no clear solubility increase with rising R ($0 \leq R \leq 1.0$).

Immersion in toluene should in principle remove all elemental sulfur that might be present.[223-225] Considering that S bound in the form of thiol groups, [SH], accounts for at most 3% of [S] (see Figure 4-4 and Figure 4-5), other S-based functionalities (or possibly even elemental sulfur) must certainly be present. Regrettably, these cannot be identified on the basis of (inexistent) chemical shifts in high-resolution XPS spectra (see Figure 4-7).

In Figure 4-10, changes in thickness, ΔT, are plotted versus R ($R \leq 0.6$) for both C_4H_6- (a) and C_2H_4-based (b) coatings.

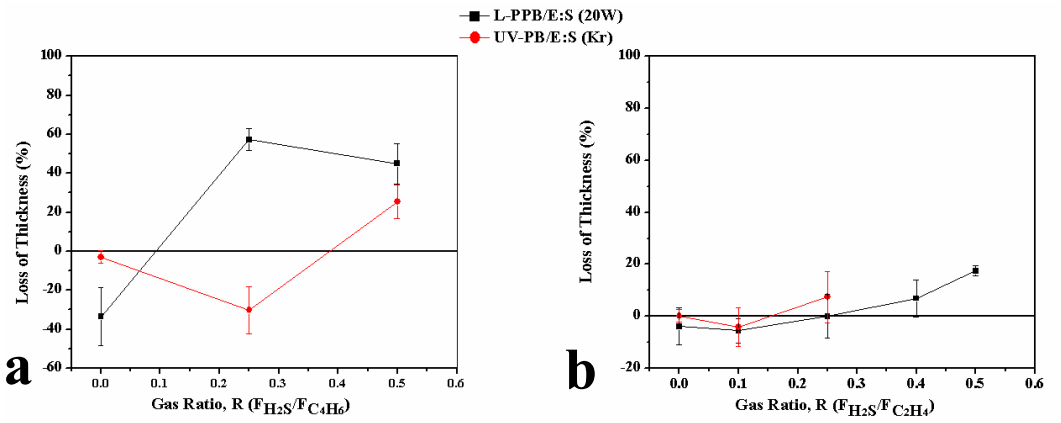

Figure 4-10: Stability in toluene of as deposited L-PPB(E):S (squares, 20 W) and UV-PB(E):S (circles, KrL) films deposited using H_2S-C_4H_6(C_2H_4) mixtures. Loss of thickness, ΔT, (in %) of: (a) L-PPB:S (squares, 20 W) and UV-PB:S (circles, KrL) and (b) L-PPE:S (squares, 20 W) and UV-PE:S (circles, KrL) as a function of gas mixture ratio, R, after immersion in toluene for 24 h. Error bars show standard deviation of three measurements.

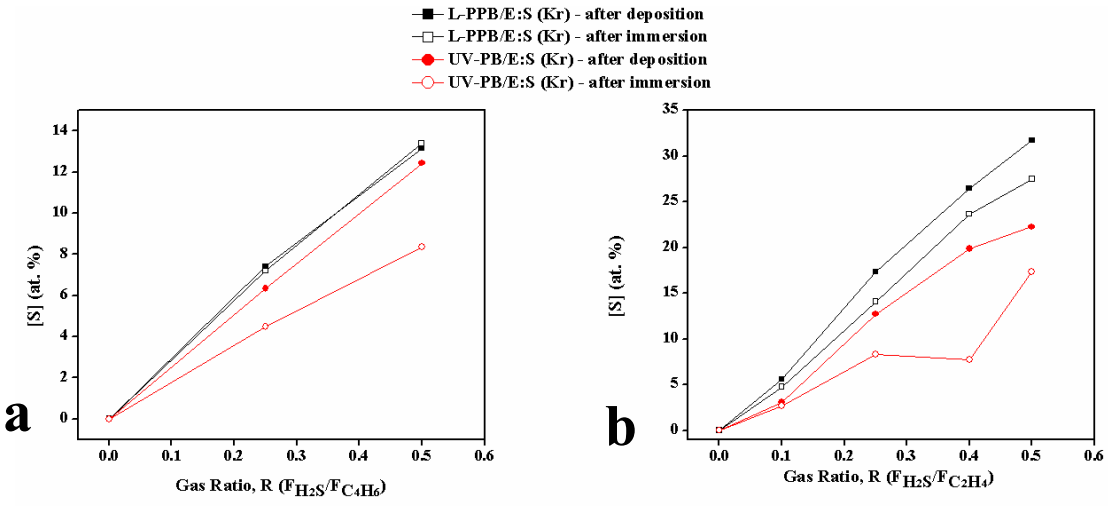

Figure 4-11: Sulfur surface concentrations, [S] (XPS, in at. %), before (full symbols) and after (open symbols) immersion in toluene of (a) L-PPB:S (squares, 20 W) and UV-PB:S (circles, KrL) and (b) L-PPE:S (squares, 20 W) and UV-PE:S (circles, KrL) as a function of gas mixture ratio, R, after immersion in toluene for 24 h. The lines are to guide the reader's eye.

Only relatively few data points have been taken, and ΔT manifests possible ambiguities (*negative* values, suggesting swelling, i.e. *gain* of T, as opposed to loss via dissolution). Comparing (a) and (b), the highest ΔT values, ca. 60% and 20%, are respectively noted for L-PPB:S ($R > 0.2$) and L-PPE:S ($R = 0.5$), while their VUV counterparts display significantly lower ΔT values, that is, greater stability in toluene. Indeed, the C_2H_4-based coatings appear to perform better.

In Figure 4-11, changes in [S] are plotted versus R ($R \leq 0.6$) for both C_4H_6- (a) and C_2H_4-based (b) coatings.

The following may be noted: over the whole range of R values investigated, PP films systematically showed smaller reductions than their VUV counterparts. While there was virtually no change for L-PPB:S, UV-PB/E:S films displayed a change in [S] ~ - 10% at the higher R values. Compared with the ΔT data discussed above, this outcome is difficult to explain, particularly for the case of L-PPB:S (highest ΔT but lowest change in [S]).

4.5 General Discussion and Conclusions

While single-molecule precursors that incorporate the desired functionality have been used to create amine-, hydroxyl- and/or carboxyl-, and thiol-rich plasma-polymer films, the "co-polymerization" approach we present here for SH-containing films is unprecedented; it improves control over experimental outcome, and it can maximize the concentration of the desired functional group. We have demonstrated, to our knowledge for the first time, the possibility to create SH-terminated surfaces by co-polymerizing mixtures of a hydrocarbon (here C_4H_6 or C_2H_4) and H_2S by both vacuum-ultraviolet photo-initiated CVD and low-pressure r.f PECVD.

In Figure 4-3 we noted that the deposition rates, *r*, of UV-PB/E:S and L-PPB/E:S coatings as a function of the gas mixture ratio, *R*, are quite different, the latter (plasma) method yielding higher *r* values. Such systematic differences were not apparent in regard to sulfur concentration, [S] (Figure 4-4), where we noted a monotonic increase with rising *R,* $2 \leq [S] \leq 48$ at. %. Furthermore, no significant distinction between photo- and plasma-polymerized films could be observed, beside that noted in Figure 4-5: the plasma-based coatings are seen to be richer in [SH] groups, up to ca. 3%. This result is somewhat surprising, considering that photo-polymerized coatings from C_2H_4-NH_3 mixtures presented in the literature proved to be highly amine (NH_2)-rich, with [NH_2]/[N] selectivity values exceeding 75%. Clearly, this does not apply in the case of C_2H_4 / H_2S or C_4H_6 / H_2S mixtures.

The different types of coatings were all found to be quite stable after 24 h of immersion in Milli-Q water, a key criterion for biomedical applications. Contrary to earlier reports for N- or O-rich coatings, we did not observe an increase in solubility with rising *R* values, nor significant differences between the photo- and plasma-polymerized coatings. Further stability tests conducted in toluene demonstrated that the sulfur in the films not in thiol form is likely of organic nature (Figure 4-10). Since the surfaces mainly showed non-oxidized sulfur, it is very difficult to identify different types of S-bonding through HR-XPS, because chemical shifts in the S2p HR-XPS spectrum are not significant.

Butadiene-based coatings show great stability over a wide range of *R* values, confirming our hypothesis for using butadiene as a hydrocarbon source gas: its higher unsaturated structure compared with C_2H_4 presumably leads to more active species in the plasma, thereby increasing the cross-link density in the resulting coatings.

In general, when comparing UV-PB/E:S and L-PPB/E:S coatings, all have proven to possess similar attributes, namely a high sulfur concentration, [S], and stability in water. The main differences occur in [-SH] values, the plasma-polymerized films being superior. Understanding this rather surprising result is of great interest, and it is the objective of ongoing further studies.

Acknowledgments

The authors gratefully acknowledge financial support from McGill University, from the *Fonds de recherche du Québec en nature et technologies* (FRQNT), and *Plasma-Québec*; from the Natural Sciences and Engineering Research Council of Canada (NSERC), and the Canadian Foundation for Innovation (CFI).

Chapter 5 Growth Mechanisms of Sulfur-rich Plasma Polymers: Binary Gas Mixtures versus Single Precursor

5.1 Preface

This chapter presents an article published in the journal of "*Plasma Processes and Polymers*". The complete citation of the published manuscript is:

> E. Kaparek, D. Thiry, J. R. Tavares, M. R. Wertheimer, R. Snyders and P.-L. Girard-Lauriault (2018), *Growth mechanisms of sulfur-rich plasma polymers: Binary gas mixtrues versus single precursor*, Plasma Processes and Polymers, 1800036.

The experimental part of this research was performed at the Materia Nova Research Center in Mons, Belgium. The research was planned, analyzed and written by E. Kasparek (Ph.D. candidate). Dr. Thiry was responsible for training and supervision, and review of the work at the foreign institution. Dr. Girard-Lauriault, Dr. Tavares, Dr. Snyders, and Dr. Wertheimer were responsible for review of the work.

In Chapter 4 we demonstrated that it is possible to synthesize stable SH-terminated films from binary gas mixtures comprising a hydrocarbon and hydrogen sulfide. The previous study also showed that the growth mechanisms of these films are not easy to predict and, contrary to our expectations, films obtained from a low-pressure r.f. plasma were richer in SH groups than ones obtained via photo-polymerization. In this article, we improved the understanding of the growth mechanisms of sulfur-rich plasma polymers. In addition, we compared our approach of using binary gas mixtures with the more conventional single-molecule precursor approach. With this study we broaden the library of hydrocarbon gases that can be used to obtain SH-terminated films.

Growth Mechanisms of Sulfur-rich Plasma Polymers: Binary Gas Mixtures versus Single Precursor

Evelyne Kasparek[a], Damien Thiry[b], Jason R. Tavares[c], Michael R. Wertheimer[d], Rony Snyders[b,e], Pierre-Luc Girard-Lauriault[a]

[a]Plasma Processing Laboratory, Department of Chemical Engineering, McGill University, Montreal, QC H3A 2B2, Canada; [b]Chimie des Interactions Plasma-Surfaces (ChIPS), CIRMAP, Université de Mons, Mons, 7000, Belgium ; [c]Photochemical Surface Engineering Laboratory, Department of Chemical, Engineering, École Polytechnique de Montréal, Montréal, QC H3C 3A7, Canada; [d]Groupe des couches minces (GCM) and Department of Engineering Physics, École Polytechnique de Montréal, Montréal, QC H3C 3A7, Canada; [e]Materia Nova Research Center, Parc Initialis, Mons, 7000, Belgium.

Abstract

Thiol (SH)-terminated surfaces have gained interest over the past years due to their potential applications, especially in the biomedical field. In this work, SH-terminated films have been prepared by "co-polymerizing" gas mixtures of acetylene (C_2H_2) and hydrogen sulfide (H_2S) using low-pressure r.f. plasma-enhanced chemical vapor deposition. R.f. power greatly influences the deposition rate, sulfur content, [S], and thiol concentration, [SH], of the films, as confirmed by XPS (both before and after chemical derivatization), FTIR, and mass spectrometry measurements. These data are compared with those obtained in a similar discharge by using a single molecule precursor, propanethiol. Among other differences, it is demonstrated that [SH] is higher when using binary gas mixtures compared to the single molecule precursor.

5.2 Introduction

The development of thiol (SH)-functionalized surfaces is of great interest in surface modification and functionalization due to their increasing fields of applications, ranging from biomedicine to optics.[40, 71, 88, 201, 226-228] The presence of SH groups on surfaces allows for further functionalization via reaction with electron-rich-enes, alkynes, electron-deficient-enes, epoxies and halogens, generating a "chemical toolbox" that offers a large variety of functional moieties for rapid manipulation of surface properties.[228, 229] Especially in the biomedical field, SH-terminated surfaces can be used for thiol-based coupling reactions, where a series of (bio) molecules (e.g. biotin, DNA, proteins) are attached to the surfaces with retention of their biological activities.[230, 231] Synthesis of surfaces supporting -SH groups through direct polymerization of monomers featuring these groups poses real challenges, since the thiol moiety is not tolerated in radical polymerization.[232] Therefore, SH-terminated surfaces have been synthesized using complex, multi-step wet-chemical approaches, often involving multiple different (toxic) solvents and long reaction times.[39, 40, 228]

In this context, low-pressure (LP) plasma deposition of plasma polymer films (PPFs) offers an alternative solvent-free, single-step, low reaction time and environmental friendly process to synthesize SH-terminated surfaces. The properties of the resulting PPFs depend on different plasma process parameters such as absorbed power, P, pressure, p, precursor flow rate(s), F, mixture ratio, R, and precursor type. Two approaches are generally used to incorporate a desired functionality into PPFs, namely the use of (i) single molecule precursors, in which the desired functionality is already present; or (ii) binary gas mixtures comprising a hydrocarbon and a sulfur-based functional gas. In the specific case of –SH containing surfaces, allylmercaptan (AM)[71, 88, 89] and more recently propanethiol (Pr)[72, 91-94, 226] are two examples of single

molecule precursors that have been used. On the other hand, we have previously reported the use of binary gas mixtures of butadiene (C_4H_6) or ethylene (C_2H_4) and hydrogen sulfide (H_2S) to create SH-terminated PPF surfaces.[233] While the single molecule approach allows for direct incorporation of the functionalities into PPFs, the use of binary mixtures has been demonstrated to be at least equal, if not superior, in terms of functional group density and stability[9, 10, 20, 77, 83, 106, 119] (e.g. for the case of nitrogen (N)-containing coatings). The controllable gas mixture ratio, *R*, allows for increased versatility to achieve coatings with tailored properties. In our previous study,[233] we were able to grow PPFs with adjustable surface-near sulfur concentrations, [S], ranging from 2 to 48 at.%, presenting thiol concentrations, [SH], up to 3%; these films exhibited high stability in aqueous solution, making them ideal candidates for further use in biomedical applications. Nevertheless, despite their promising properties, only few studies have so far been dedicated to the full characterization and understanding of the growth of SH-terminated PPFs. In addition, all those works focused on single monomer discharge plasmas. Thiry et al. reported a complete study, combining plasma diagnostics and PPF synthesis, regarding the influence of different plasma parameters on the chemical properties of propanethiol plasma polymers (Pr-PPF) deposited in r.f. discharges.[72, 91-93] These same authors also developed a derivatization method allowing specific identification of SH groups and their concentrations, [SH].[94]

Given this background, the main purpose of the present research has been to gain better understanding of growth mechanisms of S-containing PPFs prepared from binary gas mixtures of acetylene (C_2H_2) and H_2S, correlating plasma-phase and surface phenomena. Varying *R* and $\langle P \rangle$ (the mean absorbed power per cycle, see section 5.3.1), the plasma chemistry is examined by residual gas analysis (RGA) mass spectrometry,

and these data are correlated with chemical composition of the PPFs using X-ray Photoelectron Spectroscopy (XPS) and Fourier Transform Infrared Spectroscopy (FTIR), along with PPF deposition kinetics. In addition, these data are compared with those for single precursor Pr-PPF counterparts.

5.3 Experimental Section

5.3.1 Thin film deposition and characterization

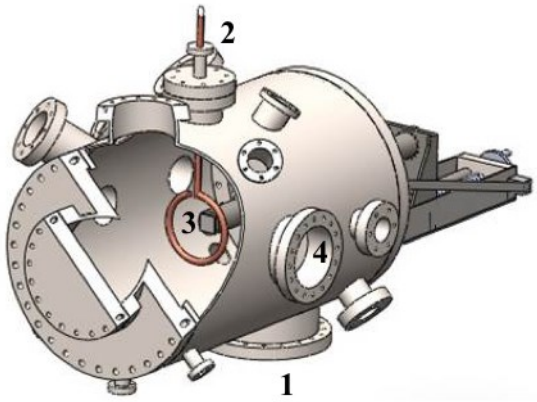

Figure 5-1: 3D view of the plasma reactor: 1 – Pumping line, 2 – Water-cooled RF copper coil, 3 – Substrate holder, 4 – Mass spectrometer inlet port.

The experimental setup (Figure 5-1) consisted of a cylindrical stainless steel vacuum chamber (65 cm in length and 35 cm in diameter), evacuated by combined turbo-molecular and primary pumps to a base pressure, $p < 2 \cdot 10^{-6}$ Torr. The power was applied using a single-turn copper coil (10 cm diameter) connected to an Advanced Energy 13.56 MHz r.f. power supply (CESAR 1310). The operating pressure during depositions was maintained at p=80 mTorr by a throttle valve connected through a capacitive gauge (both from Nor-Cal Products). The flow rate of the hydrocarbon C_2H_2 (99%, Air Liquide), $F_{(C2H2)}$, was kept constant at 30 sccm, while that of H_2S (99%, Air

Liquide), $F_{(H2S)}$, was varied between 0 and 30 sccm; this yielded values of R (=$F_{(H2S)}$/$F_{(C2H2)}$) ranging from 0 to 1. The flow rate of 1-propanethiol (99%, Sigma-Aldrich, the single molecule precursor), $F_{(Pr)}$, was fixed at 50 sccm, so as to maintain essentially the same total F as in the gas mixture experiments where the elemental feed ratio (X≡S/C=1/3) was identical (i.e. for R=0.66 in the gas mixture). The PPFs, henceforth designated "L-PPA:S" (for "low-pressure plasma-polymerized, sulfurized acetylene") or "Pr-PPF" (for "propanethiol plasma polymer") were deposited on 500 μm-thick silicon wafers (Si-Mat) using *pulsed* plasma polymerization. The (nominal) value of mean power, $<P>$, absorbed in the plasma was modulated by varying the duty cycle, Δ; the relationship between the plasma "on" time and the pulse period, is shown in equations (1) and (2), where P_{peak} is input power during the plasma "on" time.

$$< P >= P_{Peak}\Delta \tag{5-1}$$

$$\Delta = \frac{t_{on}}{t_{on} + t_{off}} \tag{5-2}$$

Table 5-1 summarizes the electrical power conditions used.

Table 5-1: Electrical conditions used in the present study.

<P> [W]	**P_{peak} [W]**	**Δ [%]**	**t_{on} [ms]**	**t_{off} [ms]**
12	120	10	0.2	1.8
48	120	40	0.8	1.2

All PPF deposits were characterized by X-ray photoelectron spectroscopy (XPS), performed in a PHI 500 VersaProbe instrument (Physical Electronics), using monochromatic Al Kα radiation (hv = 1486.6 eV). The elemental composition (in atomic %, at. %) and the chemical environment of the elements were obtained by

survey- and high-resolution, HR spectra, respectively. The former were acquired at a pass energy of 117.4 eV, a dwell time of 50 ms and energy steps of 1 eV, the latter at pass energy of 23.5 eV, dwell time of 50 ms and energy steps of 0.2 eV. Spectra were obtained at 45° emission angles; possible charging was corrected by referencing all peaks to the C1s peak at binding energy (BE)=285.0 eV. The constituent elements were quantified from survey spectra using 2.3.16 PR 1.6 Casa XPS software, by integrating the areas under relevant peaks after a Shirley-type background subtraction.

Fourier-transform infrared (FTIR) spectroscopy (Bruker IFS 66V/S) was used for further chemical characterization. PPFs (~200 nm thick) were deposited on KBr pellets and spectra (average of 32) were obtained within a spectral range from 4000 to 600 cm^{-1} in transmission mode at a resolution of 4 cm^{-1}. A blank KBr pellet served to acquire background spectra.

To quantify thiol concentrations, [SH], chemical derivatization with *N*-ethylmaleimide (99 %, Sigma-Aldrich) was used, as recently described by Thiry et al.[94] The reaction mechanism is shown in Scheme 5-1, where *N*-ethylmaleimide reacts selectively with SH via nucleophilic addition between the S atom and the double bond in the maleimide structure (thiol-ene click reaction), forming a stable thio-ether bond. The thiol-maleimide reaction offers several benefits, including high selectivity in the presence of multiple functional groups, rapid and quantitative conversion at low concentrations, and high stability in aqueous environments.[228]

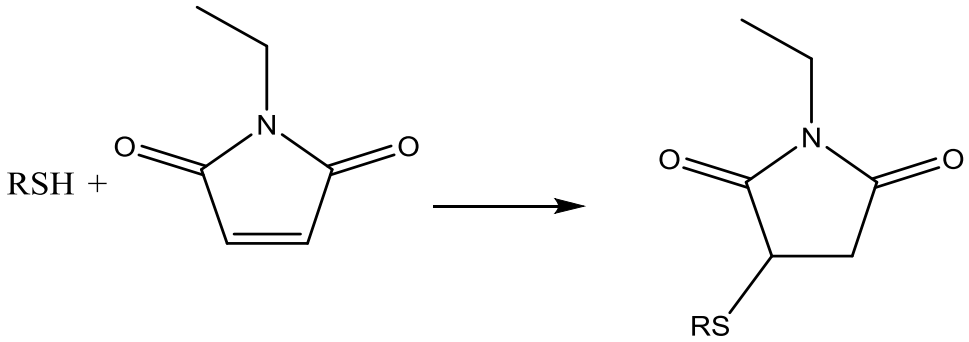

Scheme 5-1: Derivatization reaction between a thiol group and N-ethylmaleimide.

Typically, the derivatization reaction was carried out in phosphate buffer (KH_2PO_4/Na_2HPO_4, Chem Lab) solution at pH = 7, the *N*-ethylmaleimide concentration being fixed at 0.1 M. The samples were immersed in this solution for 78 h, following which they were rinsed in clean solution for 5 min to eliminate any unreacted molecules, then dried under a flow of dry nitrogen. XPS survey spectra were obtained before and after derivatization, allowing nitrogen, [N], and carbon, [C], concentrations to be quantified; [SH], was then calculated as follows:

$$[SH] = \frac{[N]}{[C] - 6[N]} \times 100\ (\%) \qquad (5\text{-}3)$$

Deposition rates were determined by measuring coating thickness, *T*, with a Dektak 150 mechanical profilometer (Veeco), using a diamond tip with 2.5 μm curvature radius and an applied force of 0.1 mN. The coatings' stability against dissolution was examined after immersion in Milli-Q water for 24 h, using the profilometer to measure possible changes in *T* (ΔT, in %) before and after immersion at three different points.

5.3.2 Plasma characterization

Gas-phase species in the plasma were investigated using a quadrupole mass spectrometer, MS (model HAL EQP 1000, Hiden Analytical), connected to the chamber by a 100 μm extraction orifice located about 30 cm from the coil. Residual gas analysis (RGA) MS measurements involved neutral species entering the instrument, which were then ionized by electron impact (EI) with electrons of kinetic energy fixed at 20 eV so as to avoid excessive fragmentation.

5.4 Results and Discussion

5.4.1 Deposition kinetics and composition of PPF coatings

Deposition rates, *r* (in nm/min), of the L-PPA:S films as a function of gas mixture ratio, *R*, for *<P>=12* and *48 W,* show that *r* decreased with rising *R* in both cases (Figure 5-2), as also observed in previous experiments with ethylene (C_2H_4), butadiene (C_4H_6), or C_2H_2 and N- or O-containing gas mixtures.[10, 77, 78, 83, 119, 234]

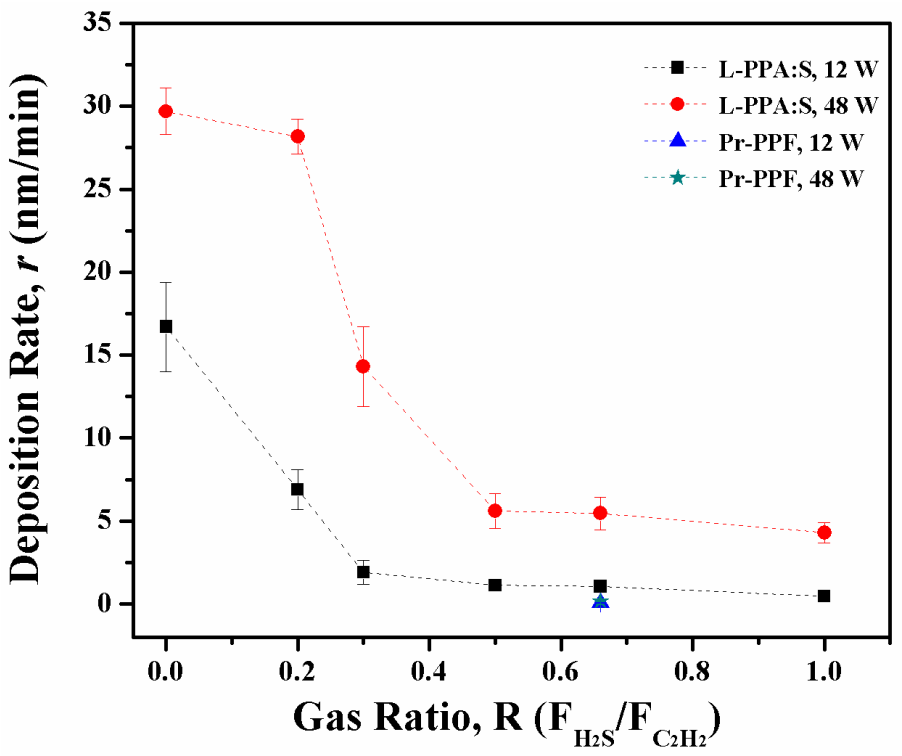

Figure 5-2: Deposition rates, r, of L-PPA:S films (squares, <P>=12 W; circles, <P>=48 W) as a function of gas mixture ratio, R, and of Pr-PPFs (triangle, <P>=12 W; star, <P>=48 W, overlapping here) at equivalent elemental feed ratio (X=S/C=1/3). Error bars show standard deviations of three measurements. The lines are to guide the reader's eye.

This is due to the decreasing relative concentrations of C_xH_y radicals that create the PPFs' polymer-like backbone. Furthermore, with increasing *R*, more H_2S in the gas mixture gives rise to more of the highly reactive $H^{\cdot}$ and $S^{\cdot\cdot}$ radicals; the former can etch the growing film and thereby lead to a transition from radical-induced deposition to an ablation regime, thus the observed decrease in *r*.[83] Similar behavior observed in the past for the case of N-rich films was also attributed to a threshold for the production of etching species.[76, 117, 214] Besides etching, quenching of radical species in the plasma, through recombination reactions, could also lead to a decrease in *r*. Indeed, radicals produced from H_2S dissociations (e.g. $H^{\cdot}$ and $S^{\cdot\cdot}$) could readily recombine with the ones

formed from C_2H_2, thus reducing the availability of radicals for film deposition, leading to a decrease in deposition rate.

Note that at $<P>$=48 W, L-PPA:S films showed significantly higher r values than at $<P>$=12 W. Referring to Table 5-1, at $<P>$=48 W the plasma "on" time was higher (0.8 vs. 0.2 ms), thereby leading to greater precursor fragmentation and higher concentration of film-forming species. Deposition rates of Pr-PPFs (Figure 5-2), prepared at the constant elemental feed rate (X≡C/S=1/3) and total flow comparable to L-PPA:S films obtained at R=0.66, revealed the same behavior, although significantly smaller, due to several reasons: (i) the saturated structure of propanethiol likely led to more dehydrogenation, which can induce increased etching; (ii) absence of unsaturations (i.e. double or triple bonds) in propanethiol, in contrast to C_2H_2, prevented uptake of unactivated precursor into the PPF; and (iii) mass spectrometry measurements (see Figure 8-1) also showed very little fragmentation of the propanethiol precursor under the applied conditions, compared with previous results of Thiry et al.

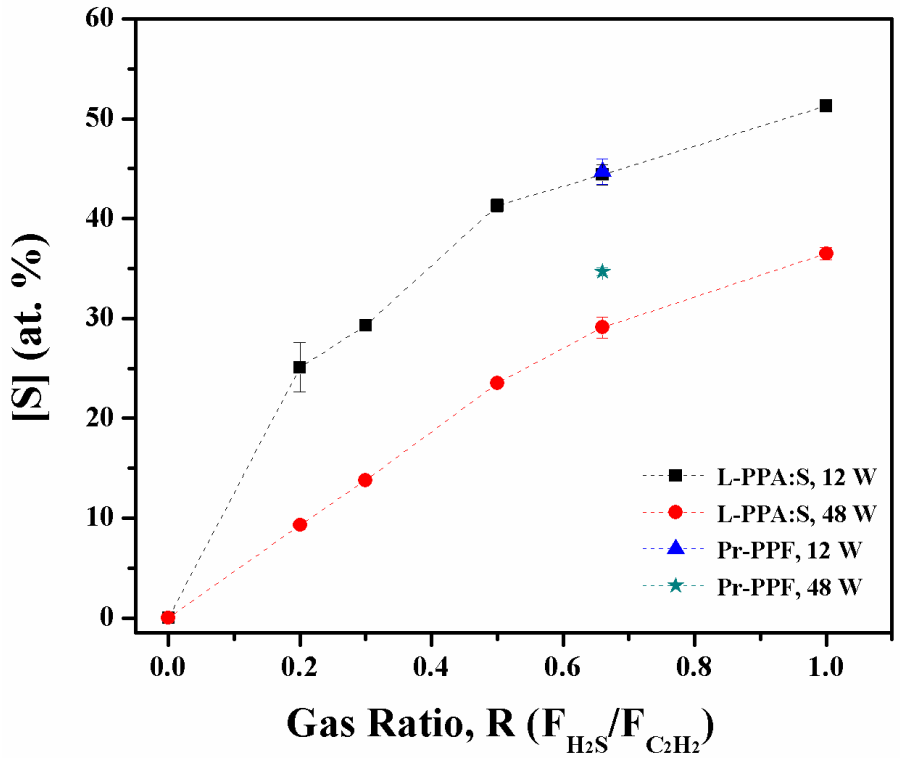

Figure 5-3: Sulfur concentrations, [S] (in at.%), as measured by XPS for L-PPA:S films (squares, <P>=12 W; circles, <P>=48 W) as a function of gas mixture ratio, R, and of Pr-PPFs (triangle, <P>=12 W; star, <P>=48 W) at equivalent elemental feed ratio (X=S/C=1/3). Error bars show standard deviations of three measurements. The lines are to guide the reader's eye.

For both <*P*> values, [S] is seen to have increased monotonically with rising *R*, up to [S] ≈ 50 at. %, tending to plateau for *R* > 0.66 (Figure 5-3). Similar behavior was also observed in our previous work, where [S] up to ~48 at. % was obtained with C_2H_4 as the hydrocarbon feed gas.[233] Lower [S] values at high <*P*> can presumably be attributed to higher fragmentation, leading to many small volatile S-rich stable molecules that were pumped out of the chamber and did not contribute to film growth;[72, 93, 173, 176, 235] the higher the fragmentation, the less S-containing moieties might then be available for incorporation into the growing films. Similar trends for [S] were observed for Pr-PPFs, namely higher [S] was obtained at lower <*P*> (more details

under section 5.4.3). These data also reveal a major difference when comparing with N- or O-based PPFs: especially at low <*P*>, [S] significantly exceeded that element's concentration in the feed gas mixture or in the precursor, an observation that was also reported when using propanethiol and attributed to trapped H_2S in the plasma polymer network.[91, 93] A major advantage of binary gas mixtures over a single molecule precursor is the following: Figure 5-3 and previous studies[77, 83, 118, 233, 234] all showed that heteroelement concentration, [X] (here: [S]), can be controlled over a remarkably wide range (here: 10 at.% < [S] < 50 at.%). This flexibility evidently opens the use of these PPFs for numerous applications where a particular [X] value is required, for example to select a specific value of refractive index.[226]

Due to the complexity of plasma-chemical reactions, a large variety of S-containing groups are created, but the measured [S] value does not reveal whether it occurs as the SH-groups desired, for example, in biomedical applications. Indeed, S can exist in different allotropes (S-S-S, C-S-C, C-SH, …), but these cannot readily be identified by XPS because different types of S-bonding do not result in appreciable chemical shifts, neither in the S2p nor in C1s HR-XPS spectra.[219-221] Therefore, in order to measure [SH] in L-PPA:S and Pr-PPFs, the selective and quantitative chemical derivatization reaction based on *N*-ethylmaleimide as labelling molecule was used.[94] Figure 5-4 plots [SH] as a function of *R* at two different <*P*> values, with FTIR measurements confirming the presence of these thiol moieties (see Figure 8-2).

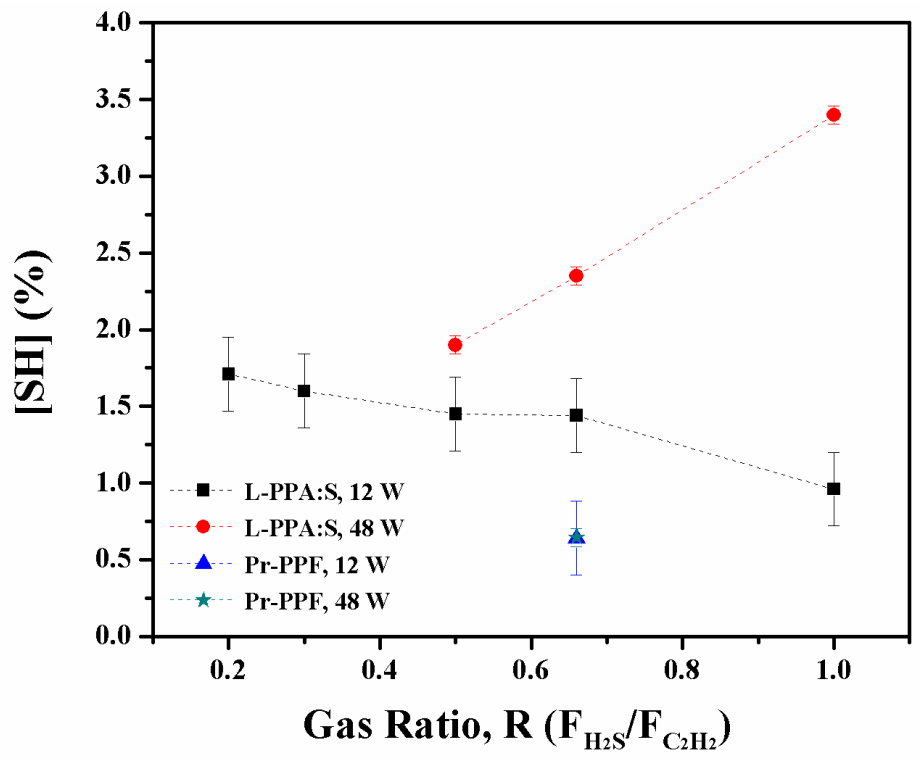

Figure 5-4: Proportion of carbon bearing the –SH group, [SH] (in %), determined using chemical derivatization XPS of L-PPA:S films (squares, <P>=12 W; circles, <P>=48 W), as a function of gas mixture ratio, R, and of Pr-PPFs (triangle, <P>=12 W; star, <P>=48 W, overlapping here) at equivalent elemental feed ratio (X=S/C=1/3). Error bars show standard deviations of three measurements. The lines are to guide the reader's eye.

For R < 0.5 and <P>=48 W it was not possible to measure [SH] of L-PPA:S films because the coatings cracked during derivatization, likely due to high internal stress caused by the higher power and carbon content.[236-238] At lower <P>, [SH] was seen to be nearly constant up to R=0.66, ~1-1.7 %, within experimental error, while the value dropped with further increase in R. At the higher <P>, [SH] increased with rising R, up to about 3.4 %. Therefore, even if [S] was overall lower at higher <P>, deposits of greater quality (higher [SH]) were obtained. Contrary to propanethiol, where higher fragmentation resulted in lower thiol retention,[7, 72, 107] in the case of gas mixtures

fragmentation was *needed* to create that desired chemical functionality. At higher <*P*>, higher fragmentation led to more of such active thiol-forming species, hence to the observed increasing [SH] values. Similar observations were reported by Buddhadasa et al.[106] for the case of ammonia / butadiene feed-gas mixtures, where the concentration of amino groups, [NH_2], was found to increase with rising *P*.

[SH] (~ 0.6%) of Pr-PPFs was apparently not affected by <*P*>, as previously observed for other electrical and pressure conditions,[72] being significantly lower than for L-PPA:S ([SH] ~ 1.5 and ~ 2.5 %). The use of binary mixtures was therefore advantageous for higher thiol incorporation. At this stage, the exact mechanism(s) remain elusive and require further experiments over wider parameter ranges.

5.4.2 Ageing in water and in air

The stability of PPFs in water and in air is of crucial importance for potential biomedical applications, for example. For the case of N- and O-rich PPF coatings, stability has already been extensively discussed:[9, 10, 78, 169] high concentrations of heteroatoms (N or O) lead to higher solubility in polar solvents (e.g. water) and a higher instability in air, commonly referred to as "ageing". This is attributed, among other factors, to the presence of soluble low molecular weight (LMW) fractions formed during deposition, which are extractable in polar solvents, and to oxidation of dangling bonds and degradation of unstable functional groups in contact with air.[9, 10, 78, 118, 172-174, 222] In the specific case of sulfur-based coatings, Thiry et al. showed that S-containing species (e.g. H_2S) were trapped in the PPF matrix and released after immersion in water.[91] Therefore, S/C ratios of our coatings were measured before and after immersion in *N*-ethylmaleimide solution (Figure 5-5). Except for the <*P*>=48 W / *R*=1 sample, conditions under which many stable molecules were created (see section 3.3), little

reduction in S/C was observed after immersion; this suggests that a small proportion of S-containing molecules were trapped in the PPF matrix and/or that the degree of chemical bonding was sufficient to prevent release of such possibly trapped molecules during immersion.

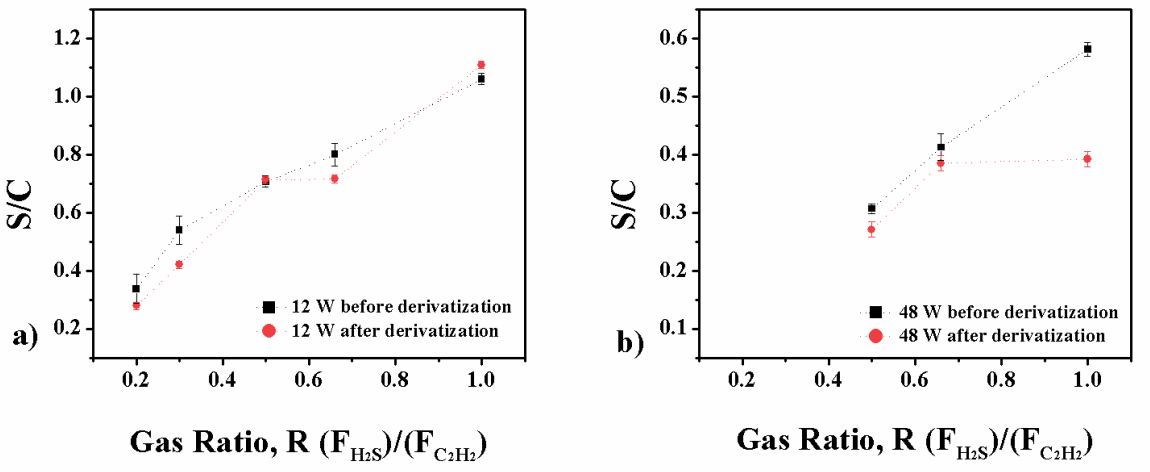

Figure 5-5: S/C ratios measured by XPS before (squares) and after (circles) immersion in N-ethylmaleimide solution: a) L-PPA:S films obtained at <P>=12 W, and b) at <P>=48 W, as a function of gas mixture ratio, R. Error bars show standard deviations of three measurements. The lines are to guide the reader's eye.

To complete this part of the study, possible thickness loss after immersion in Milli-Q water during 24 h was also examined, as extensively reported in the literature for several other families of plasma polymers.[9, 78, 79, 83, 222, 233, 239-241] Similar to the case of C_4H_6- and C_2H_4-based PPF coatings, the present L-PPA:S films were found to be largely insoluble in Milli-Q water, for $0 \leq R \leq 1$: the largest observed values of $\Delta T/T$ were about 20% (positive or negative), comparable to the cumulative measurement uncertainty (see Figure 8-3). Pr-PPFs deposited at <P>=12 W showed similar stability to the corresponding L-PPA:S films while for <P>=48 W, a higher solubility was observed (~25 % loss of thickness, see Figure 8-3). A possible explanation for their

stability might be that these coatings were particularly highly cross-linked on account of acetylene's triple bond, as also reported for L-PPA:N films.[83]

To complete the study of ageing, surface-near oxygen concentrations, [O], of the L-PPA:S films were measured by XPS as a function of *R* after storing them in ambient air for 3 days.

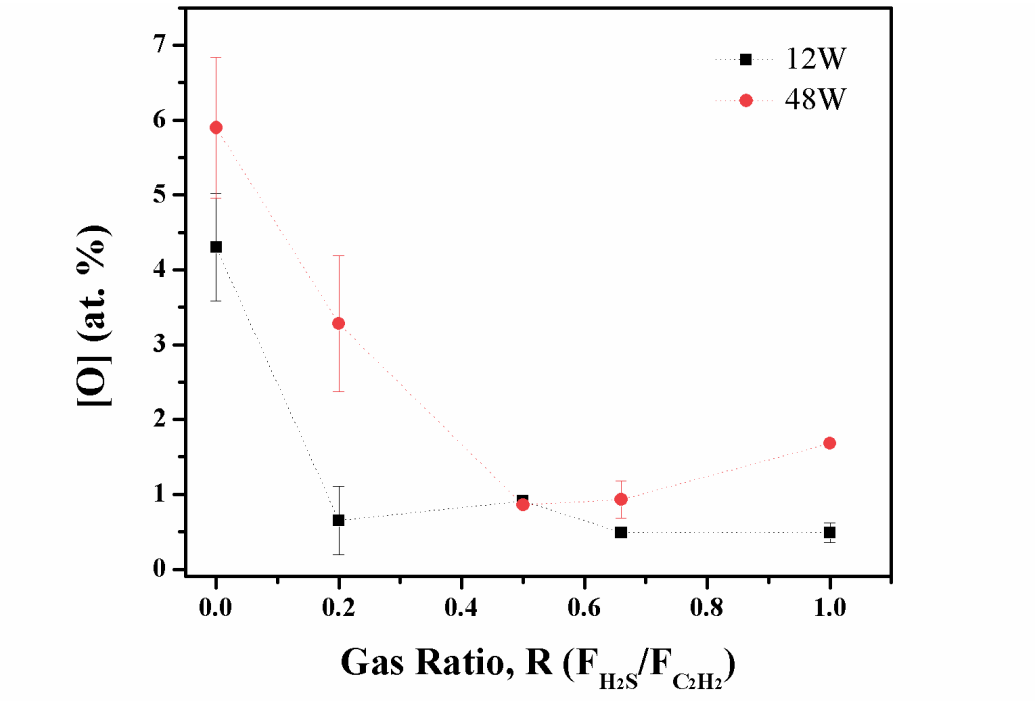

Figure 5-6: Surface-near oxygen concentrations, [O] (in at.-%, obtained by XPS) as a function of gas mixture ratio, R, of L-PPA:S films (squares, <P>=12 W; circles, <P>=48 W) stored for 3 days in ambient air. Error bars show standard deviations of three measurements. The lines are to guide the reader's eye.

Figure 5-6 shows that [O] decreased with rising *R* for both values of <*P*>. As already discussed, increasing *R* decreased the concentration of C_xH_y radicals in the plasma, hence that of C-centered radicals in the coatings (as opposed to S-bearing groups). Figure 5-5 clearly revealed proportional rise of S/C with increasing *R*; since

atmospheric oxygen presumably only reacted with C-centered radicals, the drop in [O] noted in Figure 5-6 therefore stands to reason.[242, 243]

5.4.3 Mass-spectrometry measurements

To better understand growth mechanisms of L-PPA:S films, plasma chemistry of the gas mixtures was examined by mass spectrometry measurements using residual gas analysis (RGA). Mass spectra of the precursor gases (Figure 5-7a) and b)) revealed peaks at m/z = 26 for C_2H_2 and m/z = 34 for H_2S in the absence of plasma. Additional peaks in Figure 5-7a) can presumably be assigned to slight impurities in C_2H_2.[244]

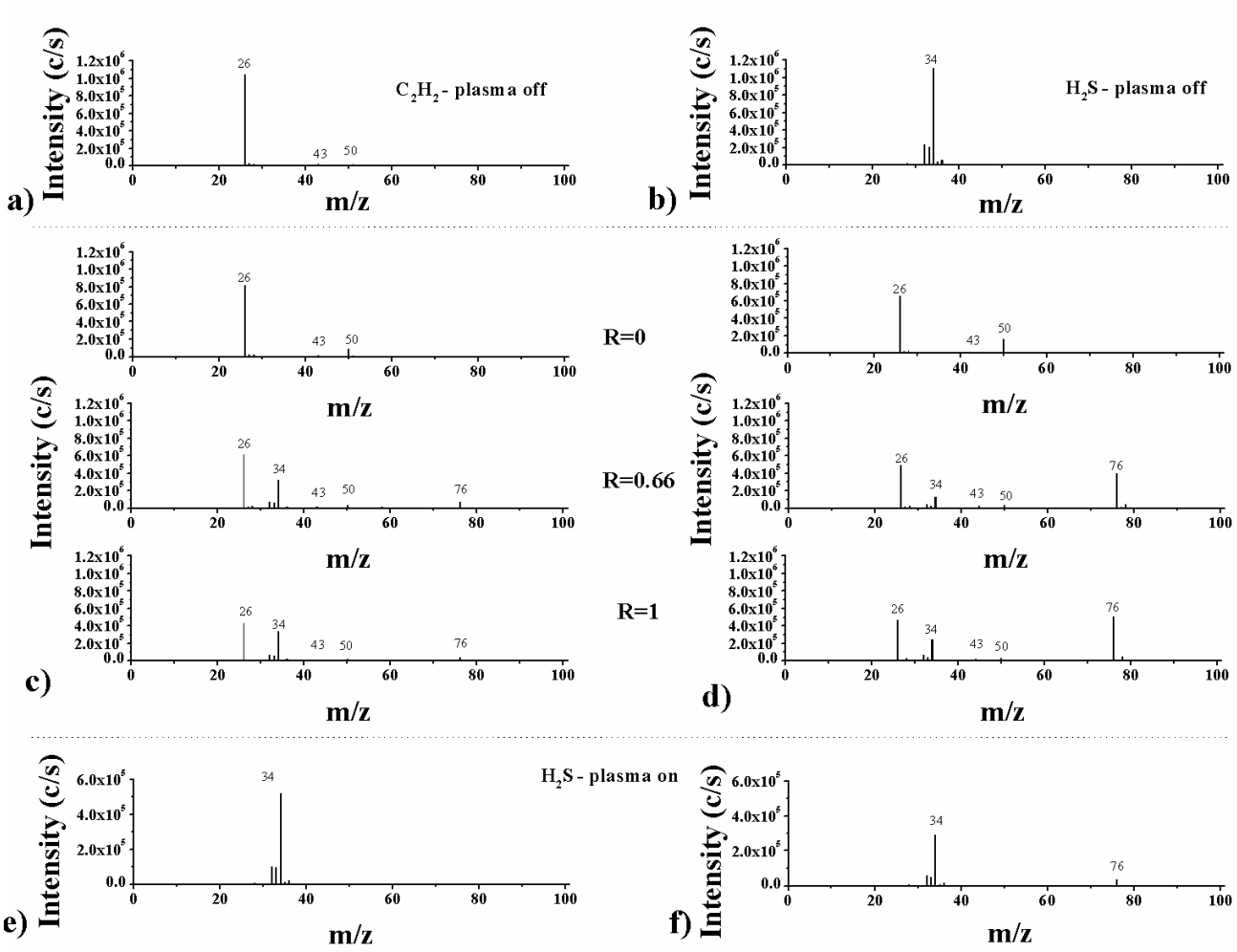

Figure 5-7: Mass spectra of a) C_2H_2 and b) H_2S at plasma "off" conditions (spectra show no significant fragmentation of the pure gases in the ionisation source of the spectrometer); of three different C_2H_2 + H_2S mixtures (R=0, R=0.66, and R=1) in plasmas sustained at c) <P>=12 W and d) <P>=48 W; and mass spectra of pure H_2S plasmas sustained at e) <P>=12 W and f) <P>=48 W (Note; creation of CS_2, m/z = 76, was observed at <P>=48 W only).

Plasma ignition led to changes in concentrations and to the production of new species, depending on R and <P> (Figure 5-7c) and d)). All peaks in the mass spectra are identified in Table 5-2.

Table 5-2: Attribution of peaks observed in the various mass spectra, Figure 5-7 (a-f).

m/z	**Ions**
25-28	$[C_2H_\chi]^+$ χ=1-4
32-34	$[H_\chi S]^+$ χ=0-2
76	$[CS_2]^+$

At *R*=0, a quite intense peak at m/z=50 corresponding to C_4H_2 was detected. As *R* increased (more H_2S was present in the gas mixture), an additional peak corresponding to CS_2 appeared at m/z=76, which increased in amplitude with rising *R* and <*P*>, whereas that corresponding to C_4H_2 decreased. The abundance of CS_2 points to reactions between feed gas species in the plasma; on the other hand, earlier studies showed little evidence of such reactions between ammonia and the hydrocarbon.[106] However, etching reactions can apparently also contribute to formation of CS_2: when a pure H_2S discharge was ignited at <*P*>=48 W (Figure 5-7f)), the m/z=76 peak revealed that etching of PPF coatings on the chamber walls must have taken place. Those etching reactions also contributed to the drop in *r*, as previously evoked. CS_2 production in S-containing discharges had already been reported for propanethiol,[72, 93] methanethiol,[245] and thiophene plasmas. Here, the creation of CS_2 can mainly be attributed to gas phase reactions between C_2H_2 and H_2S in the plasma, because its peak at m/z=76 was much higher than that corresponding to etching reactions.

Lower-mass fragments detected in previous work, especially in acetylene plasmas (e.g. H_2, H·, and C_2H·), were not noted here to any appreciable extent.[244, 246] This may have been due to a lower detection limit of the mass spectrometer, but also to the high sticking coefficient, β, of C_2H· (β~0.9),[246] which rendered detection of this

radical particularly challenging: It has been recognized as the major contributor to *a*-C:H film growth in pure acetylene plasmas.[244, 246, 247]

In order to connect mass spectrometry results with L-PPA:S film characteristics, we examined the extent of fragmentation of both precursors, α, as a function of R at different <*P*> (Figure 5-8), according to equation (5-4):

$$\alpha = I_{rel}(m)_{on} - I_{rel}(m)_{off} \tag{5-4}$$

where $I_{rel}(m)_{on}$ and $I_{rel}(m)_{off}$ are the relative peak intensities of precursor (m) when the plasma is "on" and "off", respectively. The relative abundance of mass m species, $I_{rel}(m)$, in the plasma is then defined as:

$$I_{rel}(m) = \frac{I(m)}{\sum_m I(m)} \tag{5-5}$$

where $I(m)$ are the experimentally observed values recorded in the mass spectra of mass m, respectively.

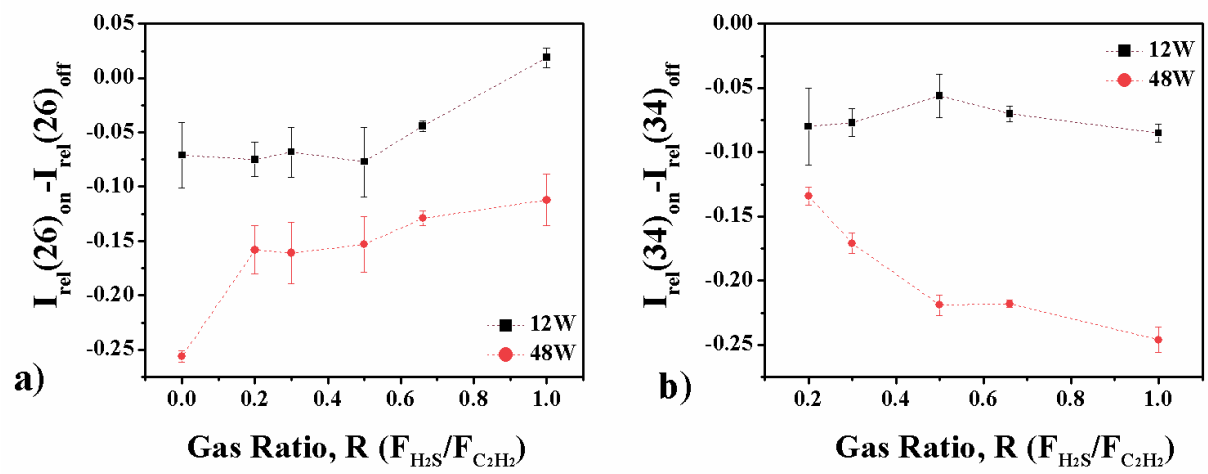

Figure 5-8: Extent of fragmentation, α, for a) C_2H_2 and b) H_2S (squares, <P>=12 W; circles, <P>=48 W) as a function of gas mixture ratio, R. Error bars show standard deviations of three measurements. The lines are to guide the reader's eye.

Based on equation (5-4), *negative* α values indicate *decreased* peak intensity, thus higher fragmentation of the precursors; the more negative, the higher the extent of fragmentation in the plasma. Some fragmentation was observed at all values of *R*, although little at low <*P*> for C_2H_2; for H_2S, increased fragmentation was observed with rising *R*, especially at the higher <*P*>. Indeed, for both gases, fragmentation was higher at <*P*>=48 W, confirming the assumptions reported in section 5.4.1: the precursors were exposed to the plasma for a longer period of time, thereby increasing the probability of collisions with energetic electrons. This led to higher fragmentation and it can explain the observed larger values of *r*, lower [S] and higher [SH]. Nevertheless, decreased [S] and increased [SH] cannot readily be explained solely by higher precursor fragmentation. We therefore also focused on the evolution of other important species, such as CS_2 (m/z=76) (Figure 5-9).

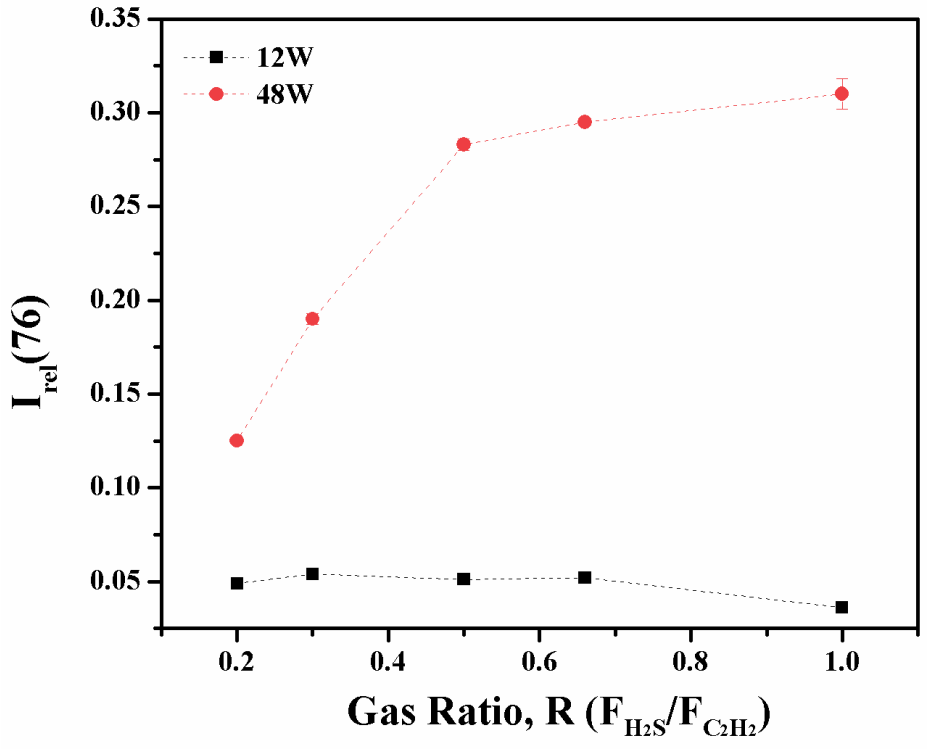

Figure 5-9: Plot of $I_{rel}(76)$(squares, <P>=12 W; circles, <P>=48 W) as a function of gas mixture ratio, R. Error bars show standard deviations of three measurements. The lines are to guide the reader's eye.

Lower amounts of CS_2 at <P>=12 W could be directly observed in the mass spectra (Figure 5-7c)) and correlated with a lower extent of precursor fragmentation (Figure 5-8); at <P>=48 W, fragmentation was high, giving rise to increasing production of CS_2 with rising R, up to saturation for R>0.66, probably due to insufficient numbers of C_xH_y radicals. The concentration of CS_2 in the discharge correlates inversely with [S] in the PPFs:[93] increased CS_2 production at high <P> could therefore help explain the reduced amount of sulfur available for incorporation into the growing films, hence the observed lower [S] values than at lower <P> (Figure 5-3).

To help better understand the evolution of [SH] with rising R (Figure 4), we next focused on fragments that could possibly insert -SH moieties into the growing L-PPA:S films, namely SH· (m/z=33) and $S^{\cdot\cdot}$ (m/z=32). Both of these already being observed in the absence of plasma (Figure 5-7b)), equation (5-6) takes into account fragments produced in the ionization source of the mass spectrometer by electron impact:[107]

$$I_c(m) = \frac{\left(I(m)_{on} - \left(I(m)_{off} \cdot \frac{I(34)_{on}}{I(34)_{off}}\right)\right)}{\sum_m I(m)} \qquad (5\text{-}6)$$

where $I_c(m)$ is the corrected intensity of mass m (here either 33 or 32), and $I(m)_{on}$ and $I(m)_{off}$ are the experimentally observed peak intensities for mass m when the plasma is on and off, respectively; I(34) is the peak intensity corresponding to the H_2S precursor gas.

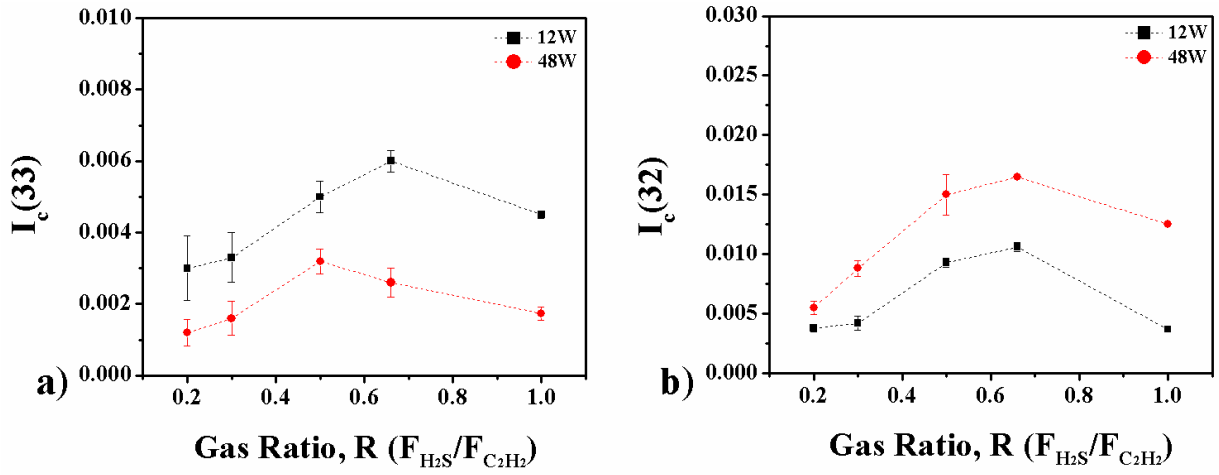

Figure 5-10: Evolution of species that could lead to SH-groups in L-PPA:S films a) SH· and b) S·· (squares, <P>=12 W; circles, <P>=48 W) as a function of gas mixture ratio, R. Error bars show standard deviations of three measurements. The lines are to guide the reader's eye.

$I_c(33)$ is seen to have increased with rising R, reaching a maximum near R=0.66 (Figure 5-10a)). Furthermore, for similar R values, the relative amount of SH· was higher at <P>=12 W. Figure 5-4 depicts a rather different trend in [SH] than the one shown here, namely a monotonic decrease with rising R. This would imply that SH· radicals were not directly responsible for SH-groups in L-PPA:S films. Now examining Figure 5-10b), the atomic S·· peak (m/z=32) was also seen to increase with rising R for both <P> values, reaching maxima at R=0.66. However, contrary to SH· (Figure 5-10a)), the creation of S·· was greater at the higher <P>, presumably on account of multistep fragmentation (i.e. H_2S → SH· → S··). This would indeed be favored at high <P> due to longer exposure time in the plasma, which in turn might help explain the increased formation of CS_2. Considering that larger amounts of atomic hydrogen were available at higher <P> with rising R (see Figure 5-8), the incorporation of S·· and accompanying formation of -SH groups in growing L-PPA:S films would therefore be favored, as indeed observed in Figure 5-4.

Summarizing, knowledge of the plasma composition from mass spectrometry measurements enables a better understanding of deposition kinetics and film composition (at least in terms of [S]); however, the evolution of [SH] cannot yet be fully explained by gas phase reactions only. Theoretical calculations could help in predicting different fragmentation pathways as a function of the employed plasma parameters and thus give a better understanding for the evolution of [SH], as was previously done for a propanethiol plasma.[72, 93]

5.5 Discussion and Conclusions

The chemistry and growth mechanisms of plasma-assisted deposition from single-molecule precursors have been extensively studied in the past, relating to the fabrication and characterization of amine-, hydroxyl- and/or carboxyl-, and thiol(SH)-rich plasma-polymer films. However, no such studies have been reported for the case of feed-gas mixtures leading to SH-terminated films, conducted by the present authors. Here, we have aimed to gain deeper knowledge of the chemistry involving a new family of SH-containing films, namely acetylene-based sulfur-rich ones (L-PPA:S), created by "co-polymerizing" mixtures of a hydrocarbon (here C_2H_2) and H_2S by low-pressure r.f plasma polymerization. The impact of varying gas mixture ratio, R, and applied power, $<P>$, was investigated by way of surface- (XPS and FTIR) and plasma-related (MS) analyses.

Deposition rates, r, of L-PPA:S coatings as a function of R followed the same trends for both values of $<P>$ investigated, higher $<P>$ leading to higher r values. This could be correlated with more pronounced precursor fragmentation at higher $<P>$, as also confirmed by MS measurements. Sulfur concentrations, [S], in the films increased

monotonically with rising *R,* up to [S] ~ 50 at. % at <*P*>=12 W, while higher <*P*> led to a decrease in [S]. This was attributed to intense precursor fragmentation that resulted in the production of many S-rich stable molecules, which did not appreciably contribute to film growth and were pumped out of the chamber. This was also confirmed by MS measurements, namely increased production of CS_2 at higher <*P*>. Somewhat surprisingly, higher thiol concentrations, [SH], were found to occur in the higher <*P*> L-PPA:S films. Contrary to the case of a single molecule precursor, extensive precursor-gas fragmentation is first needed to produce the desired functionality(ies), here [SH], when using binary gas mixture. Therefore, [SH] increase at higher <*P*> is again correlated with the higher extent of precursor fragmentation under these conditions. Nevertheless, MS measurements revealed that SH· in the gas phase was not alone responsible for [SH] in the films, but that other surface reactions need to be considered in addition.

Comparison with Pr-PPF films prepared using the single-molecule precursor, propanethiol, with a constant S/C ratio (= 1/3), revealed comparable [S], but lower *r* and [SH] values than those obtained for the case of L-PPA:S films. This is surprising because the propanethiol molecule already possesses the thiol functionality, which ought to lead to higher [SH]; this had so far been considered an advantage of the single molecule approach over the use of gas mixture.

In conclusion, binary gas mixtures offer (i) excellent control of [S] over a wide range (here: 10 at. %< [S] <50 at. %); (ii) flexibility over the desired [S] due to the ability to readily vary and control *R*; (iii) higher retention of thiol functionalities in the films; and (iv) excellent stability towards dissolution in aqueous media and ageing in air. All of these mentioned advantages together render L-PPA:S films superior candidates for applications, for example, biomedical ones.

Acknowledgments

The authors gratefully acknowledge financial support from McGill University (MEDA, GMA), from the *Fonds de recherche du Québec en nature et technologies* (FRQNT) via *Plasma-Québec*; from the Natural Sciences and Engineering Research Council of Canada (NSERC), and the Canadian Foundation for Innovation (CFI). D. Thiry thanks the "Région Wallonne" for financial support through the Cleanair project.

Chapter 6 VUV Photo-deposition of Thiol-terminated Films – A Wavelength-dependent Study

6.1 Preface

This chapter presents an article published in the journal of "*Langmuir*". The complete citation of the manuscript is:

> E. Kaparek, J. R. Tavares, M. R. Wertheimer and P.-L. Girard-Lauriault (2018), *VUV Photo-deposition of Thiol-terminated Films – A Wavelenght-dependent Study*, Langmuir, DOI:10.1021/acs.langmuir.8b01691.

The research was planned, analyzed and written by E. Kasparek (Ph.D. candidate). Dr. Girard-Lauriault, Dr. Tavares and Dr. Wertheimer were responsible for supervision and review of the work.

In Chapter 4 and Chapter 5 we examined the synthesis of SH-terminated organic coatings from different gas mixtures. The resulting films showed a great diversity of properties that can be tuned by selecting specific process parameters. We were able to show that SH-terminated films obtained from binary gas mixtures were richer in SH groups than their single-molecule precursor counterparts. This makes the former ones overall better candidates for potential biomedical applications based on their higher SH-concentration and stability. While deeper understanding of the growth mechanisms of the plasma-based SH-terminated films was gained, films obtained through photo-polymerization needed further investigation. The present article presents a wavelength-dependent deposition study, in which four different VUV sources were used to create SH-terminated films. The goal was to gain deeper insight in possible deposition mechanisms and to find an ideal combination of the correct photon energy and gas mixture ratio to create nearly "mono-functional" films.

VUV Photo-deposition of Thiol-terminated Films - A Wavelength-dependent Study

Evelyne Kasparek [a], Jason R. Tavares [b], Michael R. Wertheimer [c], Pierre-Luc Girard-Lauriault [a]

[a]Plasma Processing Laboratory, Department of Chemical Engineering, McGill University, Montreal, QC H3A 2B2, Canada; [b]Photochemical Surface Engineering Laboratory, Department of Chemical Engineering, École Polytechnique de Montréal, Montréal, QC H3C 3A7, Canada; [c]Groupe des couches minces (GCM) and Department of Engineering Physics, École Polytechnique de Montréal, Montréal, QC H3C 3A7, Canada.

Abstract

Photo-initiated chemical vapor deposition (PICVD) has become attractive for selective and specific surface functionalization, since it relies on a single energy source, the photons, to carry out (photo-) chemistry. In the present wavelength (λ)-dependent study, thiol (SH)-terminated thin film deposits have been prepared from gas mixtures of acetylene (C_2H_2) and hydrogen sulfide (H_2S) via PICVD using four different vacuum-ultraviolet (VUV) sources, namely KrL (λ_{peak}=123.6 nm), XeL (λ_{peak} =147.0 nm), XeE (λ_{peak} =172.0 nm) and Hg (λ=184.9 nm) lamps. Different λ influence the deposition kinetics and film composition, reflecting that photolytic reactions are governed by the gases' absorption coefficients, $k(\lambda)$. Thiol concentrations, [SH], up to ~7.7 %, were obtained with the XeL source, the highest reported in the literature so far. Furthermore, all films showed island-like surface morphology, irrespective of λ.

6.2 Introduction

6.2.1 General introduction

Synthetic polymers are broadly used in biomaterials due to their favorable bulk properties, such as high mechanical stability and elasticity, non-toxicity, and low degradation in the human body.[5, 6] Nevertheless, their surfaces are generally chemically inert and show poor biocompatibility, leading to inadequate interactions with cells, generating strong foreign body reactions such as inflammation, clotting and infection.[1, 248, 249] Therefore, commercial polymers must often undergo surface functionalization, which will aid their surfaces to adapt to biological demands by immobilizing biomolecules onto the polymers. The principal methods of immobilizing a biomolecule to a polymeric surface are adsorption via electrostatic interactions, ligand-receptor pairing, and covalent attachment. Non-covalent adsorption can be desirable for certain applications (e.g. in drug delivery), and there is broad evidence in the literature that nitrogen (N)- and oxygen (O)-containing functional groups, more specifically primary amines ($-NH_2$) and carboxylic acid (-COOH) or hydroxyl (-OH) functionalities, respectively, are often advantageous in promoting protein and cell adhesion via non-covalent adsorption.[7, 8, 10, 11] However, covalent immobilization of biomolecules has been shown to be superior by providing a stable bond between the biomolecules and the functionalized surface, extending the shelf-life of the biomolecule, and allowing for continued bioactivity.[6, 13] Sulfur (S)-rich, more specifically thiol (SH)-terminated surfaces offer excellent platforms for covalent immobilization of biomolecules through specific and selective thiol-ene coupling reactions. This coupling reaction has been widely exploited for the construction of immobilized antibodies, enzymes and peptides.[35-40]

So far, SH-terminated surfaces have been mainly synthesized through tedious, non-specific, multi-step wet-chemical approaches, often involving various toxic and expensive solvents.[38-40] Over the last decade, the synthesis of SH-terminated surfaces has been also accomplished through plasma-enhanced chemical vapor deposition (PECVD) techniques using single-molecule precursors (e.g. allylmercaptan,[71, 88] propanethiol[72, 92, 226]) and more recently, using gas mixtures comprising a hydrocarbon (either ethylene or butadiene) and hydrogen sulfide (H_2S).[233] Plasma-based techniques offer several benefits over the wet-chemical ones, such as low processing temperatures, no solvent requirement, and fast reaction times. Despite these advantages, the reactions occurring in a plasma are difficult to control since the main originators of chemical reactions, "hot" electrons, possess a broad, Maxwell-Boltzmann-like energy distribution,[10, 119] thereby making the reactions non-specific and non-selective.

More recently, photo-initiated CVD (PICVD) techniques have emerged. This method has been studied extensively and it has established a firm position as a CVD method capable of producing high quality, functional thin films, often comparable to traditional plasma CVD.[20, 123, 135, 136, 250] In PICVD, the energy required to induce reactions leading to deposition is provided by photons. Therefore, only one energy component carries out (photo-) chemistry, potentially allowing for better control of the overall process compared to plasma counterparts. To obtain thin films from specific precursors, absorption of photons by the precursors must be significant, and photon energies must be sufficiently high to overcome bond dissociation energies, D_0, to induce photo-dissociation.[70] Therefore, photo-absorption by molecules as a function of wavelength, $k(\lambda)$, must be considered for successful photo-induced deposition.[123] Almost all of the observed absorption continua correspond to dissociation processes; by choosing a specific photon wavelength, λ, different dissociation products can be

generated. Wavelength dependency has been observed for deposition kinetics and film quality.[251, 252] Nevertheless, selectivity in excitation has not been fully exploited so far, partly due to a lack of available light sources and other required equipment. This is of high importance since it could aid in selectively designing thin film deposits by simply using different λ values.[10, 20, 119, 127, 135]

In our previous study,[233] we synthesized SH-terminated coatings using ethylene (C_2H_4)/H_2S and butadiene (C_4H_6)/H_2S gas mixtures with a single non-coherent VUV source (λ_{KrL} = 123.6 nm). We obtained adjustable sulfur concentrations, [S], ranging from 2 to 30 at.% and thiol concentrations, [SH], up to 1.75%. In the present work, we broaden the experimental window by performing a λ-dependent deposition study of SH-terminated coatings using variable gas mixture ratios, *R*, of acetylene (C_2H_2) and H_2S and four different λ values, namely λ_{KrL} = 123.6 nm, λ_{XeL} = 147.0 nm, λ_{XeE} = 172.0 nm, and λ_{Hg} = 184.9 nm. In this context, we aimed to understand the growth mechanisms of the synthesized SH-terminated films using PICVD, since only one kind of excitation (VUV photons) at a specific wavelength is active and available for initiating reactions. Besides determining the chemical composition of the coatings, the deposition kinetics, film growth and -morphology were also studied. The dependence of these as a function of λ was investigated in detail. By exploring a broader range of photon energies, we intended to find an "ideal" combination of *R* and photon energy which gives the highest [SH] values, thereby maximizing the possibilities for further covalent immobilization of biomolecules through thiol-ene coupling reactions.

6.2.2 Wavelength-dependent photolysis of C_2H_2 and H_2S

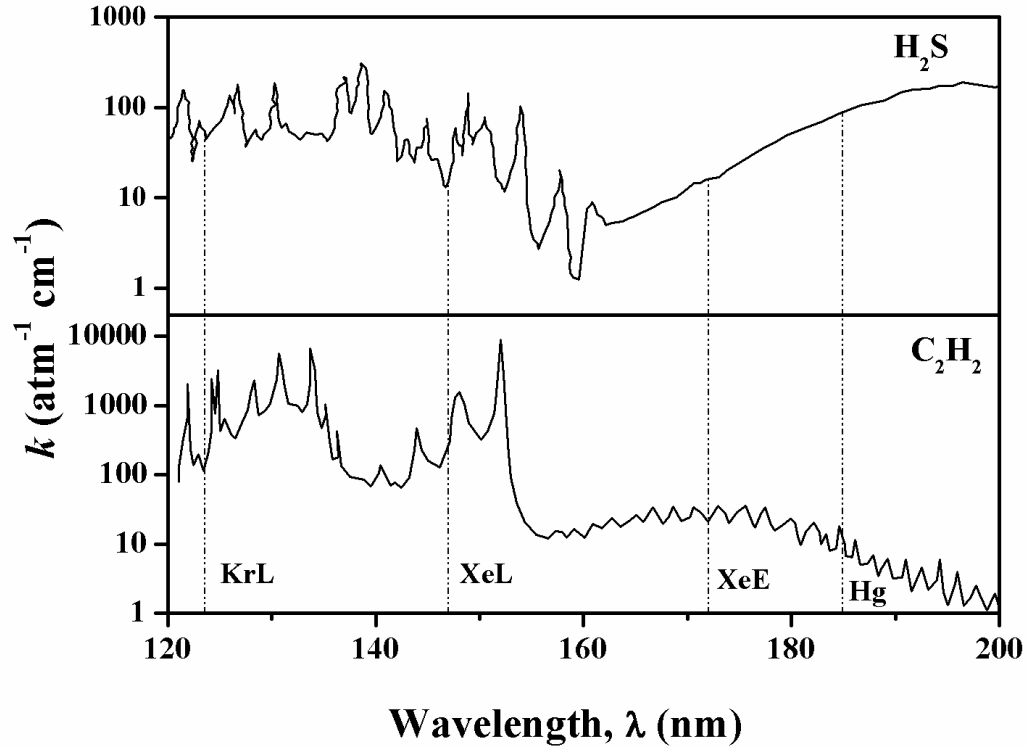

Figure 6-1: VUV-absorption, k ($atm^{-1}cm^{-1}$, base e) of gaseous H_2S[253] and C_2H_2[121]; the wavelengths, λ, of the VUV lamps used are also shown (λ_{KrL} = 123.6 nm, λ_{XeL} = 147.0 nm, λ_{XeE} = 172.0 nm, λ_{Hg} = 184.9 nm).

Activation and photo-dissociation of C_2H_2 and H_2S are expected from all four sources on account of their relatively strong absorption, $k(\lambda)$ (Figure 6-1), throughout the studied spectral range ($123.6 < \lambda < 184.9$ nm). Nevertheless, the radiation from some lamps is more strongly absorbed by the two precursor gases than others, especially in the case of C_2H_2 (Table 6-1), and these differences should be reflected in the deposition behaviour of the films at different λ.

Table 6-1: Absorption coefficients, k(λ), of H_2S[253] and C_2H_2[121] at the wavelengths, λ, of interest.

Lamp	Peak Wavelength, λ_{peak} (nm)	Absorption of C_2H_2, k_{C2H2} ($atm^{-1}cm^{-1}$)	Absorption of H_2S, k_{H2S} ($atm^{-1}cm^{-1}$)
KrL	123.6	112	48
XeL	147.0	303	15
XeE	172.0	35	16
Hg	184.9	9	92

Photo-dissociation of acetylene can occur upon absorption of photons with energies greater than 5.8 eV, or λ < 214 nm (Figure 6-1). Two primary processes have been identified to occur when C_2H_2 absorbs photons in the studied λ range:

(i) Direct dissociation:

$$C_2H_2 + h\upsilon\ (> 5.8\ eV) \rightarrow C_2H\cdot + H\cdot \qquad (6\text{-}1)$$

(ii) The formation of an excited metastable molecule, which has a relatively long lifetime (≤ 1 ms) with respect to dissociation:[154-156]

$$C_2H_2 + h\upsilon\ (> 5.8\ eV) \rightarrow C_2H_2^* \qquad (6\text{-}2)$$

Formation of organic coatings can either occur through recombination of the created radicals in reaction (6-1), or through collisions of the metastable molecule with ground-state C_2H_2 (excited molecule mode polymerization):[154, 158]

$$C_2H_2^* + C_2H_2 \rightarrow C_4H_4^* \qquad (6\text{-}3)$$

$$C_4H_4^* + C_2H_2 \rightarrow C_6H_6^*, etc. \qquad (6\text{-}4)$$

Collisions of an excited molecule with either the walls or ground-state C_2H_2 can lead to chain-terminating reactions, but can also result in the formation of stable molecules.

Although the same primary processes have been reported for all wavelengths of interest, the quantum yields of reactions (6-1) and (6-2) depend not only on λ, but also on pressure, *p*. The quantum yield is of interest, since it influences the route of coating formation.[158, 159] At λ=123.6 and 147.0 nm and low *p* (<106 Pa=0.8 Torr), the quantum yield of reaction (6-1) is high, and direct dissociation is immediate.[121, 157, 160] At low *p*, continuous absorption of photons by the restricted number of C_2H_2 molecules leads to direct dissociation. As *p* increases and more C_2H_2 molecules are available, the creation of an excited state (reaction (6-2)) becomes more important since not all molecules can continuously absorb the available photons. As reaction (6-2) becomes more important, deactivation and/or collisions of the excited molecule with ground-state C_2H_2 can lead to formation of major photochemical (stable) products, namely diacetylene, ethylene, hydrogen, and small amounts of vinylacetylene and benzene.[121, 157, 160] At λ=172.0 and 184.9 nm and low *p* (<106 Pa=0.8 Torr), the quantum yield of reaction (6-1) was reported to be 1/5 as large as at the above-mentioned shorter λ values, indicating that direct dissociation is less important.[161] Therefore, deactivation of $C_2H_2^*$ at the reactor walls is more probable than further reactions that could lead to coating formation. With increasing *p*, more collisions occur, reaction (6-1) becomes more significant, and deactivation less relevant through higher probability of radical creation; thus, increased polymer formation can be observed.[161] Due to this particular photolytic behavior of

C_2H_2, not only λ but also *p* needs to be considered in order to account for quantity of organic coating formation. Based on these theoretical considerations and experimental trials, a rather high *p* value (*p*=400 Pa=3 Torr) was chosen in this work as a compromise, so as to obtain appreciable coatings formation at all of the λ values investigated.

Hydrogen sulfide, H_2S, the second gaseous reagent in this study, strongly absorbs in the 120-250 nm VUV spectral range (Figure 6-1). Upon absorption at λ<309 nm, direct photolysis occurs leading to cleavage of the H-SH bond:[162, 163]

$$H_2S + h\upsilon\ (> 4.0\ eV) \rightarrow SH\cdot + H\cdot \qquad (6\text{-}5)$$

Reaction (6-5) has been identified as the primary process for all λ of interest. Secondary reactions include the formation of H and S through the reaction of the created radicals with each other or with H_2S.

Formation of polymer-like sulfur-rich thin films can occur through propagation of the excited states acetylenes (reactions (6-2) to (6-4)) or through thiol-yne chain reactions, initiated by the addition of SH· radicals, formed in reaction (6-5), to acetylene:

$$SH\cdot + C_2H_2 \rightarrow HS - CH = CH\cdot \qquad (6\text{-}6)$$

$$HS - CH = CH\cdot + H_2S \rightarrow HS - CH = CH_2 + SH\cdot \qquad (6\text{-}7)$$

The product of reaction (6-7) can further react with SH· radicals forming even larger chains that can be incorporated into the organic coatings.

6.3 Experimental Section

6.3.1 VUV photo-polymerization

The experimental set-up used for VUV photo-chemical experiments (Figure 6-2) was based on the design developed by Truica-Marasescu et al.[20, 119, 127, 135], and was similar to the one used in our earlier work.[233]

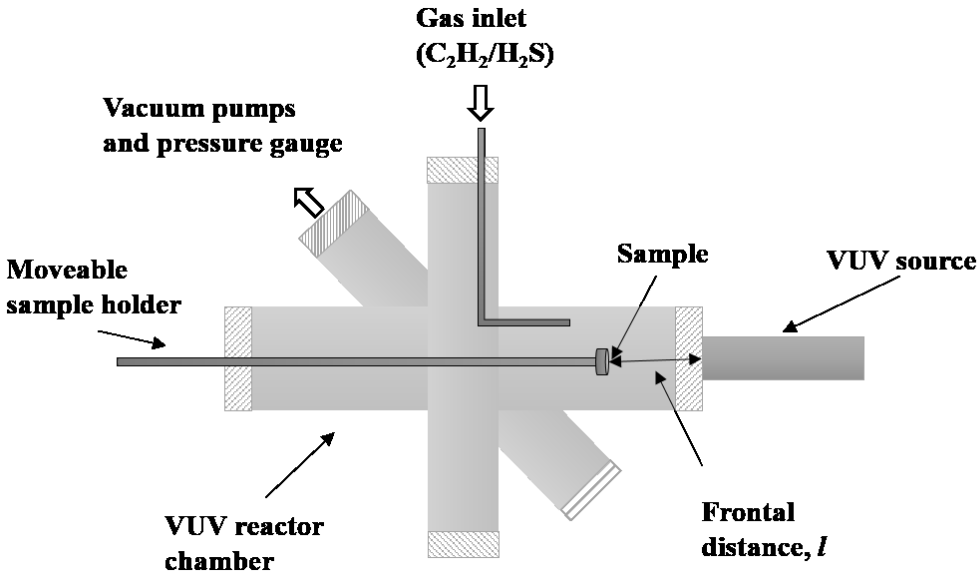

Figure 6-2: Cross section of the vacuum ultra-violet (VUV) photo-chemical reactor chamber used for depositing thiol-terminated organic thin films.

Briefly, it consisted of a stainless steel six-way cross chamber, evacuated to low p (base pressure $p < 10^{-6}$ Pa=7.5·10^{-8} Torr) using a turbo-molecular pump in tandem with a two-stage rotary vane pump. The operating pressure was maintained at p=400 Pa=3 Torr. The flow rate of the hydrocarbon, C_2H_2 (99.6%, MEGS Inc., Montreal, QC, Canada), $F_{(C2H2)}$, was kept constant at 10 sccm using a mass flow controller (Brooks Instruments, Hatfield, PA, USA), while that of H_2S (99.5%, MEGS Inc., Montreal, QC, Canada), $F_{(H2S)}$, was varied between 0 and 10 sccm; this yielded values of the gas mixture ratio R ($=\frac{F_{(H2S)}}{F_{(C2H2)}}$) ranging from 0 to 1. The purity of C_2H_2, which is commonly supplied

dissolved in acetone in bottles filled with a porous medium,[244] was assured by connecting the reservoir to a C_2H_2 filter (Balston 95A-1/4 Acetylene Filter, Parker, Haverhill, MA, USA). The removal of acetone from C_2H_2 was important since acetone is photochemically active at the wavelengths used in this study and could contribute to the formation of the organic coatings.[254] A removal efficiency of 70 % was achieved with the above-mentioned filter. Polymer-like[216] coatings resulting from the photo-chemical reactions, hereafter designated "UV-PA:S" (for "ultraviolet-polymerized sulfurized acetylene"), were deposited on 500 µm-thick (100) p-type silicon wafers (University Wafer, Boston, MA,USA).

Four different VUV sources were used in the present λ-dependent study to deposit UV-PA:S films, namely a low-pressure mercury (Hg) lamp (STER-L-RAY®, Hauppauge, NY, USA) and three non-coherent commercial resonant or excimer noble gas VUV lamps (Resonance Ltd., Barrie, ON, Canada), based on an electrodeless radio-frequency (r.f., 100 MHz)-powered discharge. Depending on the particular lamp, noble gas such as Krypton (Kr) or Xenon (Xe) is sealed into a high-grade Pyrex ampoule with a MgF_2 window (cut-off wavelength, λ=112 nm), as described in detail elsewhere.[20, 119, 135] The spectral characteristics of the different VUV sources are summarized in Figure 6-3 and Table 6-2. Compared to the "Resonance" sources, the Hg lamp shows several emission lines, the most pronounced being at λ=253.7 nm. However, only the emission at λ=184.9 nm was of importance in this work based on $k(\lambda)$ of the two precursor gases, and it represents about 7% of the lamps' total output, $I_{184.9\ nm,\ 5.08\ cm,\ air}$ =177 µW/cm^2. In order to integrate this lamp to the VUV reactor chamber, it was placed in front of a flanged fused silica window, which assured good vacuum in the reactor chamber.

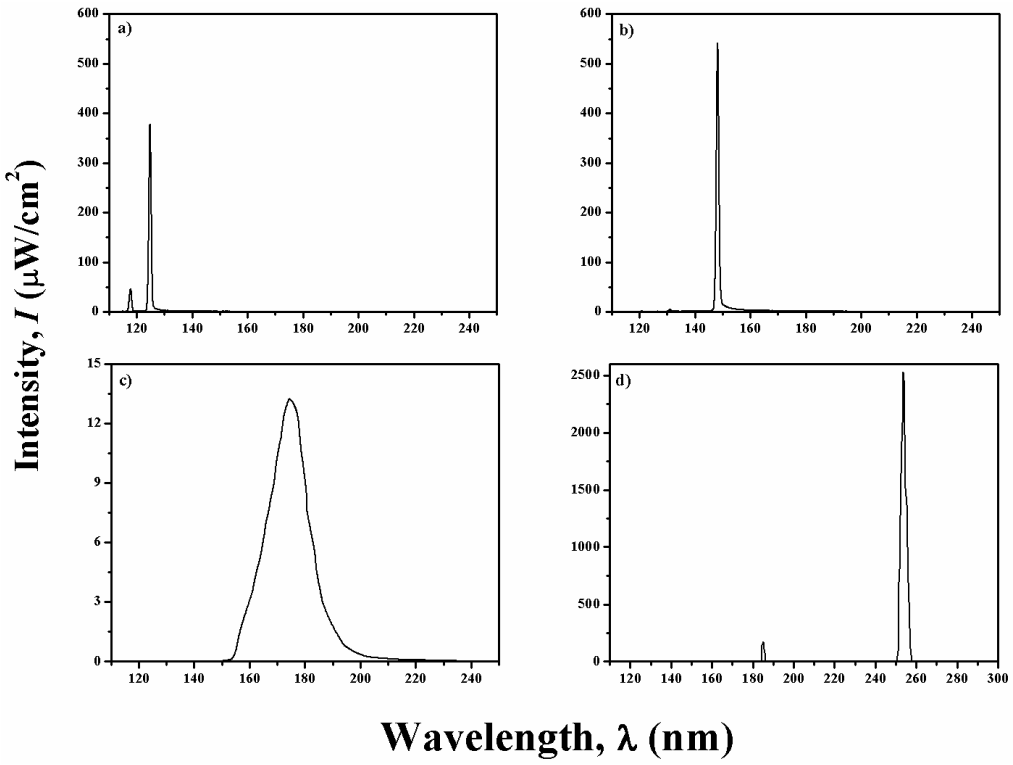

Figure 6-3: Intensities and spectral distributions of the VUV radiation emitted by the a) resonant Kr; b) resonant Xe; c) Xe excimer (as measured by Truica et al.[20, 127, 135] at d=6 cm under high vacuum); and d) Hg lamps (spectrum obtained from the manufacturer, corresponding to d=5.08 cm[255] in air).

Table 6-2: Characteristics of the VUV sources used, measured under high vacuum at the respective frontal distances, *d* (see text).

Lamp	Peak Wavelength, λ_{peak} (nm)	Photon Energy, E_p (eV)	Photon Flux, Φ (ph/cm^2/s)
KrL	123.6	10.0	$1.4 \cdot 10^{15}$
XeL	147.0	8.4	$2.5 \cdot 10^{15}$
XeE	172.0	7.2	$6.3 \cdot 10^{14}$
Hg	184.9	6.7	$7.1 \cdot 10^{15}$

The c-Si substrates were mounted on a stainless-steel sample holder, which could be moved axially within the VUV reactor chamber, to frontal distances of d_{KrL}=0.9 cm, d_{XeL}=0.9 cm, and d_{XeE}=0.7 cm. Varying d between the substrate and the VUV source allowed us to vary the photon flux, Φ, impinging on the gas mixture in the gap. In the case of the Hg source, the lamp was moved to d_{Hg}=8.0 cm away from the fused silica window, behind which the c-Si substrate was placed. This allowed us to achieve comparable experimental Φ values (see Table 2) while guaranteeing deposit creation on the c-Si substrates. Earlier work by Truica et al.[20, 127, 135] had shown that a $\Phi \sim d^{-2}$ relationship quite closely applied to the "Resonance" lamps at the sample holder/substrate, even though these were far from being "point-sources". To determine Φ, the photocurrent, i, of each source was measured at different d from the respective source under high vacuum inside the chamber, using two NIST-calibrated photodiodes (Resonance Ltd., Barrie, ON, Canada). This allowed us to obtain Φ as a function of d and thus to determine the above-mentioned distances for each source at which comparable photon fluxes would act at the position of the c-Si substrates. Coatings of comparable thicknesses (~ 50 nm) were obtained by varying the treatment duration between 1 and 5 h (depending on the VUV source and gas mixture ratio).

For reasons of safety in handling the toxic H_2S, the experimental chamber was housed inside a N_2-filled glovebox; this had the additional benefit of inhibiting oxygen-exposure and "aging" of the freshly-deposited UV-PA:S films when the chamber was opened.

6.3.2 Characterization studies

6.3.2.1 X-ray photoelectron spectroscopy

All deposits were characterized by X-ray photoelectron spectroscopy (XPS), performed in a Thermo Scientific K-Alpha^{TM} instrument (Waltham, MA, USA) using monochromatic Al Kα radiation (hv=1486.6 eV). The samples were mounted onto a vacuum transfer module (VTM, Thermo Scientific K-Alpha^{TM}) inside the glovebox and directly transferred to the instrument without exposure to air; this allowed us to determine the UV-PA:S films' native chemical composition without exposure to atmospheric O_2. The elemental compositions (in atomic %, at. %) and chemical environments of the constituent elements were obtained by survey- and high-resolution (HR) spectra, respectively. The former were acquired at a pass energy of 160 eV, a dwell time of 200 ms and energy steps of 1 eV, the latter at pass energy of 20 eV, dwell time of 200 ms and energy steps of 0.1 eV. No evidence of X-ray induced damage was observed, based on measurements of the C1s peaks before and after analyses. Spectra were acquired at 0° emission angles, and possible charging was corrected by referencing all peaks to the HR C1s peak at binding energy (BE) = 285.0 eV. The constituent elements were quantified from the broad-scan spectra using CasaXPS v2.3.16 (CasaSoftware Ltd., Teignmouth, England), by integrating the areas under relevant peaks after a Shirley-type background subtraction, and by using sensitivity factors from the Wagner table.[256] Throughout this study, we refer to the atomic sulfur concentration, [S], of UV-PA:S coatings; however, since hydrogen atoms cannot be detected by XPS, [S] is approximated by:

$$[S] = \frac{S}{S + O + C} \times 100 \qquad (6\text{-}8)$$

6.3.2.2 Chemical derivatization with N-ethylmaleimide

Chemical derivatization with *N*-ethylmaleimide (98%, BioShop Canada Inc., Burlington, ON, Canada) was used to quantify thiol concentrations, [SH], as recently described by Thiry et al.[94] The reaction mechanism is shown in Scheme 6-1, where *N*-ethylmaleimide reacts selectively with SH via nucleophilic addition between the S atom and the double bond in the maleimide structure (thiol-ene click reaction), forming a stable thio-ether bond. The thiol-maleimide reaction offers several advantages, including high selectivity in the presence of multiple functional groups, rapid and quantitative conversion at low thiol concentrations, and high stability in aqueous environments.[257]

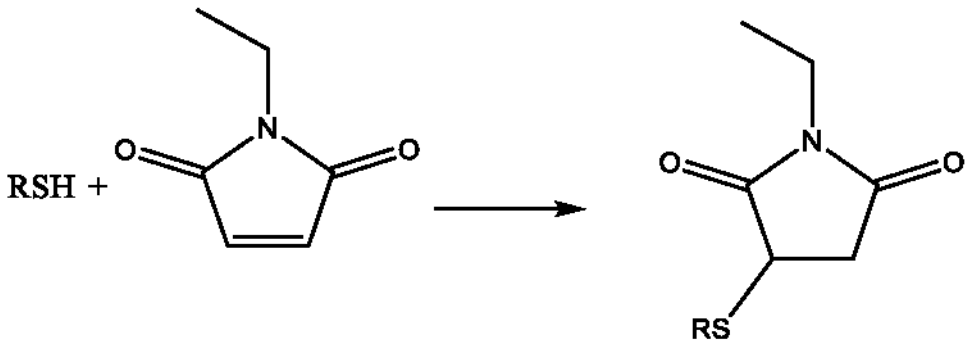

Scheme 6-1: Derivatization reaction between a thiol group and N-ethylmaleimide.

The derivatization reaction was carried out in phosphate buffer solution at pH=7, the *N*-ethylmaleimide concentration being fixed at 0.1 M. Since free thiol functionalities are sensitive towards oxidation upon exposure to oxygen,[38, 258] the samples were mounted into closed vials, equipped with a septum, before removal from the glovebox, thereby eliminating possible exposure to air. The derivatization solution was then injected through the septum and the samples were kept immersed in this solution for 78 h, following which they were rinsed in clean solution for 5 min to eliminate any unreacted molecules, then finally dried under a flow of dry nitrogen. XPS survey

spectra were obtained before and after derivatization, allowing nitrogen, [N], and carbon, [C], concentrations to be quantified; [SH], was then calculated as follows:

$$[SH] = \frac{[N]}{[C] - 6[N]} \times 100\ (\%) \quad (6\text{-}9)$$

6.3.2.3 Profilometry

The coating thickness, *T*, was measured by scratching down to the c-Si substrate using a sharp needle. The resulting step height was measured with a Dektak XTTM Stylus Profilometer (Bruker, Tucson, AZ, USA), using a diamond tip and an applied force of 3 mg. The measured *T* was used to determine deposition rates, *r* (nm/min), which in turn were used to determine the normalized deposition rates shown in Figure 6-5, using the respective photon flux of each source listed in Table 2.

6.3.2.4 Atomic Force Microscopy

The surface morphology of the films was investigated by atomic force microscopy (AFM) using a MFP-3D instrument (Asylum Research, Santa Barbara, CA, USA). All samples were measured in tapping mode using silicon cantilevers (ACTA model, AppNano) with a nominal spring constant of 37 N/m, nominal resonant frequency of 300 kHz, and nominal tip radius of 6 nm. Gwyddion 2.48 software was used to process the AFM images.

6.4 Results and Discussion

6.4.1 Deposition kinetics

As explained in the section entitled *Wavelength-dependent photolysis of C_2H_2 and H_2S*, the photo-dissociation and therefore deposition was dependent on *k* (λ) of the individual

precursor gases. However, when considering mixtures as in this present study, *k(λ)* must first be used to calculate absorption coefficients of the gas mixtures, α, considering the mixture ratios , $R = \frac{F(H_2S)}{F(C_2H_2)}$, the intensity of the sources, *I*, and the pressure, *p*. Truica et al.[10, 119] reported the following equation to calculate α:

$$\alpha = \int \left(\frac{1}{R+1}k(\lambda)_{C2H2} + \frac{R}{R+1}k(\lambda)_{H2S}\right)\frac{I(\lambda)}{\int I(\lambda)d\lambda}pd\lambda \quad (6\text{-}10)$$

where $\frac{I(\lambda)}{\int I(\lambda)d\lambda}$ is the relative contribution (in %) of each λ value in the overall emission spectrum of the respective source, and *p* the gas pressure (here kept constant at 400 Pa=3 Torr).

The calculated absorption coefficients of the H_2S/C_2H_2 mixtures, α, as a function of *R* are presented in Figure 6-4.

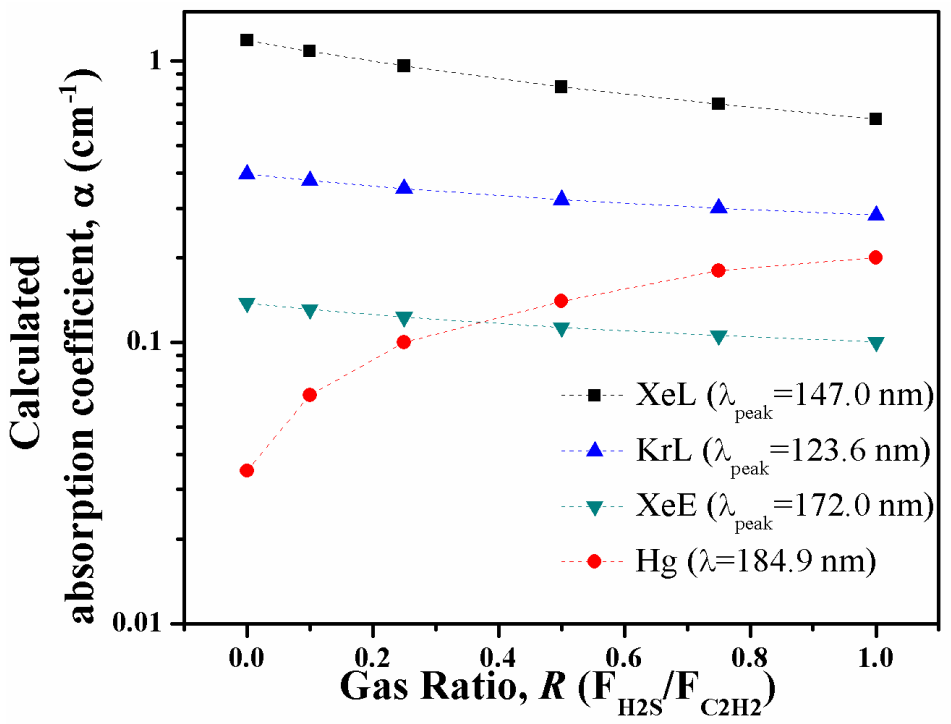

Figure 6-4: Calculated absorption coefficients, α (in cm^{-1}), calculated using equation (6-7) for H_2S/C_2H_2 gas mixtures; the corresponding wavelengths are those of the XeL (squares), KrL (triangles), XeE (upside down triangles), Hg (circles) VUV sources.

Calculated α values of the H_2S/C_2H_2 mixtures are seen to vary significantly for the different λ, being highest at λ=147.0 nm, followed by λ=123.6 nm, λ=172.0 nm, and λ=184.9 nm, respectively. Based on this, one would expect substantial differences in the photo-induced deposition kinetics at different λ. This was indeed the case, Figure 6-5, where deposition rates normalized with respect to photon flux, r/Φ, are seen to have followed the same trend as α. The ratio r/Φ is being considered, so as to remove

possible dependence of r on the number of photons, in other words, focusing only on the λ–dependence.

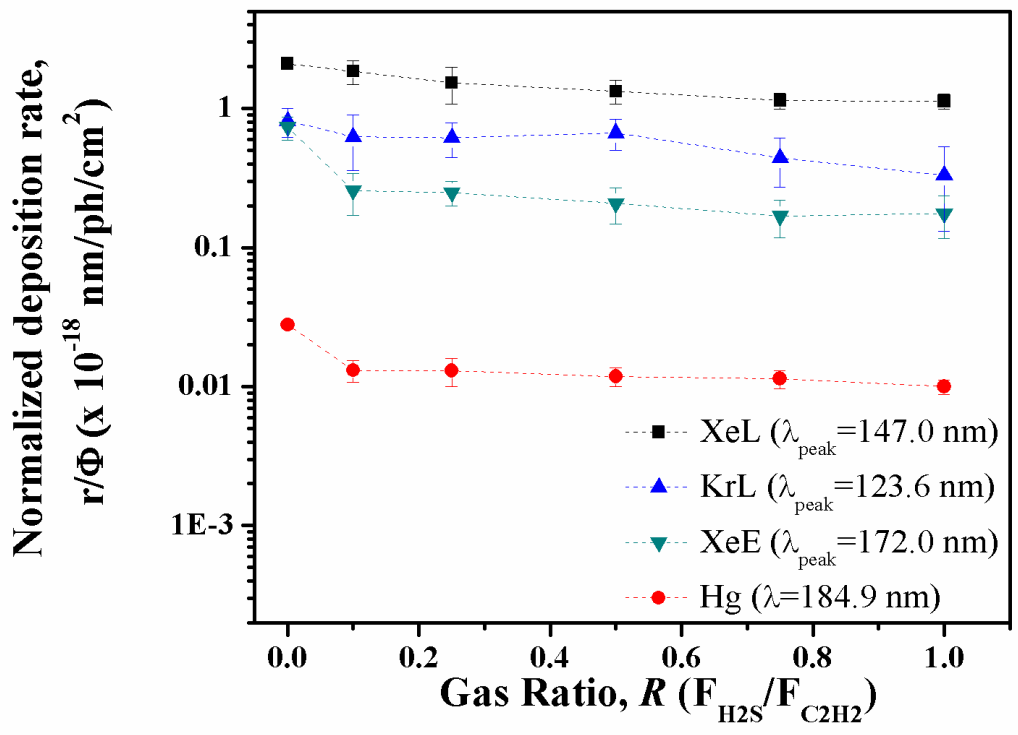

Figure 6-5: Normalized deposition rates, r/Φ, as a function of gas mixture ratio, R, for UV-PA:S films deposited using the XeL (squares), KrL (triangles), XeE (upside down triangles), Hg (circles) sources. The values of r are normalized with respect to photon flux, Φ. Error bars indicate 95% confidence interval. The lines are to guide the reader's eye.

Overall, *r/Φ* values are seen to have decreased with rising *R*, for XeL from 2.1 (*R*=0) to 1.1x10^{-18} nm/ph/cm^2 (*R*=1); from 0.8 to 0.3 x10^{-18} nm/ph/cm^2 for KrL; from 0.7 to 0.2 x10^{-18} nm/ph/cm^2 for XeE; and from 0.03 to 0.01 x10^{-18} nm/ph/cm^2 for Hg. This comes as no surprise, since, except for Hg, all α values decreased with rising *R*. For Hg, an increase in α was due to higher *k* of H_2S at λ=184.9 nm. The overall rate at which precursor radicals were produced decreased with increasing *R*, which also reduced the relative concentration of C_xH_y· radicals, and thereby also the formation of

UV-PA:S.[10, 20, 119] Furthermore, increasing *R* also gave rise to a greater concentration of reactive H atoms, leading to competing etching reactions, hence to the decrease in r/Φ for all four VUV sources.[10, 233]

It is noteworthy that pure acetylene-based, amorphous carbon films (R=0) had been obtained in the past through PICVD by Danno et al.[259] using a low-pressure Hg lamp. The carbon films were deposited at elevated temperatures (150 and 300°C), under conditions resulting in r/Φ values of $1.8\text{x}10^{-17}$ nm/ph/cm^2 and $7.2\text{x}10^{-18}$ nm/ph/cm^2, respectively, compared to $3\text{x}10^{-20}$ nm/ph/cm^2 in the present work (at room temperature). Differences between setup geometries and process parameters (even though Danno also used p=400 Pa= 3 Torr) could help explain the higher deposition rates obtained by the Japanese authors.

6.4.2 Chemical composition of deposited UV-PA:S films

Chemical compositions, more particularly [S] as a function of *R*, are seen to have displayed different trends among the four different UV-PA:S film families (Figure 6-6). An example of an XPS survey spectrum, which was used to obtain [S], is demonstrated in Figure 8-4 in Appendix B.

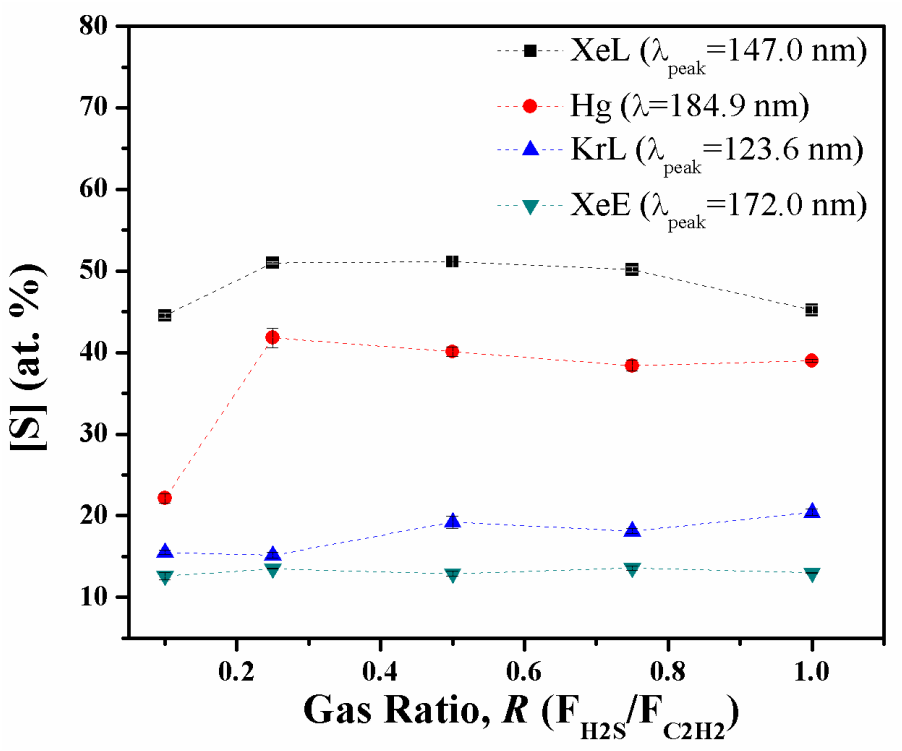

Figure 6-6: Sulfur concentrations, [S] (in at.- %) of UV-PA:S films deposited using XeL (squares), KrL (triangles), XeE (upside down triangles), Hg (circles) VUV sources, as a function of gas mixture ratio, R. The lines are to guide the reader's eye.

On the basis of Figure 6-1 and Table 6-1, the highest $k(\lambda)$ values of H_2S at λ=184.9 nm might lead one to expect the highest [S] for the case of the Hg VUV lamp, but the most efficient S-incorporation in fact was observed for XeL. In order to incorporate S-containing groups into UV-PA:S, the polymer-like backbone needs to be created first and foremost. For the case of XeL the probability of $C_xH_y\cdot$ radical creation by photo-dissociation of C_2H_2 was obviously high, thereby possibly also allowing higher incorporation of S. However, for the case of the Hg source, the rate of creating $C_xH_y\cdot$ radicals was much smaller, even though the possibility of S incorporation was higher Tentatively, this would explain why [S] ~ 50 and ~ 40 at.% for the XeL and Hg lamps, respectively, as observed in Figure 6-6. In terms of possible reaction mechanisms, if only "pure" thiol-yne chain reactions ((6-6) and (6-7)) would take place, a film

composition of $(SCH_2CH_2)_n$, resulting in [S]=33 at.% could be expected. However, since [S]>33 at.% (in the case of the Hg and XeL sources), we can assume that this is not the only formation mechanism. Many subsequent reactions are possible, resulting in a broad product distribution. Contrary to trends of increasing heteroatom concentration (here: S) with rising *R* values reported in the literature and in our previous work,[10, 83, 233] Figure 6-6 did not bear witness to such an increase in [S]. Here, [S] of the UV-PA:S films tended to rise between *R*=0.1 and 0.25, but it then remained nearly constant when *R* further increased. We attribute this to the higher pressure (*p*=400 Pa=3 Torr) used in the present experiments, compared to *p* « 133 Pa=1 Torr in previous studies. In an attempt to better understand this rather unusual behavior noted in Figure 6-6, UV-PA:S films were deposited at *p*=13 Pa=0.1 and 133 Pa=1 Torr using only the KrL and XeL VUV sources (Figure 6-7). Only these two yielded sufficiently high *r* values at the lower *p*, due to the dependence of quantum yield on *p* discussed in the earlier section entitled *Wavelength-dependent photolysis of C_2H_2 and H_2S.*

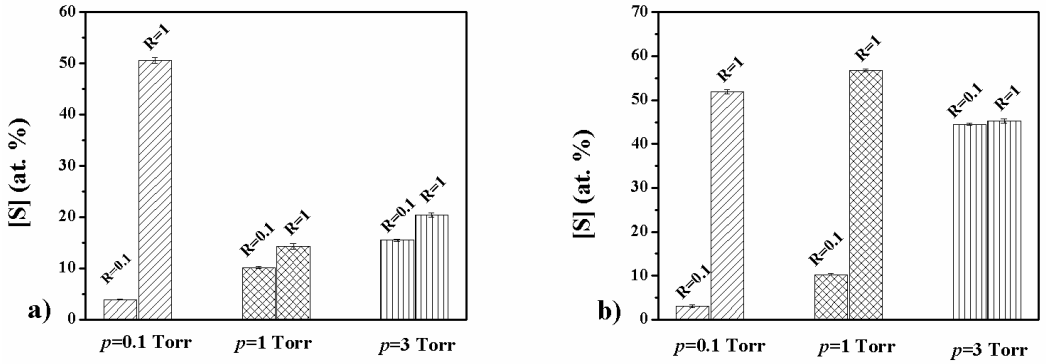

Figure 6-7: Sulfur concentrations, [S] (in at.- %), for UV-PA:S films deposited using the a) KrL and b) XeL VUV sources at three different pressures (p=13, 133, and 400 Pa=0.1, 1 and 3 Torr) and two gas mixture ratios (R=0.1 and 1).

At low *p* (*p*=13 Pa=0.1 Torr), a dramatic increase in [S] with rising *R* was observed, as also reported in the literature and in our own previous work. As *p* increased, numbers

of molecular collisions of course also increased, leading to more S-bearing reactive species and more sulfur incorporation into the films. In Figure 6-7, [S] values at R=1 and lower p were seen to significantly exceed those at higher p, especially for XeL radiation, while at p=400 Pa=3 Torr [S] values were almost independent of R, as observed in Figure 6-6.

Changing p could also lead to transitions among different flow regimes, of which one can distinguish three, depending on p and on geometry: these are molecular, continuum and transition flows. They can be quantitatively distinguished by their respective dimensionless Knudsen numbers, K_n:

$$K_n = \frac{l}{d} \tag{6-11}$$

where l is the molecular mean free path and d a characteristic length of the experimental apparatus; in this case we chose d to be the distance between lamp and substrate where deposition occurred. Mean free path, l, the average distance between collisions among gas molecules, is given by[260, 261]

$$l = \frac{k_B T}{\sqrt{2}\sigma p} = \frac{k_B T}{\sqrt{2}\pi \left(\frac{1}{2}d_1 + \frac{1}{2}d_2\right)^2 p_1 p_2} \tag{6-12}$$

for the case of gas mixtures with dissimilar particles. In equation (6-12), k_B is Boltzmann's constant, T the temperature, σ the collisional cross-section, and p the pressure. To consider collisions between the dissimilar particles here, the molecular diameters of H_2S (d_1=3.6·10^{-10} m) and of C_2H_2 (d_2=3.3·10^{-10} m), and their partial pressures (p_1 and p_2) need to be considered. Knudsen numbers, K_n<0.01 describe continuum flow, whereas K_n>1 represent molecular or discrete particle flow. Between those values both gas-gas and gas-wall collisions are important, and the flow regime is

termed transition or slip flow.[260-262] Here, the two mixture ratios (R=0.1 and 1) and three different pressures (p=13, 133 and 400 Pa=0.1, 1 and 3 Torr) yielded K_n ~0.1 at p=13 Pa=0.1; ~0.001 at p=133 Pa=1 Torr; and ~$5 \cdot 10^{-5}$ at p=400 Pa=3 Torr (see Appendix B for detailed calculations). Therefore, we have observed a shift between transition and continuum flow regimes. As p increased and transition towards continuum flow occurred, collisions gained in importance, transition towards continuum flow being observed between p=13 and 133 Pa (=0.1 and 1 Torr) ($K_n << 0.01$). We propose that this transition may explain the different [S] versus R behaviors observed in Figure 6-6 and Figure 6-7. Such a dependence of chemical composition on p is an important observation, one which to the authors' knowledge has so far not yet been reported in connection with transitions among flow regimes. This aspect of very different heteroatom incorporation rates may well need to be taken into consideration when in future designing new CVD processes.

Because [S] does not reveal in what functional form this element was incorporated in the UV-PA:S films, the selective and quantitative derivatization reaction based on *N*-ethylmaleimide was used to determine [SH], as shown in Figure 6-8. A typical XPS survey spectrum obtained after the derivatization reaction is shown in Figure 8-4 in Appendix B.

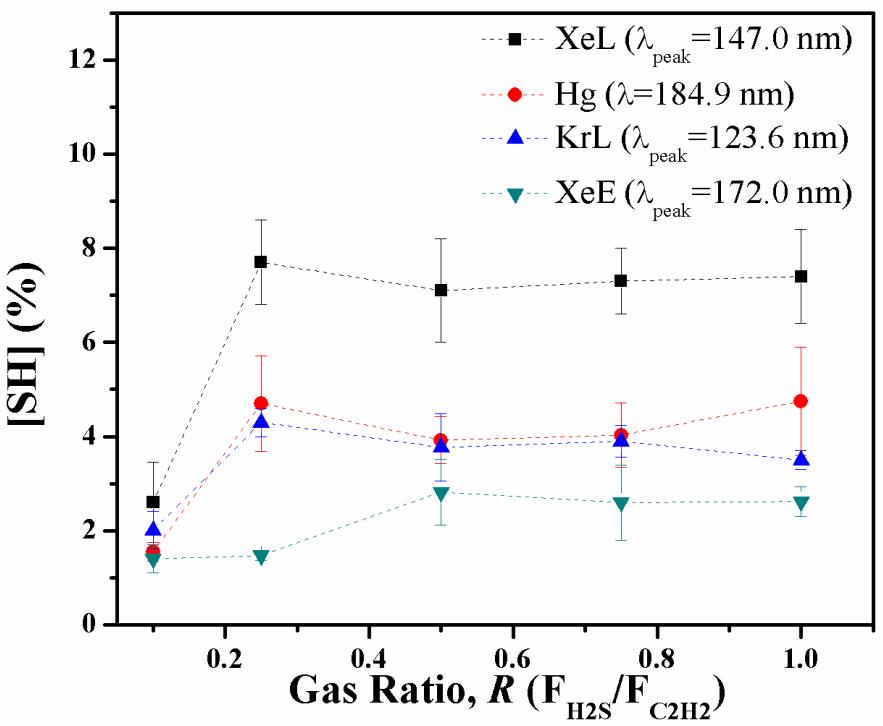

Figure 6-8: Proportion of C bearing -SH groups, [SH] (in %), determined using chemical derivatization XPS for UV-PA:S films based on XeL (squares), KrL (triangles), XeE (upside down triangles), Hg (circles) VUV sources, versus gas mixture ratio, R. Error bars show standard deviations of three measurements. The lines are to guide the reader's eye.

This plot of [SH] versus *R* displays similar trends as that of [S] versus *R* in Figure 6-6, the highest incorporation of thiol groups having occurred for the case of XeL-based deposits, followed by Hg, KrL and XeE ones. Following an initial increase in [SH] between *R*=0.1 and 0.25, [SH] values are seen to have remained nearly constant. These UV-PA:S films, especially in the case of XeL, were much richer in SH groups than their L-PPA:S ("low-pressure plasma-polymerized, sulfurized acetylene") counterparts, reported in our previous study;[263] here, [SH] values up to ~7.7 % were achieved by photo-polymerization, in sharp contrast with the maximum of only ~3.4 % for L-PPA:S. This was not only the case for the present gas mixtures, but also for a single molecule precursor, propanethiol, where a maximum [SH] of ~5 % was

obtained.[94] It is noteworthy that comparable [SH] (~5 %) was achieved using the Hg lamp, far more affordable and readily available than the other three VUV sources used here.

The observed higher photochemical [SH] values for UV-PA:S films compared with their plasma-chemical L-PPA:S counterparts is not entirely surprising, because this has already been observed and reported for N- and O-rich films.[10, 119] Indeed, Truica reported UV-PE:N deposits with up to more than 70 % [-NH_2] concentration (versus roughly 30 % for L-PPE:N) when using C_2H_4-NH_3 reagent gas mixtures. In low-pressure plasma, the gaseous precursors are subjected to many collisions with "hot" electrons that possess Boltzmann-like energy distribution. However, as stated earlier, photolysis of H_2S creates only SH· radicals, which react with hydrocarbon radicals under much lesser disruption than in a discharge plasma. For this reason [SH] values for the XeL-based UV-PA:S were the highest ones reported in the literature so far for any preparation method or type of precursor. They greatly exceeded ones previously reported (up to ~1.75 %),[233] where photo-polymerized S-containing films were prepared using mixtures of C_2H_4 or butadiene (C_4H_6) with H_2S using the KrL source. Beside the selective and specific VUV-photochemical reactions via the present gas mixtures, a further reason for the high [SH] can be attributed to the exclusion of oxygen during derivatization, i.e. no oxidation of free thiol groups. To the authors' best knowledge such air-excluding derivatization had not been reported before, but it can evidently have contributed significantly to increased retention of SH-groups.

While stability studies were beyond the scope of the present work, previous studies suggest that these photo-derived films should be stable in aqueous media, suitable for further applications.[10, 233, 263]

6.4.3 Surface morphology

Growth mechanisms and resulting surface-topological features are also known to affect the performance of thin coatings for biomaterial uses.[179, 181] In designing new biomaterials, it is critically important to consider how cells respond to specific surface-chemical and -topographical features. Therefore, we have examined the surface morphologies of UV-PA:S films deposited using the four different VUV sources at *R*=0.1 and *R*=1, see Figure 6-9.

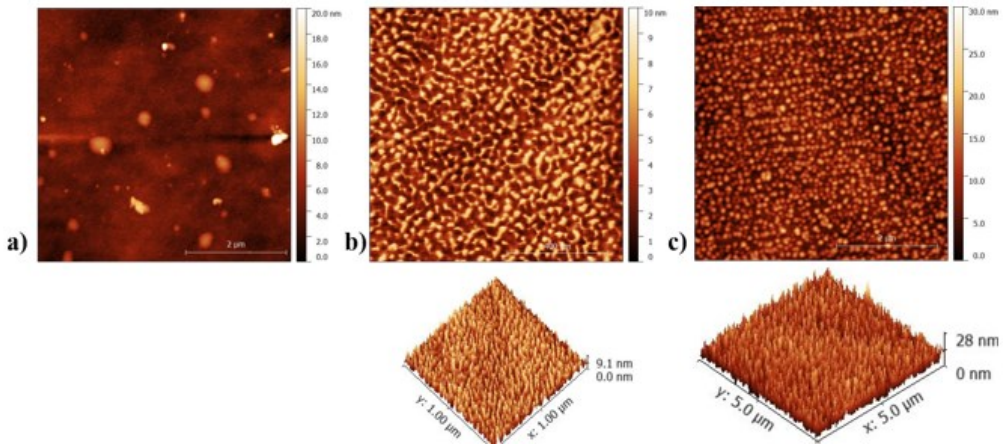

Figure 6-9: Atomic force microscopy topography images of UV-PA:S films deposited using the KrL VUV source at a) R=0.1 (5x5 μm²); b) R=0.1 (1x1 μm²); and (c) R=1 (1x1 μm²). The bottom images represent 3D portrayals of the respective surfaces.

At lower magnification (5x5 μm², Figure 6-9a)), the *R*=0.1 film appeared smooth , but at higher magnification (i.e. smaller area, 1x1 μm²) the AFM images reveal a rougher surface with island-like features up to ~4 nm in height (Figure 6-9b)). These were more pronounced at *R*=1 and were seen to grow in height up to ~14 nm (Figure 6-9c)): The films' RMS roughness increased with rising *R*, from ~1.5 nm to ca. 5.4 nm. Similar island-like features with increasing *R* were also observed for the other VUV sources. For example, Figure 6-10 represents UV-PA:S films obtained with the Hg source, from

which we conclude that surface morphology of UV-PA:S was essentially independent of λ, but that it was strongly influenced by *R*.

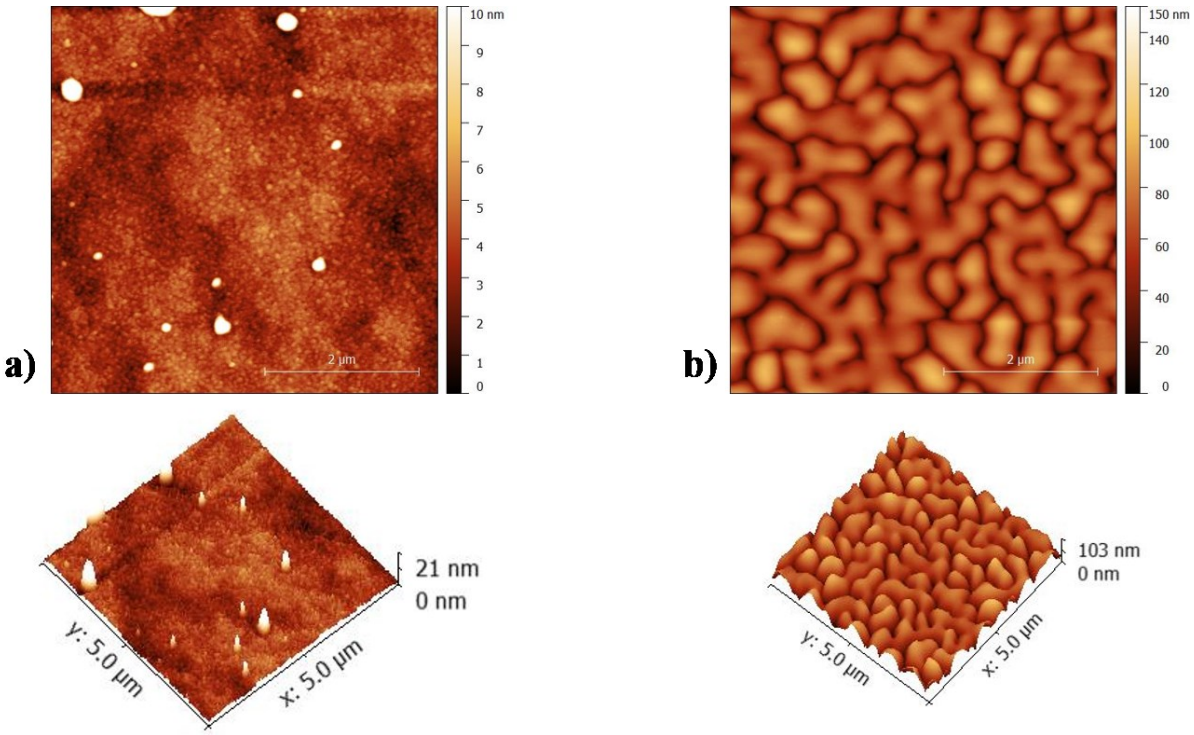

Figure 6-10: Atomic force microscopy topography images of UV-PA:S films deposited using the Hg VUV source at a) R=0.1 (5x5 µm²); and b) R=1 (5x5 µm²). The bottom images represent 3D portrayals of the respective surfaces.

Plasma polymers with diverse surface topographies are well known in the literature.[179, 182, 183, 264] UV-PA:S appears to present Volmer-Weber growth morphology, where incoming film-forming precursors have more affinity for one another than for the (c-Si) substrate surface. As a result, they tend to form clusters which grow into 3D islands that can eventually coalesce and merge into a continuous film.[181, 182, 265] In terms of surface energy, γ, the deposit tends to form islands minimizing its surface, if its γ is significantly different from that of the underlying substrate, since no intermolecular

interactions with the substrate occur. From this, we could infer that the surface energy of the UV-PA:S films deviates from γ of the substrate with rising *R* and thus with [S].

6.5 Summary and Conclusions

PICVD techniques have been gaining interest over the past years, for example for selective, specific organic surface functionalization. Simply by selecting different photon energies (i.e. values of λ), thin films with different properties could be obtained in this present work. Although different VUV photon energies could be useful in surface engineering, very few wavelength (λ)-dependent deposition studies had been carried out so far. The present study aimed to understand λ-dependent deposition of thiol-terminated films using four different VUV sources covering roughly 123 nm ≤ λ ≤ 185 nm. We have shown that UV-PA:S coatings could be successfully deposited by VUV irradiation of acetylene (C_2H_2) / hydrogen sulfide (H_2S) mixtures, growth rates and properties of the resulting films being highly λ-dependent. The results clearly showed that photolytic reactions of C_2H_2 and H_2S are governed by the gases' absorption coefficients, $k(\lambda)$, obviously also that of the H_2S/C_2H_2 gas mixtures, α. The latter was found to be highest for the XeL VUV source, and was found to yield the highest sulfur, [S], and thiol, [SH], concentrations. [SH] values reported here are the highest in the literature so far, a good choice if high [SH] are desired for further (biomedical) applications. Slightly lower [SH] (~5%) were obtained with the more economic and readily accessible Hg lamp. The importance of pressure, *p*, another key CVD process parameter was also amply demonstrated in the section entitled *Wavelength-dependent photolysis of C_2H_2 and H_2S*. This was especially evident from the [S] versus *R* dependence: surprisingly, at the relatively high *p*=400 Pa=3 Torr, used here, [S] remained nearly constant with *R* contrary to all previous studies by others and by

ourselves.[10, 77, 83, 233] Independent of λ, UV-PA:S deposits showed island-like growth morphology, more pronounced with increasing [S].

In summary, this λ-dependent VUV photo-deposition study demonstrated the importance of single, well-characterized VUV sources for selective and specific deposition of organic coatings. This UV-PA:S deposition technique can be useful for creating optimized films with desired biomedical properties simply by adjusting the source's wavelength.

Acknowledgments

The authors gratefully acknowledge financial support from McGill University (MEDA), from the *Fonds de recherche du Québec en nature et technologies* (FRQNT), and *Plasma-Québec*; from the Natural Sciences and Engineering Research Council of Canada (NSERC) and the Canadian Foundation for Innovation (CFI).

Chapter 7 Conclusions and recommendations for future work

7.1 Summary

This body of work details novel syntheses of stable thiol (SH)-terminated organic coatings with high SH concentrations, which could potentially find use among others in biomedical applications. Reviewing the literature (Chapter 2), it is evident that SH-terminated materials are gaining importance due to their ability to covalently immobilize (bio)molecules via thiol-ene click reactions. The conventional synthesis of SH-terminated surfaces involves wet-chemical approaches, such as bulk polymerization, gas or acid sulfonation, or photochemical grafting. These wet-chemical approaches are found to be non-specific, lengthy, hazardous, and can degrade the substrate, making their fabrication challenging. Finding new fabrication methods that are simpler, faster, and more environmentally friendly was the main driver for the present work. Plasma enhanced chemical vapor deposition (PECVD) and photo-initiated CVD (PICVD) are viable synthesis alternatives, as they represent one-step, solvent free processes, in which the waste production and CO_2 emissions are reduced since all chemical reactions are driven using electricity. PECVD has been used in the past to produce SH-terminated organic coatings using single-molecule precursors already containing the desired SH functionality, such as allylmercaptan,[71, 88, 89] thiophene,[44, 51, 73, 90] and propanethiol.[72, 91-94] This approach can be beneficial in obtaining high concentrations of SH groups on the surfaces, however, it is limited in the number of process parameters available to tune the properties of the organic coatings. Even though some groups have obtained SH-terminated organic coating through PECVD, only Thiry et al. have reported a complete study combining plasma

diagnostics and plasma polymer synthesis, connecting the influence of different plasma process parameters on the chemical properties of propanethiol plasma polymers.[72, 91-93] In the present work we chose to use the "co-polymerization" approach, in which binary gas mixtures (BGMs) comprising a hydrocarbon and a sulfur-rich gas were used to create functional SH-terminated coatings. This approach allows to adjust the gas mixture ratio, *R,* enabling better fine-tuning of the films' properties.

Using both above-mentioned CVD techniques, SH-terminated surfaces were obtained through "co-polymerization" of BGMs comprising ethylene (C_2H_4) or 1,3-butadiene (C_4H_6) and hydrogen sulfide (H_2S) (see Chapter 4). Irrespective of the deposition technique, coatings were found to have very similar properties and remained stable after 24 h of immersion in water. However, contrary to our expectations and previous results from nitrogen- and oxygen-rich coatings, the plasma-based coatings were richer in SH compared to their VUV counterparts. Overall, the use of BGMs offers excellent control of the sulfur content, [S], flexibility over the desired [S] due to the ability to readily vary and control *R*, acceptable retention of SH functionalities in the films, and excellent stability towards dissolution in aqueous media and in air compared to the more traditional use of single-molecule precursors.

Deeper investigation of the growth mechanisms of a further BGM comprising acetylene (C_2H_2) and H_2S resulting in SH-terminated coatings revealed that in the case of BGMs pronounced precursor fragmentation at higher powers resulted in increased deposition rates, *r*, decreased [S], and increased SH concentrations, which was also confirmed by mass spectrometry measurements (see Chapter 5). All above-mentioned benefits related to the use of BGMs also applied in this second portion of the project. A comparison of the resulting SH-terminated coatings with coatings obtained from a single-molecule precursor (propanethiol) in a similar discharge demonstrated lower SH

concentrations on their surfaces. This result was unexpected as the use of a single-molecule precursor normally yields higher concentration of functional groups, as they are already present in the molecule.

The last part of this research focused on the implementation of a wavelength (λ)-dependent study, therefore broadening the initial work presented in Chapter 4, by using four photon energies (i.e. four VUV sources) to deposit SH-terminated organic coatings from the previously used BGM of C_2H_2 and H_2S (see Chapter 6). This work aimed to verify if the PICVD technique can be optimized in a sense that a material richer in SH can be obtained, as previously reported for nitrogen- and oxygen-rich organic coatings. By matching the absorption coefficients, *k*, of the precursor gases with the emission of the lamps, maximum amounts of active species, and therefore more SH on the surfaces, should be created. Indeed, different photon energies influenced the deposition kinetics and film composition, reflecting that photolytic reactions are governed by the gases' absorption profile. SH concentrations up to ~7.7 % were obtained, the highest reported in the literature to date. Overall, the presented λ-dependent photo-deposition study demonstrates the importance of single, well-characterized VUV sources for selective and specific deposition of organic coatings. This deposition technique can be useful for creating optimized films with desired biomedical properties.

This thesis aimed to investigate the formation of SH-terminated organic coatings from BGMs (comprising a hydrocarbon and a sulfur-rich gas) using two different CVD methods. The importance of process parameters when designing new functional organic coatings with desired properties was highlighted throughout this research. Especially *R* can be of great use in tuning the sulfur or SH concentrations. The results obtained during this study lay a foundation for understanding the

mechanisms occurring during different CVD methods leading to SH-terminated surfaces. With this, applications on the created SH-terminated organic coatings can now be tested.

7.2 Contribution to knowledge

As a result of the present work, various contributions to the field of surface engineering have been provided. In particular, the development of two new approaches to create SH-terminated surfaces with potential for biomedical applications.

The following original contributions to scientific knowledge resulted from this Ph.D. project:

- Creation and comparison of SH-terminated organic coatings using PECVD and PICVD techniques with tunable and controllable sulfur and SH concentrations from BGMs.
- Investigation of growth mechanisms of sulfur-rich plasma polymers using BGMs and comparison with a single-molecule precursor.
- Implementation of a wavelength (λ)-dependent VUV photo-deposition study to optimize SH concentrations using PICVD and investigation of the influence of specific photon energies on deposition kinetics and chemical composition of the SH-terminated organic coatings. This yielded highest SH concentrations on the surfaces reported in the literature so far.

7.3 Future work recommendations

After having developed new processes that can be used to create stable SH-terminated organic coatings, the following recommendations are suggested for future work:

1. Investigation of interactions of biomolecules with the created SH-terminated surfaces. This also includes understanding the influence of varying SH concentrations on their survival and spreading rate, and determining an optimal SH concentration, for maximum adhesion for example. To better understand interactions between biomolecules and SH-terminated surfaces, their growth and morphology, as well as their ageing behavior and stability in solution need to be studied in more detail. Especially the morphology of the created SH-terminated surfaces is of interest for the immobilization and growth of biomolecules since they are known to orient themselves along patterns. As stated in Chapter 6, the surface morphology of the created SH-terminated coatings was seen to be independent of the used photon energy as all coatings demonstrated island-like features. However, a dependence of feature size on wavelength was noted, as the features obtained at lower wavelengths were significantly smaller compared to the ones obtained at higher wavelengths. These changes in size and orientation of the features might affect the immobilization and growth of biomolecules on the surface and can be used to alter their conformation but also their attachment pattern. Additionally, stability test of the SH-terminated coatings can be improved by using non-polar solvents in addition to the polar ones already used throughout this research.
2. Preparation of SH-terminated organic coatings using alternative sulfur-containing precursors (e.g. CS_2, OCS) and study their impact on the films' properties, especially the SH concentration, and stability. The use of further sulfur-containing precursors with broad absorption spectra could be of special interest for PICVD.

3. Development of diagnostic strategies for PICVD experiments and correlate results with surface characteristics to gain deeper understanding on the deposition mechanisms.
4. Development of wavelength dependent studies for other functional gases (e.g. nitrogen- or oxygen-containing) to maximize functional group concentrations.
5. Deeper analysis of the influence of the hydrocarbon component in the plasma on deposition behavior. It was shown in Chapter 4 that using C_2H_4/H_2S and C_4H_6/H_2S gas mixtures lead to the formation of film-forming species, demonstrated in an increase in deposition rate (until reaching saturation). However, using C_2H_2/H_2S (Chapter 5) yielded a strong reduction in deposition rate. Besides the possible influences coming from the different plasma reactors it would therefore be significant to study if S-containing species might yield both film-forming and/or etchant species depending on the reactivity and hydrogen availability of the used hydrocarbon component in the plasma.
6. Implementation of new technologies for potential scale-up of the obtained SH-terminated coatings. For plasma-based coatings, atmospheric plasma technologies could be considered (if toxic gases are replaced) to eliminate the high costs introduced through the vacuum systems. For photo-based coatings, the main consideration should be to use gases with strong absorption profiles at wavelengths greater than 160 nm to eliminate the need of vacuum systems and expensive (optical) materials. At these wavelengths cheaper materials, such as the readily available Suprasil and Quartz can be used as window materials. Furthermore, lamps that are readily available and possess high intensities should be used for increased deposition. Such available, powerful lamps could be the different excimer UV and VUV lamps based on dielectric-barrier discharges.

More readily available and affordable light sources that could be used are low-pressure UVC as well as LED sources.

Chapter 8 Appendices

Appendix A: Supporting Information for Chapter 5

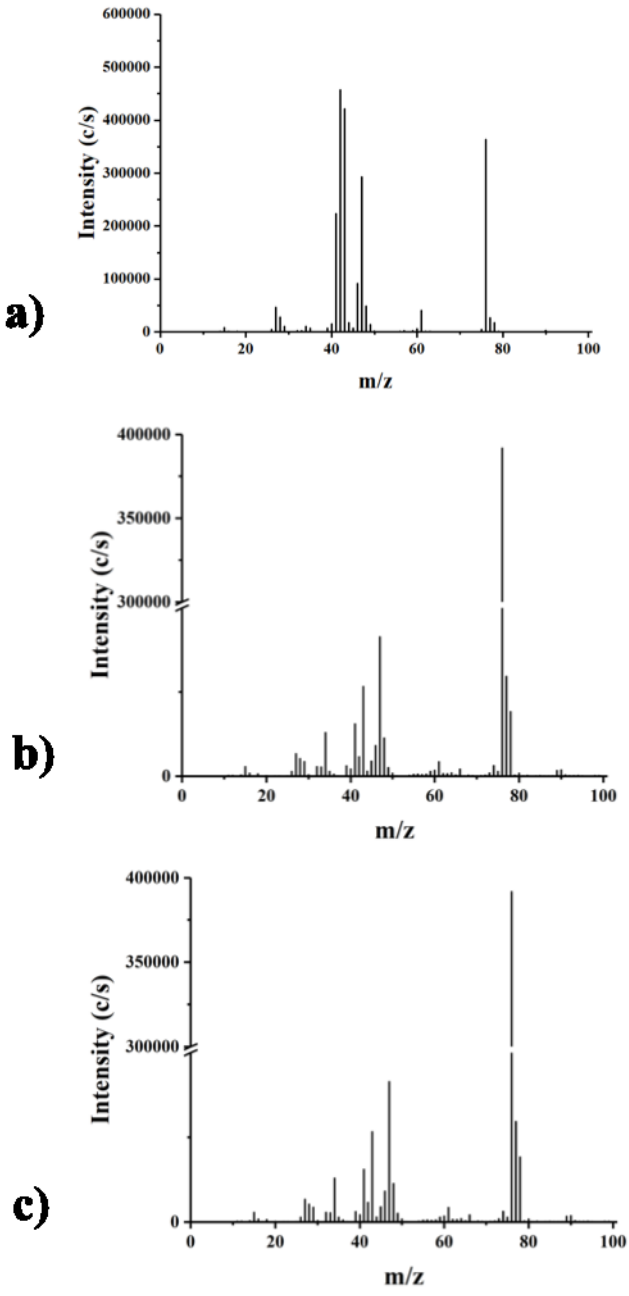

Figure 8-1: Mass spectrum of a) propanethiol vapor (plasma off) and mass spectra of plasmas sustained at b) <P>=12 W and c) <P>=48 W.

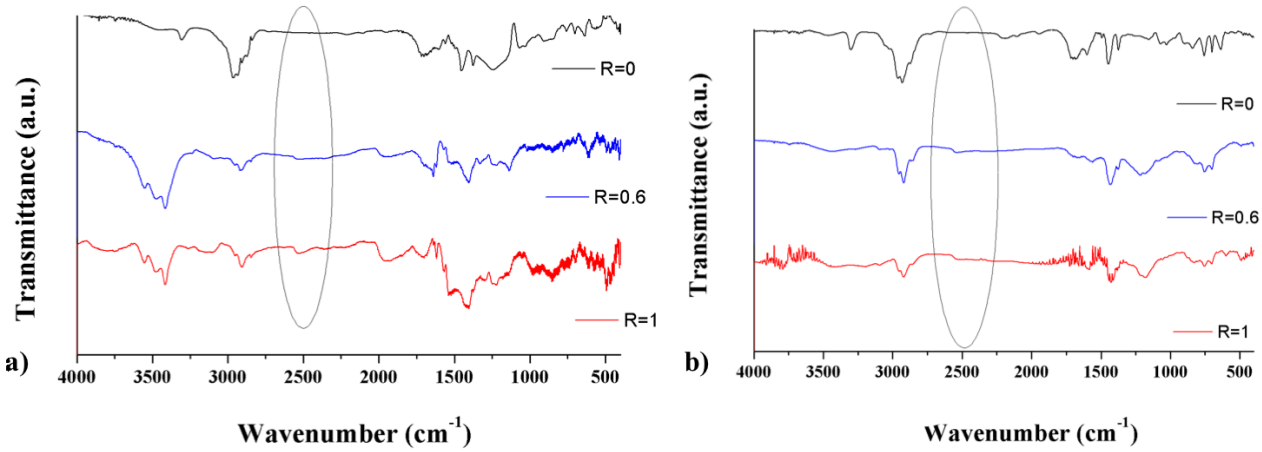

Figure 8-2: FTIR spectra of L-PPA:S films obtained at a) <P>=12 W and b) <P>=48 W. Comparison between L-PPA:S films deposited at three different R values. Circled area shows the appearance of the SH stretch band when H_2S is added to the gas mixture (R>0).

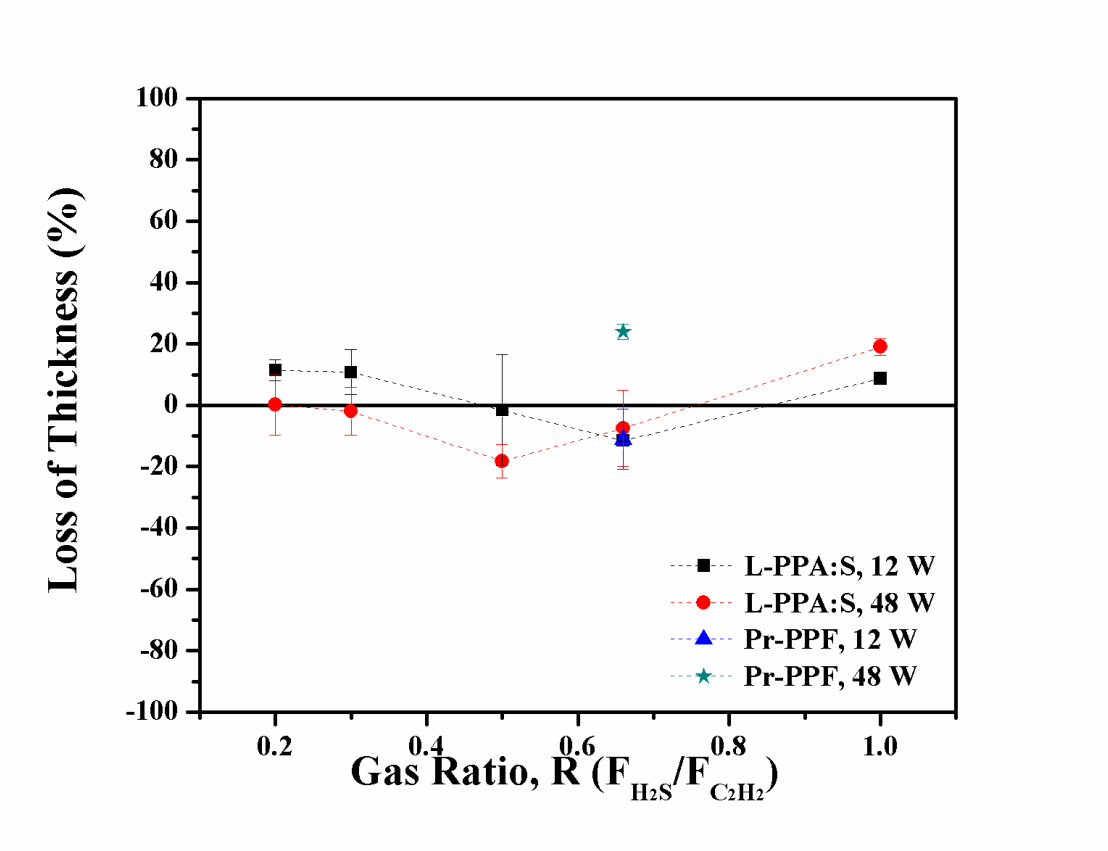

Figure 8-3: Loss of thickness, ΔT, (in %) of L-PPA:S films (squares, <P>=12 W; circles, <P>=48 W) as a function of gas mixture ratio, R, and of Pr-PPFs (triangle, <P>=12 W; star, <P>=48 W) at equivalent elemental feed ratio (X=S/C=1/3) after immersion in Milli-Q water for 24 h. Error bard show standard deviation of three measurements. The lines are to guide the readers' eye.

As in our previous study, all types of coatings were found to be quite stable after 24 h of immersion in Milli-Q water, a key criterion for biomedical applications. Furthermore, we noted an increased stability towards ageing with *R*. Contrary to earlier reports for N- or O-rich coatings, we did not observe an increase in solubility with rising *R* values, nor significant differences between the two powers applied.

Appendix B: Supporting Information for Chapter 6

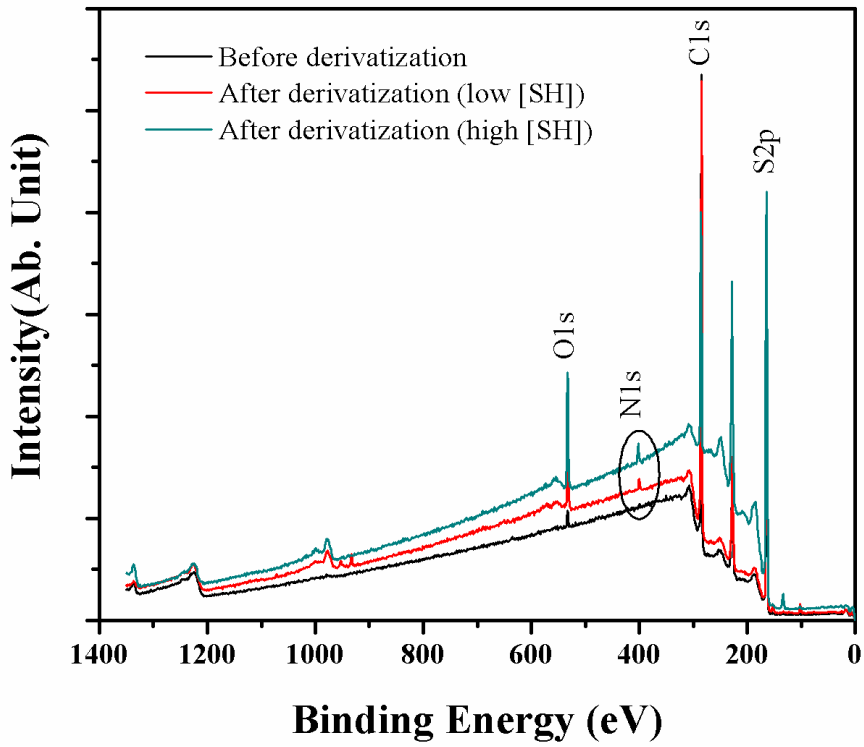

Figure 8-4: XPS survey spectra of an as-deposited (black) UV-PA:S films and after derivatization (low [SH] in red, high [SH] in green).

Throughout this study, sulfur concentrations, [S], were obtained from peak integration of XPS survey spectra of different UV-PA:S films (Figure 8-4 black curve). In order to calculate thiol concentrations, [SH], the procedure developed by Thiry et al.[94] was followed. The presence of nitrogen in the XPS spectra after derivatization (Figure 8-4 red and green curves) can be attributed to the incorporation of *N*-ethylmaleimide into the UV-PA:S coatings, most likely by following the mechanism described in Scheme 6-1. The incorporation of *N*-ethylmaleimide can also be verified by analyzing the C1s peak before and after derivatization, as discussed in detail elsewhere.[94, 233] The concentration of carbon-bearing thiol groups, [SH], can be calculated using equation (6-9) from [S], [C], and [N] obtained from XPS peak integrations.

Estimation of Knudsen number for C_2H_2/H_2S gas mixtures at three different pressures

The nature of a gas (mixture) can be determined using the Knudsen number, defined as:

$$K_n = \frac{l}{d}$$

Where *l* is the mean free path and *d* the characteristic length of a given system.

The mean free path or average distance between collisions for gas molecules is defined as:

$$l = \frac{k_B T}{\sqrt{2}\sigma p}$$

Where k_B is the Boltzmann constant, T the temperature, σ the effective area/cross-section for collisions, and *p* the pressure.

For gas mixtures with dissimilar particles, the collisional cross-section is given by:

$$\sigma = \pi \left(\frac{1}{2}d_1 + \frac{1}{2}d_2\right)^2$$

Where d_1 is the molecule diameter of H_2S and d_2 the molecule diameter of C_2H_2.

Giving the following expression for the mean free path of gas mixtures:

$$l = \frac{k_B T}{\sqrt{2}\pi \left(\frac{1}{2}d_1 + \frac{1}{2}d_2\right)^2 p_1 p_2}$$

To consider dissimilar particles and their collisions between each other, partial pressures (p_1 and p_2) need to be considered in gas mixtures.

Different relative proportions of H_2S and C_2H_2 within the gas mixtures (=*x*) were used during the experiments resulting in different gas mixture ratios. These relative proportions of the different gases can be used to calculate the partial pressures of H_2S and C_2H_2 at different total pressures (R=0.1 implies 9% H_2S and 91% C_2H_2, and R=1 implies 50% H_2S and 50% C_2H_2):

$$p_1 = x * p_{total}$$

Table 8-1: Calculated partial pressures for H2S and C2H2 at different gas mixture ratios, *R*.

Total pressure (Torr)	**Gas ratio R**	p_{H2S} **(Torr)**	p_{C2H2} **(Torr)**
0.1	0.1	0.009	0.091
	1	0.05	0.05
1	0.1	0.09	0.91
	1	0.5	0.5
3	0.1	0.27	2.73
	1	1.5	1.5

Given the different partial pressures for different gas mixture ratios, the mean free path for different pressures can be calculated and are summarized in the following table:

Table 8-2: Calculated mean free paths, l, at different gas mixture ratios, *R*.

Pressure (Torr)	**Gas ratio R**	**Mean free path,** ***l*** **(m)**
0.1	0.1	$5.3 * 10^{-4}$
	1	$1.7 * 10^{-4}$
1	0.1	$5.3 * 10^{-6}$
	1	$1.7 * 10^{-6}$
3	0.1	$5.8 * 10^{-7}$

	1	$1.9 * 10^{-7}$

For the characteristic length of the reactor, only the length where deposition is actually occurring was considered, i.e. the distance between the lamp and the sample, d=0.4 cm. Using those simplifying assumptions, the following Knudsen numbers were obtained for the three different pressures for R=0.1 and R=1:

Table 8-3: Calculated Knudsen numbers, K_n, at different gas mixture ratios, R.

Pressure (Torr)	**Gas ratio R**	**Knudsen number**
0.1	0.1	0.13
	1	0.14
1	0.1	0.001
	1	$4.3 * 10^{-4}$
3	0.1	$1.4 * 10^{-4}$
	1	$4.8 * 10^{-5}$

Knudsen numbers smaller than 0.01 describe a continuous/viscous flow. Values between 1 and 0.01 describe a transition or slip flow. From the results obtained above we see that a transition from a slip into a continuous flow is approached when increasing the pressure.

References

[1] P. K. Chu, J. Chen, L. Wang, and N. Huang, "Plasma-surface modification of biomaterials," *Materials Science and Engineering: R: Reports,* vol. 36, no. 5, pp. 143-206, 2002.

[2] T. Desmet, R. Morent, N. D. Geyter, C. Leys, E. Schacht, and P. Dubruel, "Nonthermal plasma technology as a versatile strategy for polymeric biomaterials surface modification: a review," *Biomacromolecules,* vol. 10, no. 9, pp. 2351-2378, 2009.

[3] D. F. Williams and J. Cunningham, *Materials in clinical dentistry*. Oxford University Press, USA, 1979.

[4] U. Hersel, C. Dahmen, and H. Kessler, "RGD modified polymers: biomaterials for stimulated cell adhesion and beyond," *Biomaterials,* vol. 24, no. 24, pp. 4385-4415, 2003.

[5] Y. Ikada, "Surface modification of polymers for medical applications," *Biomaterials,* vol. 15, no. 10, pp. 725-736, 1994.

[6] J. M. Goddard and J. Hotchkiss, "Polymer surface modification for the attachment of bioactive compounds," *Progress in polymer science,* vol. 32, no. 7, pp. 698-725, 2007.

[7] K. S. Siow, L. Britcher, S. Kumar, and H. J. Griesser, "Plasma methods for the generation of chemically reactive surfaces for biomolecule immobilization and cell colonization-a review," *Plasma Processes and Polymers,* vol. 3, no. 6-7, pp. 392-418, 2006.

[8] R. Förch *et al.*, "Recent and expected roles of plasma-polymerized films for biomedical applications," *Chemical Vapor Deposition,* vol. 13, no. 6-7, pp. 280-294, 2007.

[9] J.-C. Ruiz, A. St-Georges-Robillard, C. Thérésy, S. Lerouge, and M. R. Wertheimer, "Fabrication and Characterisation of Amine-Rich Organic Thin Films: Focus on Stability," *Plasma Processes and Polymers,* vol. 7, no. 9-10, pp. 737-753, 2010.

[10] F. Truica-Marasescu, J.-C. Ruiz, and M. R. Wertheimer, "Vacuum-ultraviolet (VUV) Photo-polymerization of Amine-rich Thin Films from Ammonia-Hydrocarbon Gas Mixtures," *Plasma Processes and Polymers,* vol. 9, no. 5, pp. 473-484, 2012.

[11] P. L. Girard-Lauriault, F. Mwale, M. Iordanova, C. Demers, P. Desjardins, and M. R. Wertheimer, "Atmospheric pressure deposition of micropatterned nitrogen-rich plasma-polymer films for tissue engineering," *Plasma Processes and Polymers,* vol. 2, no. 3, pp. 263-270, 2005.

[12] R. Förch, Z. Zhang, and W. Knoll, "Soft plasma treated surfaces: tailoring of structure and properties for biomaterial applications," *Plasma Processes and Polymers,* vol. 2, no. 5, pp. 351-372, 2005.

[13] J. M. Harris, *Poly (ethylene glycol) chemistry: biotechnical and biomedical applications*. Springer Science & Business Media, 2013.

[14] M. J. Kade, D. J. Burke, and C. J. Hawker, "The power of thiol-ene chemistry," *Journal of Polymer Science Part A: Polymer Chemistry,* vol. 48, no. 4, pp. 743-750, 2010.

[15] S. Sakiyama-Elbert and J. Hubbell, "Functional Biomaterials: Design of Novel Biomaterials," *Annual Review of Materials Research,* vol. 31, no. 1, pp. 183-201, 2001.

[16] D. L. Elbert and J. A. Hubbell, "Surface treatments of polymers for biocompatibility," *Annual Review of Materials Science,* vol. 26, no. 1, pp. 365-394, 1996.
[17] F. Truica-Marasescu, S. Guimond, and M. Wertheimer, "VUV-induced nitriding of polymer surfaces: Comparison with plasma treatments in nitrogen," *Nuclear Instruments and Methods in Physics Research Section B: Beam Interactions with Materials and Atoms,* vol. 208, pp. 294-299, 2003.
[18] A. Fozza, J. Klemberg-Sapieha, and M. R. Wertheimer, "Vacuum ultraviolet irradiation of polymers," *Plasmas and Polymers,* vol. 4, no. 2-3, pp. 183-206, 1999.
[19] H. Esrom and U. Kogelschatz, "Modification of surfaces with new excimer UV sources," *Thin Solid Films,* vol. 218, no. 1, pp. 231-246, 1992.
[20] F. Truica-Marasescu, S. Pham, and M. R. Wertheimer, "VUV processing of polymers: Surface modification and deposition of organic thin films," *Nuclear Instruments and Methods in Physics Research Section B: Beam Interactions with Materials and Atoms,* vol. 265, no. 1, pp. 31-36, 2007.
[21] A. Meyer-Plath, K. Schröder, B. Finke, and A. Ohl, "Current trends in biomaterial surface functionalization—nitrogen-containing plasma assisted processes with enhanced selectivity," *Vacuum,* vol. 71, no. 3, pp. 391-406, 2003.
[22] K. S. Siow, L. Britcher, S. Kumar, and H. J. Griesser, "Plasma Polymers Containing Sulfur and Their Co-Polymers With 1, 7-Octadiene: Chemical and Structural Analysis," *Plasma Processes and Polymers,* vol. 14, no. 3, pp. 1600044-1-1600044-10, 2017.
[23] P. Mungli, M. S. Shetty, P. Tilak, and N. Anwar, "Total thiols: biomedical importance and their alteration in various disorders," *Online journal of health and allied sciences,* vol. 8, no. 2, 2009.
[24] D. Klee, R. V. Villari, H. Höcker, B. Dekker, and C. Mittermayer, "Surface modification of a new flexible polymer with improved cell adhesion," *Journal of Materials Science: Materials in Medicine,* vol. 5, no. 9, pp. 592-595, 1994.
[25] N. Inagaki, S. Tasaka, and Y. Horikawa, "Nafion-like thin film plasma-polymerized from perfluorobenzene/SO2 mixture," *Journal of Polymer Science Part A: Polymer Chemistry,* vol. 27, no. 10, pp. 3495-3501, 1989.
[26] N. Inagaki, S. Tasaka, and H. Miyazaki, "Sulfonic acid group-containing thin films prepared by plasma polymerization," *Journal of applied polymer science,* vol. 38, no. 10, pp. 1829-1838, 1989.
[27] J. Gu, X. Yang, and H. Zhu, "Surface sulfonation of silk fibroin film by plasma treatment and in vitro antithrombogenicity study," *Materials Science and Engineering: C,* vol. 20, no. 1, pp. 199-202, 2002.
[28] L. Jui-Che and S. Cooper, "Surface characterization and ex vivo blood compatibility study of plasmamodified small diameter tubing: effect of sulphur dioxide and hexamethyl-disiloxane plasmas," *Biomaterials,* vol. 16, no. 13, pp. 1017-1023, 1995.
[29] M. T. Gokmen, J. Brassinne, R. A. Prasath, and F. E. Du Prez, "Revealing the nature of thio-click reactions on the solid phase," *Chemical Communications,* vol. 47, no. 16, pp. 4652-4654, 2011.
[30] A. Dondoni, "The emergence of thiol–ene coupling as a click process for materials and bioorganic chemistry," *Angewandte Chemie International Edition,* vol. 47, no. 47, pp. 8995-8997, 2008.

[31] M. C. Fritz, G. Hähner, N. D. Spencer, R. Bürli, and A. Vasella, "Self-assembled hexasaccharides: Surface characterization of thiol-terminated sugars adsorbed on a gold surface," *Langmuir,* vol. 12, no. 25, pp. 6074-6082, 1996.
[32] T. N. Gevrek, R. N. Ozdeslik, G. S. Sahin, G. Yesilbag, S. Mutlu, and A. Sanyal, "Functionalization of reactive polymeric coatings via Diels–Alder reaction using microcontact printing," *Macromolecular Chemistry and Physics,* vol. 213, no. 2, pp. 166-172, 2012.
[33] C. E. Hoyle, T. Y. Lee, and T. Roper, "Thiol–enes: Chemistry of the past with promise for the future," *Journal of Polymer Science Part A: Polymer Chemistry,* vol. 42, no. 21, pp. 5301-5338, 2004.
[34] A. B. Lowe, "Thiol-ene "click" reactions and recent applications in polymer and materials synthesis," *Polymer Chemistry,* vol. 1, no. 1, pp. 17-36, 2010.
[35] S. Ravi, V. R. Krishnamurthy, J. M. Caves, C. A. Haller, and E. L. Chaikof, "Maleimide–thiol coupling of a bioactive peptide to an elastin-like protein polymer," *Acta biomaterialia,* vol. 8, no. 2, pp. 627-635, 2012.
[36] S. S. Ghosh, P. M. Kao, A. W. McCue, and H. L. Chappelle, "Use of maleimide-thiol coupling chemistry for efficient syntheses of oligonucleotide-enzyme conjugate hybridization probes," *Bioconjugate chemistry,* vol. 1, no. 1, pp. 71-76, 1990.
[37] Y.-T. Tsai *et al.*, "Topologically Controlled Cell Differentiation Based on Vapor-Deposited Polymer Coatings," *Langmuir,* vol. 33, no. 36, pp. 8943-8949, 2017.
[38] C. M. Nimmo and M. S. Shoichet, "Regenerative biomaterials that "click": simple, aqueous-based protocols for hydrogel synthesis, surface immobilization, and 3D patterning," *Bioconjugate chemistry,* vol. 22, no. 11, pp. 2199-2209, 2011.
[39] P. Jonkheijm *et al.*, "Photochemical Surface Patterning by the Thiol-Ene Reaction," *Angewandte Chemie,* vol. 120, no. 23, pp. 4493-4496, 2008.
[40] D. Weinrich *et al.*, "Oriented immobilization of farnesylated proteins by the thiol-ene reaction," *Angew Chem Int Ed Engl,* vol. 49, no. 7, pp. 1252-1257, 2010.
[41] Z. Ogumi, Y. Uchimoto, Z. Takehara, and F. Foulkes, "Ionically Conductive Thin Polymer Films Prepared by Plasma Polymerization III. Preparation and Characterization of Ultrathin Films Having Fixed Sulfonic Acid Groups with Only One Mobile Species," *Journal of The Electrochemical Society,* vol. 137, no. 1, pp. 29-34, 1990.
[42] N. Bhat and D. Wavhal, "Preparation and characterization of plasma-polymerized thiophene films," *Journal of applied polymer science,* vol. 70, no. 1, pp. 203-209, 1998.
[43] A. Kiesow and A. Heilmann, "Deposition and properties of plasma polymer films made from thiophenes," *Thin Solid Films,* vol. 343-344, pp. 338-341, 1999.
[44] M. Silverstein and I. Visoly-Fisher, "Plasma polymerized thiophene: molecular structure and electrical properties," *Polymer,* vol. 43, no. 1, pp. 11-20, 2002.
[45] F. Basarir, E. Y. Choi, S. H. Moon, K. C. Song, and T. H. Yoon, "Electrochemical properties of polypropylene membranes modified by the plasma polymerization coating of SO2/acetylene," *Journal of Applied Polymer Science,* vol. 99, no. 6, pp. 3692-3699, 2006.

[46] H. Mahdjoub, S. Roualdes, P. Sistat, N. Pradeilles, J. Durand, and G. Pourcelly, "Plasma-Polymerised Proton Conductive Membranes for a Miniaturised PEMFC," *Fuel Cells,* vol. 5, no. 2, pp. 277-286, 2005.
[47] F. Liu *et al.*, "High-temperature synthesis of magnetically active and SO3H-functionalized ordered mesoporous carbon with good catalytic performance," *Catalysis today,* vol. 186, no. 1, pp. 115-120, 2012.
[48] S. Shylesh, S. Sharma, S. Mirajkar, and A. Singh, "Silica functionalised sulphonic acid groups: synthesis, characterization and catalytic activity in acetalization and acetylation reactions," *Journal of Molecular Catalysis A: Chemical,* vol. 212, no. 1-2, pp. 219-228, 2004.
[49] I. J. Dijs, H. L. van Ochten, C. A. van Walree, J. W. Geus, and L. W. Jenneskens, "Alkyl sulphonic acid surface-functionalised silica as heterogeneous acid catalyst in the solvent-free liquid-phase addition of acetic acid to camphene," *Journal of Molecular Catalysis A: Chemical,* vol. 188, no. 1-2, pp. 209-224, 2002.
[50] D. Zuo, J. Lane, D. Culy, M. Schultz, A. Pullar, and M. Waxman, "Sulfonic acid functionalized mesoporous SBA-15 catalysts for biodiesel production," *Applied Catalysis B: Environmental,* vol. 129, pp. 342-350, 2013.
[51] B. Akhavan, K. Jarvis, and P. Majewski, "Plasma Polymer-Functionalized Silica Particles for Heavy Metals Removal," *ACS Applied Materials & Interfaces,* vol. 7, no. 7, pp. 4265-4274, 2015.
[52] P. Majewski, "Interaction of functionalised surfaces on silica with dissolved metal cations in aqueous solutions," *Zeitschrift für Metallkunde,* vol. 97, no. 6, pp. 784-788, 2006.
[53] Y. Shin, G. E. Fryxell, W. Um, K. Parker, S. V. Mattigod, and R. Skaggs, "Sulfur-Functionalized Mesoporous Carbon," *Advanced Functional Materials,* vol. 17, no. 15, pp. 2897-2901, 2007.
[54] A. Okkema, S. Visser, and S. Cooper, "Physical and blood-contacting properties of polyurethanes based on a sulfonic acid-containing diol chain extender," *Journal of Biomedical Materials Research Part A,* vol. 25, no. 11, pp. 1371-1395, 1991.
[55] Y. H. Kim, D. K. Han, K. D. Park, and S. H. Kim, "Enhanced blood compatibility of polymers grafted by sulfonated PEO via a negative cilia concept," *Biomaterials,* vol. 24, no. 13, pp. 2213-2223, 2003.
[56] T. G. Grasel and S. L. Cooper, "Properties and biological inteactions of polyurethane anionomers: Effect of sulfonate incorporation," *Journal of Biomedical Materials Research Part A,* vol. 23, no. 3, pp. 311-338, 1989.
[57] Z. Huang, G. Shi, L. Qu, and X. Hong, "Electrochemical polymerization of β-naphthalene sulfonic acid in the mixed electrolyte of boron trifluoride diethyl etherate and trifluoroacetic acid," *Journal of Electroanalytical Chemistry,* vol. 544, pp. 41-46, 2003.
[58] J. H. Silver, J.-C. Lin, F. Lim, V. A. Tegoulia, M. K. Chaudhury, and S. L. Cooper, "Surface properties and hemocompatibility of alkyl-siloxane monolayers supported on silicone rubber: effect of alkyl chain length and ionic functionality," *Biomaterials,* vol. 20, no. 17, pp. 1533-1543, 1999.
[59] M. Lestelius, B. Liedberg, and P. Tengvall, "In vitro plasma protein adsorption on ω-functionalized alkanethiolate self-assembled monolayers," *Langmuir,* vol. 13, no. 22, pp. 5900-5908, 1997.
[60] J. C. Lin and W. H. Chuang, "Synthesis, surface characterization, and platelet reactivity evaluation for the self-assembled monolayer of alkanethiol with

sulfonic acid functionality," *Journal of Biomedical Materials Research Part A,* vol. 51, no. 3, pp. 413-423, 2000.

[61] N. Saman, K. Johari, and H. Mat, "Adsorption Characteristics of Sulfur-Functionalized Silica Microspheres with Respect to the Removal of Hg(II) from Aqueous Solutions," *Industrial & Engineering Chemistry Research,* vol. 53, no. 3, pp. 1225-1233, 2014.

[62] Q. Qu, P. Xu, D. Mangelings, C. Yang, and X. Hu, "Facile synthesis and size control of highly monodispersed hybrid silica spheres through a novel nuclei controlling method," *Journal of Non-Crystalline Solids,* vol. 357, no. 3, pp. 976-980, 2011.

[63] D. V. Quang, J. E. Lee, J.-K. Kim, Y. N. Kim, G. N. Shao, and H. T. Kim, "A gentle method to graft thiol-functional groups onto silica gel for adsorption of silver ions and immobilization of silver nanoparticles," *Powder technology,* vol. 235, pp. 221-227, 2013.

[64] E. M. Claesson and A. P. Philipse, "Thiol-functionalized silica colloids, grains, and membranes for irreversible adsorption of metal (oxide) nanoparticles," *Colloids and Surfaces A: Physicochemical and Engineering Aspects,* vol. 297, no. 1-3, pp. 46-54, 2007.

[65] J. H. Seo, D.-S. Shin, P. Mukundan, and A. Revzin, "Attachment of hydrogel microstructures and proteins to glass via thiol-terminated silanes," *Colloids and Surfaces B: Biointerfaces,* vol. 98, pp. 1-6, 2012.

[66] T. Nakamura, Y. Yamada, and K. Yano, "Direct synthesis of monodispersed thiol-functionalized nanoporous silica spheres and their application to a colloidal crystal embedded with gold nanoparticles," *Journal of Materials Chemistry,* vol. 17, no. 35, pp. 3726-3732, 2007.

[67] C. D. Dion, W. Raphael, E. Tong, and J. R. Tavares, "Photo-initiated chemical vapor deposition of thin films using syngas for the functionalization of surfaces at room temperature and near-atmospheric pressure," *Surface and Coatings Technology,* vol. 244, pp. 98-108, 2014.

[68] H. O. Pierson, *Handbook of chemical vapor deposition: principles, technology and applications*. William Andrew, 1999.

[69] K. L. Choy, "Chemical vapour deposition of coatings," *Progress in Materials Science,* vol. 48, no. 2, pp. 57-170, 2003.

[70] C. D. Dion and J. R. Tavares, "Photo-initiated chemical vapor deposition as a scalable particle functionalization technology (a practical review)," *Powder technology,* vol. 239, pp. 484-491, 2013.

[71] W. Schofield, J. McGettrick, T. Bradley, J. Badyal, and S. Przyborski, "Rewritable DNA microarrays," *Journal of the American Chemical Society,* vol. 128, no. 7, pp. 2280-2285, 2006.

[72] D. Thiry, R. Francq, D. Cossement, M. Guillaume, J. Cornil, and R. Snyders, "A detailed description of the chemistry of thiol supporting plasma polymer films," *Plasma Processes and Polymers,* vol. 11, no. 6, pp. 606-615, 2014.

[73] B. Akhavan, K. Jarvis, and P. Majewski, "Development of oxidized sulfur polymer films through a combination of plasma polymerization and oxidative plasma treatment," *Langmuir,* vol. 30, no. 5, pp. 1444-1454, 2014.

[74] S. A. Voronin, M. Zelzer, C. Fotea, M. R. Alexander, and J. W. Bradley, "Pulsed and continuous wave acrylic acid radio frequency plasma deposits: plasma and surface chemistry," *The Journal of Physical Chemistry B,* vol. 111, no. 13, pp. 3419-3429, 2007.

[75] K. Vasilev *et al.*, "Early Stages of Growth of Plasma Polymer Coatings Deposited from Nitrogen- and Oxygen-Containing Monomers," *Plasma Processes and Polymers,* vol. 7, no. 9-10, pp. 824-835, 2010.
[76] F. Truica-Marasescu, P.-L. Girard-Lauriault, A. Lippitz, W. E. S. Unger, and M. R. Wertheimer, "Nitrogen-rich plasma polymers: Comparison of films deposited in atmospheric- and low-pressure plasmas," *Thin Solid Films,* vol. 516, no. 21, pp. 7406-7417, 2008.
[77] J.-C. Ruiz, P.-L. Girard-Lauriault, F. Truica-Marasescu, and M. R. Wertheimer, "Plasma-and vacuum-ultraviolet (VUV) photo-polymerisation of N-and O-rich thin films," *Radiation Physics and Chemistry,* vol. 79, no. 3, pp. 310-314, 2010.
[78] J. C. Ruiz, P. L. Girard-Lauriault, and M. R. Wertheimer, "Fabrication, Characterization, and Comparison of Oxygen-Rich Organic Films Deposited by Plasma- and Vacuum-Ultraviolet (VUV) Photo-Polymerization," *Plasma Processes and Polymers,* vol. 12, no. 3, pp. 225-236, 2015.
[79] S. Lerouge *et al.*, "Nitrogen-Rich Plasma Polymer Coatings for Biomedical Applications: Stability, Mechanical Properties and Adhesion Under Dry and Wet Conditions," *Plasma Processes and Polymers,* vol. 12, no. 9, pp. 882-895, 2015.
[80] M. M. Hossain, J. Müssig, A. S. Herrmann, and D. Hegemann, "Ammonia/acetylene plasma deposition: An alternative approach to the dyeing of poly(ethylene terephthalate) fabrics at low temperatures," *Journal of Applied Polymer Science,* vol. 111, no. 5, pp. 2545-2552, 2009.
[81] D. Hegemann, E. Körner, K. Albrecht, U. Schütz, and S. Guimond, "Growth Mechanism of Oxygen-Containing Functional Plasma Polymers," *Plasma Processes and Polymers,* vol. 7, no. 11, pp. 889-898, 2010.
[82] A. Harsch, J. Calderon, R. Timmons, and G. Gross, "Pulsed plasma deposition of allylamine on polysiloxane: a stable surface for neuronal cell adhesion," *Journal of neuroscience methods,* vol. 98, no. 2, pp. 135-144, 2000.
[83] A. Contreras-Garcia and M. R. Wertheimer, "Low-Pressure Plasma Polymerization of Acetylene-Ammonia Mixtures for Biomedical Applications," *Plasma Chemistry and Plasma Processing,* vol. 33, no. 1, pp. 147-163, 2013.
[84] N. Inagaki, *Plasma surface modification and plasma polymerization*. CRC Press, 1996.
[85] A. J. Ward and R. D. Short, "A spectroscopic analysis of plasma polymers prepared from a series of vinyl sulphones," *Surface and Interface Analysis,* vol. 22, no. 1-12, pp. 477-482, 1994.
[86] K. S. Siow, L. Britcher, S. Kumar, and H. J. Griesser, "Sulfonated Surfaces by Sulfur Dioxide Plasma Surface Treatment of Plasma Polymer Films," *Plasma Processes and Polymers,* vol. 6, no. 9, pp. 583-592, 2009.
[87] K. S. Siow, S. Kumar, and H. J. Griesser, "Low-Pressure Plasma Methods for Generating Non-Reactive Hydrophilic and Hydrogel-Like Bio-Interface Coatings - A Review," *Plasma Processes and Polymers,* vol. 12, no. 1, pp. 8-24, 2015.
[88] L. G. Harris, W. C. E. Schofield, K. J. Doores, B. G. Davis, and J. P. S. Badyal, "Rewritable Glycochips," *Journal of the American Chemical Society,* vol. 131, no. 22, pp. 7755-7761, 2009.
[89] L. G. Harris, W. C. E. Schofield, and J. P. S. Badyal, "Multifunctional molecular scratchcards," *Chemistry of Materials,* vol. 19, no. 7, pp. 1546-1551, 2007.

[90] B. Akhavan, K. Jarvis, and P. Majewski, "Plasma polymerization of sulfur-rich and water-stable coatings on silica particles," *Surface and Coatings Technology,* vol. 264, pp. 72-79, 2015.
[91] D. Thiry, F. J. Aparicio, N. Britun, and R. Snyders, "Concomitant effects of the substrate temperature and the plasma chemistry on the chemical properties of propanethiol plasma polymer prepared by ICP discharges," *Surface and Coatings Technology,* vol. 241, pp. 2-7, 2014.
[92] D. Thiry, N. Britun, S. Konstantinidis, J.-P. Dauchot, L. Denis, and R. Snyders, "Altering the sulfur content in the propanethiol plasma polymers using the capacitive-to-inductive mode transition in inductively coupled plasma discharge," *Applied Physics Letters,* vol. 100, no. 7, pp. 071604-1-071604-3, 2012.
[93] D. Thiry *et al.*, "Experimental and theoretical study of the effect of the inductive-to-capacitive transition in propanethiol plasma polymer chemistry," *The Journal of Physical Chemistry C,* vol. 117, no. 19, pp. 9843-9851, 2013.
[94] D. Thiry, R. Francq, D. Cossement, D. Guerin, D. Vuillaume, and R. Snyders, "Establishment of a derivatization method to quantify thiol function in sulfur-containing plasma polymer films," *Langmuir,* vol. 29, no. 43, pp. 13183-13189, 2013.
[95] J. Friedrich, *The plasma chemistry of polymer surfaces: advanced techniques for surface design*. John Wiley & Sons, 2012.
[96] K. Yanagihara, M. Kimura, M. Niinomi, Y. Nishikawa, and Y. Mukaida, "Process for producing plasma polymerized film," ed: Google Patents, 1987.
[97] D. Frank-Kamenetskii, *Plasma: the fourth state of matter*. Springer Science & Business Media, 2012.
[98] R. Sreenivasan and K. K. Gleason, "Overview of strategies for the CVD of organic films and functional polymer layers," *Chemical Vapor Deposition,* vol. 15, no. 4-6, pp. 77-90, 2009.
[99] H. Yasuda, "Glow discharge polymerization," *Journal of Polymer Science: Macromolecular Reviews* vol. 16, no. 1, pp. 199-293, 1981.
[100] R. A. Haefer, *Oberflächen-und Dünnschicht-Technologie: Teil I: Beschichtungen von Oberflächen*. Springer-Verlag, 2013.
[101] R. Hippler, H. Kersten, M. Schmidt, and K. H. Schoenbach, "Low temperature plasmas," *Eds R Hippler et al, Berlin: Wiley,* vol. 787, 2008.
[102] M. Shen and A. T. Bell, "A review of recent advances in plasma polymerization," in *Plasma polymerization*: ACS Publications, 1979.
[103] H. Yasuda, *Plasma polymerization*. Orlando: Academic Press, 1985.
[104] M. Jacob, C. Easton, G. Woods, and C. Berndt, "Fabrication of a novel organic polymer thin film," *Thin Solid Films,* vol. 516, no. 12, pp. 3884-3887, 2008.
[105] L. Groenewoud, G. Engbers, J. Terlingen, H. Wormeester, and J. Feijen, "Pulsed plasma polymerization of thiophene," *Langmuir,* vol. 16, no. 15, pp. 6278-6286, 2000.
[106] M. Buddhadasa, C. R. Vandenabeele, R. Snyders, and P. L. Girard-Lauriault, "Single source precursor vs. precursor mixture for N-rich plasma polymer deposition: Plasma diagnostics and thin film analyses," *Plasma Processes and Polymers,* vol. 14, no. 11, 2017.
[107] D. Thiry, S. Konstantinidis, J. Cornil, and R. Snyders, "Plasma diagnostics for the low-pressure plasma polymerization process: A critical review," *Thin Solid Films,* vol. 606, pp. 19-44, 2016.

[108] R. D'Agostino, "Plasma deposition, treatment, and etching of polymers," *Materials & Manufacturing Processes,* vol. 8, no. 3, pp. 385-390, 1993.
[109] W. Knoll and R. C. Advincula, *Functional Polymer Films, 2 Volume Set*. John Wiley & Sons, 2013.
[110] J. Friedrich, "Mechanisms of plasma polymerization–reviewed from a chemical point of view," *Plasma Processes and Polymers,* vol. 8, no. 9, pp. 783-802, 2011.
[111] H. Kobayashi, A. Bell, and M. Shen, "Plasma polymerization of saturated and unsaturated hydrocarbons," *Macromolecules,* vol. 7, no. 3, pp. 277-283, 1974.
[112] S. Saboohi, M. Jasieniak, B. R. Coad, H. J. Griesser, R. D. Short, and A. Michelmore, "Comparison of plasma polymerization under collisional and collision-less pressure regimes," *The Journal of Physical Chemistry B,* vol. 119, no. 49, pp. 15359-15369, 2015.
[113] J. F. O'Hanlon, *A user's guide to vacuum technology*. Wiley-Interscience, 2003.
[114] R. d'Agostino and F. Palumbo, "Comment on "Ion-Assisted Processes of Polymerization in Low-Pressure Plasmas"," *Plasma Processes and Polymers,* vol. 9, no. 9, pp. 844-849, 2012.
[115] A. Michelmore, D. A. Steele, J. D. Whittle, J. W. Bradley, and R. D. Short, "Nanoscale deposition of chemically functionalised films via plasma polymerisation," *Rsc Advances,* vol. 3, no. 33, pp. 13540-13557, 2013.
[116] S. Lerouge *et al.*, "Nitrogen-rich coatings for promoting healing around stent-grafts after endovascular aneurysm repair," *Biomaterials,* vol. 28, no. 6, pp. 1209-1217, 2007.
[117] M. M. Hossain, D. Hegemann, G. Fortunato, A. S. Herrmann, and M. Heuberger, "Plasma Deposition of Permanent Superhydrophilic a-C:H:N Films on Textiles," *Plasma Processes and Polymers,* vol. 4, no. 4, pp. 471-481, 2007.
[118] F. Truica-Marasescu and M. R. Wertheimer, "Nitrogen-rich plasma-polymer films for biomedical applications," *Plasma processes and polymers,* vol. 5, no. 1, pp. 44-57, 2008.
[119] F. Truica-Marasescu and M. R. Wertheimer, "Vacuum-Ultraviolet Photopolymerisation of Amine-Rich Thin Films," *Macromolecular Chemistry and Physics,* vol. 209, no. 10, pp. 1043-1049, 2008.
[120] C. G. Roffey, *Photopolymerization of surface coatings*. Wiley, 1982.
[121] H. Okabe, *Photochemistry of small molecules*. Wiley, 1978.
[122] W. A. Noyes and P. A. Leighton, *Photochemistry of gases*. Dover Publications, 1966.
[123] M. Hanabusa, "Photoinduced deposition of thin films," *Materials Science Reports,* vol. 2, no. 2, pp. 51-97, 1987.
[124] E. Stauffer, J. A. Dolan, and R. Newman, *Fire Debris Analysis*. Academic Press, 2008, pp. 49-83.
[125] S. J. Blanksby and G. B. Ellison, "Bond Dissociation Energies of Organic Molecules," *Accounts of Chemical Research,* vol. 36, no. 4, pp. 255-263, 2003.
[126] S. H. Baxamusa, L. Montero, J. M. Dubach, H. A. Clark, S. Borros, and K. K. Gleason, "Protection of sensors for biological applications by photoinitiated chemical vapor deposition of hydrogel thin films," *Biomacromolecules,* vol. 9, no. 10, pp. 2857-2862, 2008.
[127] F.-E. Truica-Marasescu and M. R. Wertheimer, "Vacuum Ultraviolet Photolysis of Hydrocarbon Polymers," *Macromolecular Chemistry and Physics,* vol. 206, no. 7, pp. 744-757, 2005.

[128] B. Eliasson and U. Kogelschatz, "UV excimer radiation from dielectric-barrier discharges," *Applied Physics B,* vol. 46, no. 4, pp. 299-303, 1988.
[129] U. Kogelschatz, H. Esrom, J.-Y. Zhang, and I. Boyd, "High-intensity sources of incoherent UV and VUV excimer radiation for low-temperature materials processing," *Applied Surface Science,* vol. 168, no. 1-4, pp. 29-36, 2000.
[130] U. Kogelschatz, B. Eliasson, and H. Esrom, "Industrial applications of excimer ultraviolet sources," *Materials & Design,* vol. 12, no. 5, pp. 251-258, 1991.
[131] I. W. Boyd and J.-Y. Zhang, "Photo-induced growth of dielectrics with excimer lamps," *Solid-State Electronics,* vol. 45, no. 8, pp. 1413-1431, 2001.
[132] W. Kern, *Thin film processes II*. Elsevier, 2012.
[133] M. Ackerman, *Mesospheric models and related experiments*. Springer, 1971, pp. 149-159.
[134] A. St-Georges-Robillard *et al.*, "Adhesion of U-937 Monocytes on Different Amine-functionalised Polymer Surfaces," *Plasma Processes and Polymers,* vol. 9, no. 3, pp. 243-252, 2012.
[135] F. Truica-Marasescu and M. Wertheimer, "Vacuum ultraviolet–induced photochemical nitriding of polyolefin surfaces," *Journal of applied polymer science,* vol. 91, no. 6, pp. 3886-3898, 2004.
[136] D. Farhanian, G. De Crescenzo, and J. R. Tavares, "Kinetics, Chemistry, and Morphology of Syngas Photoinitiated Chemical Vapor Deposition," *Langmuir,* vol. 33, no. 8, pp. 1780-1791, 2017.
[137] G. Franz, *Low pressure plasmas and microstructuring technology*. Springer Science & Business Media, 2009.
[138] A. Fahr and A. H. Laufer, "Quantum yield of vinylidene (3B) from the vacuum UV photolysis of acetylene and ethylene," *Journal of photochemistry,* vol. 34, no. 3, pp. 261-266, 1986.
[139] D. M. P. Holland *et al.*, "A photoabsorption, photodissociation and photoelectron spectroscopy study of C2H4 and C2D4," *Chemical Physics,* vol. 219, no. 1, pp. 91-116, 1997.
[140] M. Zelikoff and K. Watanabe, "Absorption Coefficients of Ethylene in the Vacuum Ultraviolet," *Journal of the Optical Society of America,* vol. 43, no. 9, pp. 756-759, 1953.
[141] J. R. McNesby and H. Okabe, *Advances in Photochemistry*. John Wiley & Sons, Inc., 2007, pp. 157-240.
[142] W. C. Price and W. T. Tutte, "The Absorption Spectra of Ethylene, Deutero-Ethylene and Some Alkyl-Substituted Ethylenes in the Vacuum Ultra-Violet," *Proceedings of the Royal Society of London. Series A, Mathematical and Physical Sciences,* vol. 174, no. 957, pp. 207-220, 1940.
[143] R. A. Back and D. W. L. Griffiths, "Flash Photolysis of Ethylene," *The Journal of Chemical Physics,* vol. 46, no. 12, pp. 4839-4843, 1967.
[144] H. Okabe and J. R. McNesby, "Vacuum Ultraviolet Photochemistry. II. Photolysis of Ethylene," *The Journal of Chemical Physics,* vol. 36, no. 3, pp. 601-604, 1962.
[145] P. Borrell, A. Cervenka, and J. Turner, "Pressure effects and quantum yields in the photolysis of ethylene and propene at 185 nm," *Journal of the Chemical Society B: Physical Organic,* pp. 2293-2298, 1971.
[146] L. Giroux, M. H. Back, and R. A. Back, "The photolysis of ethylene at 193 nm," *Canadian Journal of Chemistry,* vol. 67, no. 7, pp. 1166-1173, 1989.
[147] H. Hiroshi and T. Ikuzo, "Photolysis of Ethylene at 1634 Å and 1849 Å," *Bulletin of the Chemical Society of Japan,* vol. 46, no. 10, pp. 3012-3015, 1973.

[148] P. Potzinger, L. Glasgow, and G. Bünau, "Photolyse des Äthylens im Bereich 147 — 193 nm / Ethylene Photolysis At 147 — 193," *Zeitschrift für Naturforschung A,* vol. 27, no. 4, pp. 628-638, 1972.
[149] A. Fahr and A. K. Nayak, "Temperature dependent ultraviolet absorption cross sections of 1,3-butadiene and butadiyne," *Chemical Physics,* vol. 189, no. 3, pp. 725-731, 1994.
[150] R. I. Schoen, "Absorption, Ionization, and Ion-Fragmentation Cross Sections of Hydrocarbon Vapors under Vacuum-Ultraviolet Radiation," *The Journal of Chemical Physics,* vol. 37, no. 9, pp. 2032-2041, 1962.
[151] W. C. Price and A. D. Walsh, "The Absorption Spectra of Conjugated Dienes in the Vacuum Ultra-Violet (1)," *Proceedings of the Royal Society of London. Series A, Mathematical and Physical Sciences,* vol. 174, no. 957, pp. 220-234, 1940.
[152] R. D. Doepker, "Vacuum-ultraviolet photolysis of the C4H6 isomers. I. 1, 3-Butadiene," *The Journal of Physical Chemistry,* vol. 72, no. 12, pp. 4037-4042, 1968.
[153] J. C. Robinson, S. A. Harris, W. Sun, N. E. Sveum, and D. M. Neumark, "Photofragment Translational Spectroscopy of 1,3-Butadiene and 1,3-Butadiene-1,1,4,4-d4 at 193 nm," *Journal of the American Chemical Society,* vol. 124, no. 34, pp. 10211-10224, 2002.
[154] L. Stief, V. DeCarlo, and R. Mataloni, "Vacuum-Ultraviolet Photolysis of Acetylene," *The Journal of Chemical Physics,* vol. 42, no. 9, pp. 3113-3121, 1965.
[155] A. H. Laufer and A. M. Bass, "Photochemistry of acetylene - bimolecular rate constant for the formation of butadiyne and reactions of ethynyl radicals," *Journal of Physical Chemistry,* vol. 83, no. 3, pp. 310-313, 1979.
[156] W. Lichten, "Some New Metastable States of Molecules," *The Journal of Chemical Physics,* vol. 37, no. 9, pp. 2152-2154, 1962.
[157] H. Okabe, "Photochemistry of acetylene," *Canadian Journal of Chemistry-Revue Canadienne De Chimie,* vol. 61, no. 5, pp. 850-855, 1983.
[158] M. Zelikoff and L. M. Aschenbrand, "Vacuum ultraviolet photochemistry. Part III. Acetylene at 1849 A," *Journal of Chemical Physics,* vol. 24, no. 5, pp. 1034-1037, 1956.
[159] M. Irion and K. Kompa, "UV laser photochemistry of acetylene at 193 nm," *Applied Physics B,* vol. 27, no. 4, pp. 183-186, 1982.
[160] H. Okabe, "Photochemistry of acetylene at 1470 A," *Journal of Chemical Physics,* vol. 75, no. 6, pp. 2772-2778, 1981.
[161] H. Okabe, "Photochemistry of acetylene at 1849 A," *Journal of Chemical Physics,* vol. 78, no. 3, pp. 1312-1317, 1983.
[162] J. Xu, C. Li, P. Liu, D. He, J. Wang, and Q. Zhang, "Photolysis of low concentration H2S under UV/VUV irradiation emitted from high frequency discharge electrodeless lamps," *Chemosphere,* vol. 109, no. Supplement C, pp. 202-207, 2014.
[163] B. d. B. Darwent, R. L. Wadlinger, and M. J. Allard, "The photochemical decomposition of hydrogen sulfide. The reactions of hydrogen atoms and HS radicals," *The Journal of Physical Chemistry,* vol. 71, no. 7, pp. 2346-2347, 1967.
[164] G. S. Forbes, J. E. Cline, and B. C. Bradshaw, "The Photolysis of Gaseous Hydrogen Sulfide," *Journal of the American Chemical Society,* vol. 60, no. 6, pp. 1431-1436, 1938.

[165] D. Perner and T. Franken, "Untersuchung von Primärprozessen an gasförmigem Schwefelwasserstoff mit Hilfe der Pulsradiolyse," *Berichte der Bunsengesellschaft für physikalische Chemie,* vol. 73, no. 8-9, pp. 897-901, 1969.
[166] S. N. Ahmed, *Physics and Engineering of Radiation Detection (Second Edition)*. Elsevier, 2015, pp. 65-155.
[167] C. Decker, "Photoinitiated curing of multifunctional monomers," *Acta Polymerica,* vol. 45, no. 5, pp. 333-347, 1994.
[168] F. Truica-Marasescu, S. Guimond, P. Jedrzejowski, and M. R. Wertheimer, "Hydrophobic recovery of VUV/NH3 modified polyolefin surfaces: Comparison with plasma treatments in nitrogen," *Nuclear Instruments and Methods in Physics Research Section B: Beam Interactions with Materials and Atoms,* vol. 236, no. 1-4, pp. 117-122, 2005.
[169] M. Vandenbossche and D. Hegemann, "Recent approaches to reduce aging phenomena in oxygen-and nitrogen-containing plasma polymer films: An overview," *Current Opinion in Solid State and Materials Science,* vol. 22, no. 1, pp. 26-38, 2018.
[170] R. E. Hansen and J. R. Winther, "An introduction to methods for analyzing thiols and disulfides: Reactions, reagents, and practical considerations," *Analytical biochemistry,* vol. 394, no. 2, pp. 147-158, 2009.
[171] M. Collaud Coen, B. Keller, P. Groening, and L. Schlapbach, "Functionalization of graphite, glassy carbon, and polymer surfaces with highly oxidized sulfur species by plasma treatments," *Journal of applied physics,* vol. 92, no. 9, pp. 5077-5083, 2002.
[172] Z. Zhang, Q. Chen, W. Knoll, and R. Forch, "Effect of aqueous solution on functional plasma polymerized films," *Surface & Coatings Technology,* vol. 174, pp. 588-590, 2003.
[173] P. Rupper, M. Vandenbossche, L. Bernard, D. Hegemann, and M. Heuberger, "Composition and stability of plasma polymer films exhibiting vertical chemical gradients," *Langmuir,* vol. 33, no. 9, pp. 2340-2352, 2017.
[174] F. Truica-Marasescu, P. Jedrzejowski, and M. R. Wertheimer, "Hydrophobic recovery of vacuum ultraviolet irradiated polyolefin surfaces," *Plasma Processes and Polymers,* vol. 1, no. 2, pp. 153-163, 2004.
[175] V. E. Skurat and Y. I. Dorofeev, "The transformations of organic polymers during the illumination by 147.0 and 123.6 nm light," *Macromolecular Materials and Engineering,* vol. 216, no. 1, pp. 205-224, 1994.
[176] D. Hegemann, E. Körner, N. Blanchard, M. Drabik, and S. Guimond, "Densification of functional plasma polymers by momentum transfer during film growth," *Applied Physics Letters,* vol. 101, no. 21, pp. 211603-1-211603-4, 2012.
[177] D. Hegemann *et al.*, "Suppression of hydrophobic recovery by plasma polymer films with vertical chemical gradients," *Langmuir,* vol. 32, no. 3, pp. 651-654, 2016.
[178] P. L. Girard-Lauriault, P. M. Dietrich, T. Gross, T. Wirth, and W. E. Unger, "Chemical Characterization of the Long-Term Ageing of Nitrogen-Rich Plasma Polymer Films under Various Ambient Conditions," *Plasma Processes and Polymers,* vol. 10, no. 4, pp. 388-395, 2013.
[179] R. Gristina *et al.*, "Increasing cell adhesion on plasma deposited fluorocarbon coatings by changing the surface topography," *Journal of Biomedical Materials Research Part B: Applied Biomaterials,* vol. 88, no. 1, pp. 139-149, 2009.

[180] M. Ohring, *Materials science of thin films : deposition and structure*. Academic Press, 2002.
[181] A. Michelmore, "Thin film growth on biomaterial surfaces," in *Thin Film Coatings for Biomaterials and Biomedical Applications*, 2016, pp. 29-47.
[182] A. Michelmore, P. Martinek, V. Sah, R. D. Short, and K. Vasilev, "Surface Morphology in the Early Stages of Plasma Polymer Film Growth from Amine-Containing Monomers," *Plasma Processes and Polymers,* vol. 8, no. 5, pp. 367-372, 2011.
[183] S. Hwang *et al.*, "Growth kinetics of plasma-polymerized films," *Scientific Reports,* vol. 5, pp. 11201-1-11201-5, 2015.
[184] F.-E. Truica-Marasescu, "Vacuum Ultraviolet Photo-Physical Chemistry of Hydrocarbon Polymers," PhD, Univeristé de Montreal; École Polytechnique de Montréal, 2005.
[185] B. O. C. Resonance Ltd. [Online].
[186] A. Ulman, *An Introduction to Ultrathin Organic Films: From Langmuir--Blodgett to Self--Assembly*. Academic press, 2013.
[187] D. L. Smith, *Thin-film deposition: principles and practice*. McGraw Hill Professional, 1995.
[188] R. Förch, H. Schönherr, and A. T. A. Jenkins, *Surface design: applications in bioscience and nanotechnology*. John Wiley & Sons, 2009.
[189] J. C. Ruiz *et al.*, "Approaches to quantify amine groups in the presence of hydroxyl functional groups in plasma polymerized thin films," *Plasma Processes and Polymers,* vol. 11, no. 9, pp. 888-896, 2014.
[190] A. Choukourov, H. Biederman, D. Slavinska, M. Trchova, and A. Hollander, "The influence of pulse parameters on film composition during pulsed plasma polymerization of diaminocyclohexane," *Surface and Coatings Technology,* vol. 174-175, pp. 863-866, 2003.
[191] C. L. Rinsch, X. Chen, V. Panchalingam, R. C. Eberhart, J.-H. Wang, and R. B. Timmons, "Pulsed radio frequency plasma polymerization of allyl alcohol: Controlled deposition of surface hydroxyl groups," *Langmuir,* vol. 12, no. 12, pp. 2995-3002, 1996.
[192] R. Snyders *et al.*, "Mechanism of adhesion between protein-based hydrogels and plasma treated polypropylene backing," *Surface science,* vol. 601, no. 1, pp. 112-122, 2007.
[193] G. T. Hermanson, *Bioconjugate techniques*. Academic press, 2013.
[194] J. R. Winther and C. Thorpe, "Quantification of thiols and disulfides," *Biochimica et Biophysica Acta (BBA)-General Subjects,* vol. 1840, no. 2, pp. 838-846, 2014.
[195] S. Chemtob, T. Glotch, and G. Rossman, "ATR-IR Spectroscopy for in situ mineral analysis on planetary surfaces: steps toward a forward model," in *Lunar and Planetary Science Conference*, 2010, vol. 41, p. 2198.
[196] B. Stuart, *Infrared spectroscopy : fundamentals and applications*. J. Wiley, 2004.
[197] M. Hesse, H. Meier, and B. Zeeh, *Spektroskopische Methoden in der organischen Chemie*. Georg Thieme Verlag, 2005.
[198] J. Coates, "Interpretation of infrared spectra, a practical approach," *Encyclopedia of analytical chemistry,* 2000.
[199] G. Binnig, C. F. Quate, and C. Gerber, "Atomic force microscope," *Physical review letters,* vol. 56, no. 9, p. 930, 1986.

[200] J. Benedikt, A. Hecimovic, D. Ellerweg, and A. v. Keudell, "Quadrupole mass spectrometry of reactive plasmas," *Journal of Physics D: Applied Physics,* vol. 45, no. 40, p. 403001, 2012.
[201] A. Niklewski, W. Azzam, T. Strunskus, R. A. Fischer, and C. Wöll, "Fabrication of Self-Assembled Monolayers Exhibiting a Thiol-Terminated Surface," *Langmuir,* vol. 20, no. 20, pp. 8620-8624, 2004.
[202] D. Guerin, C. Merckling, S. Lenfant, X. Wallart, S. Pleutin, and D. Vuillaume, "Silicon−Molecules−Metal Junctions by Transfer Printing: Chemical Synthesis and Electrical Properties," *The Journal of Physical Chemistry C,* vol. 111, no. 22, pp. 7947-7956, 2007.
[203] W. Azzam, B. I. Wehner, R. A. Fischer, A. Terfort, and C. Wöll, "Bonding and Orientation in Self-Assembled Monolayers of Oligophenyldithiols on Au Substrates," *Langmuir,* vol. 18, no. 21, pp. 7766-7769, 2002.
[204] E. A. Smith, M. J. Wanat, Y. Cheng, S. V. Barreira, A. G. Frutos, and R. M. Corn, "Formation, spectroscopic characterization, and application of sulfhydryl-terminated alkanethiol monolayers for the chemical attachment of DNA onto gold surfaces," *Langmuir,* vol. 17, no. 8, pp. 2502-2507, 2001.
[205] Z. Novotna, A. Reznickova, O. Kvitek, N. S. Kasalkova, Z. Kolska, and V. Svorcik, "Cells adhesion and growth on gold nanoparticle grafted glass," *Applied Surface Science,* vol. 307, pp. 217-223, 2014.
[206] V. Svorcik *et al.*, "Deposition of gold nano-particles and nano-layers on polyethylene modified by plasma discharge and chemical treatment," *Nuclear Instruments & Methods in Physics Research Section B-Beam Interactions with Materials and Atoms,* vol. 267, no. 15, pp. 2484-2488, 2009.
[207] O. Kvitek, M. Bot, and V. Svorcik, "Gold nanoparticles grafting on glass surface," *Applied Surface Science,* vol. 258, no. 22, pp. 8991-8995, 2012.
[208] V. Svorcík, Z. Kolska, J. Siegel, and P. Slepicka, ""Short" Dithiol and Au Nanoparticles Grafting on Plasma Treated Polyethyleneterephthalate," *Journal of Nano Research,* vol. 25, pp. 40-48, 2013.
[209] H. Muguruma, "Plasma-Polymerized Films for Biochip Design," *Plasma Processes and Polymers,* vol. 7, no. 2, pp. 151-162, 2010.
[210] P. C. Lin *et al.*, "Site-specific protein modification through Cu-I-catalyzed 1,2,3-triazole formation and its implementation in protein microarray fabrication," *Angewandte Chemie-International Edition,* vol. 45, no. 26, pp. 4286-4290, 2006.
[211] M. R. Wertheimer *et al.*, "Amine-Rich Organic Thin Films for Cell Culture: Possible Electrostatic Effects in Cell-Surface Interactions," *Japanese Journal of Applied Physics,* vol. 51, no. 11, pp. 1-5, 2012.
[212] A. Holländer and S. Kröpke, "Polymer Surface Treatment with SO2-Containing Plasmas," *Plasma Processes and Polymers,* vol. 7, no. 5, pp. 390-402, 2010.
[213] Z. Gugala and S. Gogolewski, "Attachment, growth, and activity of rat osteoblasts on polylactide membranes treated with various low-temperature radiofrequency plasmas," *Journal of Biomedical Materials Research Part A,* vol. 76, no. 2, pp. 288-299, 2006.
[214] D. Hegemann and M.-M. Hossain, "Influence of Non-Polymerizable Gases Added During Plasma Polymerization," *Plasma Processes and Polymers,* vol. 2, no. 7, pp. 554-562, 2005.
[215] E. Korner, G. Fortunato, and D. Hegemann, "Influence of RF Plasma Reactor Setup on Carboxylated Hydrocarbon Coatings," *Plasma Processes and Polymers,* vol. 6, no. 2, pp. 119-125, 2009.

[216] Chun Q. Yong, Jongryang Joo, and Donggeun Jung, "Polymer-like Organic Thin Films Deposited by Plasma Enhanced Chemical Vapor Deposition Using the Para-xylene Precursor as Low Dielectric Constant Interlayer Dielectrics for Multilevel Metallization," *Japanese Journal of Applied Physics,* vol. 38, no. 3R, p. 1356, 1999.
[217] G. Beamson and D. Briggs, *High resolution XPS of organic polymers : the Scienta ESCA300 database*. Wiley, 1992.
[218] D. Lin-Vien, N. B. Colthup, W. G. Fateley, and J. G. Grasselli, *The Handbook of infrared and raman characteristic frequencies of organic molecules*. Academic Press, 1991.
[219] J. A. Gardella Jr, S. A. Ferguson, and R. L. Chin, "π*← π shakeup satellites for the analysis of structure and bonding in aromatic polymers by X-Ray Photoelectron Spectroscopy," *Applied spectroscopy,* vol. 40, no. 2, pp. 224-232, 1986.
[220] H. Peisert, T. Chassé, P. Streubel, A. Meisel, and R. Szargan, "Relaxation energies in XPS and XAES of solid sulfur compounds," *Journal of Electron Spectroscopy and Related Phenomena,* vol. 68, pp. 321-328, 1994.
[221] M. Volmer, M. Stratmann, and H. Viefhaus, "Electrochemical and electron spectroscopic investigations of iron surfaces modified with thiols," *Surface and Interface Analysis,* vol. 16, no. 1-12, pp. 278-282, 1990.
[222] K. Vasilev, L. Britcher, A. Casanal, and H. J. Griesser, "Solvent-induced porosity in ultrathin amine plasma polymer coatings," *Journal of Physical Chemistry B,* vol. 112, no. 35, pp. 10915-10921, 2008.
[223] Y. Q. Ren, H. Z. Shui, C. J. Peng, H. L. Liu, and Y. Hu, "Solubility of elemental sulfur in pure organic solvents and organic solvent-ionic liquid mixtures from 293.15 to 353.15K," *Fluid Phase Equilibria,* vol. 312, pp. 31-36, 2011.
[224] S. Jay, P. Cezac, J. P. Serin, F. Contamine, C. Martin, and J. Mercadier, "Solubility of Elemental Sulfur in Toluene between (267.15 and 313.15) K under Atmospheric Pressure," *Journal of Chemical and Engineering Data,* vol. 54, no. 12, pp. 3238-3241, 2009.
[225] R. Steudel, *Elemental sulfur and sulfur-rich compounds*. Springer, 2003.
[226] F. J. Aparicio, D. Thiry, P. Laha, and R. Snyders, "Wide Range Control of the Chemical Composition and Optical Properties of Propanethiol Plasma Polymer Films by Regulating the Deposition Temperature," *Plasma Processes and Polymers,* vol. 13, no. 8, pp. 814-822, 2016.
[227] S. D. Bhagat, J. Chatterjee, B. Chen, and A. E. Stiegman, "High Refractive Index Polymers Based on Thiol–Ene Cross-Linking Using Polarizable Inorganic/Organic Monomers," *Macromolecules,* vol. 45, no. 3, pp. 1174-1181, 2012.
[228] A. B. Lowe and C. N. Bowman, *Thiol-X chemistries in polymer and materials science*. Royal Society of Chemistry, 2013.
[229] W. J. Yang, K.-G. Neoh, E.-T. Kang, S. L.-M. Teo, and D. Rittschof, "Stainless steel surfaces with thiol-terminated hyperbranched polymers for functionalization via thiol-based chemistry," *Polymer Chemistry,* vol. 4, no. 10, pp. 3105-3115, 2013.
[230] S. Chen and L. M. Smith, "Photopatterned Thiol Surfaces for Biomolecule Immobilization," *Langmuir,* vol. 25, no. 20, pp. 12275-12282, 2009.
[231] M. A. C. Campos, J. M. J. Paulusse, and H. Zuilhof, "Functional monolayers on oxide-free silicon surfaces via thiol-ene click chemistry," *Chemical Communications,* vol. 46, no. 30, pp. 5512-5514, 2010.

[232] D. Liu and D. J. Broer, *Responsive Polymer Surfaces: Dynamics in Surface Topography*. John Wiley & Sons, 2017.
[233] E. Kasparek, J. R. Tavares, M. R. Wertheimer, and P.-L. Girard-Lauriault, "Sulfur-Rich Organic Films Deposited by Plasma- and Vacuum-Ultraviolet (VUV) Photo-Polymerization," *Plasma Processes and Polymers,* vol. 13, no. 9, pp. 888-899, 2016.
[234] M. Buddhadasa and P.-L. Girard-Lauriault, "Plasma co-polymerisation of ethylene, 1,3-butadiene and ammonia mixtures: Amine content and water stability," *Thin Solid Films,* vol. 591, pp. 76-85, 2015.
[235] L. Denis *et al.*, "Physico-Chemical Characterization of Methyl Isobutyrate-based Plasma Polymer Films," *Plasma Processes and Polymers,* vol. 8, no. 2, pp. 127-137, 2011.
[236] S. Vasquez, C. A. Achete, C. P. Borges, D. F. Franceschini, F. L. Freire, and E. Zanghellini, "Structure and properties of a-C:H films deposited onto polymeric substrates," *Diamond and Related Materials,* vol. 6, no. 5, pp. 551-554, 1997.
[237] G. A. Abbas, S. S. Roy, P. Papakonstantinou, and J. A. McLaughlin, "Structural investigation and gas barrier performance of diamond-like carbon based films on polymer substrates," *Carbon,* vol. 43, no. 2, pp. 303-309, 2005.
[238] Zajı *et al.*, "Study of plasma polymerization from acetylene in pulsed r.f. discharges," *Thin Solid Films,* vol. 425, no. 1, pp. 72-84, 2003.
[239] D. Hegemann, B. Hanselmann, S. Guimond, G. Fortunato, M.-N. Giraud, and A. G. Guex, "Considering the degradation effects of amino-functional plasma polymer coatings for biomedical application," *Surface and Coatings Technology,* vol. 255, pp. 90-95, 2014.
[240] A. Manakhov *et al.*, "Optimization of Cyclopropylamine Plasma Polymerization toward Enhanced Layer Stability in Contact with Water," *Plasma Processes and Polymers,* vol. 11, no. 6, pp. 532-544, 2014.
[241] D. Hegemann, B. Hanselmann, N. Blanchard, and M. Amberg, "Plasma-Substrate Interaction during Plasma Deposition on Polymers," *Contributions to Plasma Physics,* vol. 54, no. 2, pp. 162-169, 2014.
[242] J. P. Booth, G. Cunge, P. Chabert, and N. Sadeghi, "CFx radical production and loss in a CF4 reactive ion etching plasma: Fluorine rich conditions," *Journal of Applied Physics,* vol. 85, no. 6, pp. 3097-3107, 1999.
[243] M. J. Sowa, M. E. Littau, V. Pohray, and J. L. Cecchi, "Fluorocarbon polymer deposition kinetics in a low-pressure, high-density, inductively coupled plasma reactor," *Journal of Vacuum Science & Technology A: Vacuum, Surfaces, and Films,* vol. 18, no. 5, pp. 2122-2129, 2000.
[244] J. Benedikt, "Plasma-chemical reactions: low pressure acetylene plasmas," *Journal of Physics D: Applied Physics,* vol. 43, no. 4, p. 043001, 2010.
[245] C.-H. Tsai, W.-J. Lee, C.-Y. Chen, P.-J. Tsai, G.-C. Fang, and M. Shih, "Difference in conversions between dimethyl sulfide and methanethiol in a cold plasma environment," *Plasma chemistry and plasma processing,* vol. 23, no. 1, pp. 141-157, 2003.
[246] A. Baby, C. Mahony, and P. Maguire, "Acetylene–argon plasmas measured at a biased substrate electrode for diamond-like carbon deposition: I. Mass spectrometry," *Plasma Sources Science and Technology,* vol. 20, no. 1, pp. 015003-015019, 2011.
[247] J. R. Doyle, "Chemical kinetics in low pressure acetylene radio frequency glow discharges," *Journal of applied physics,* vol. 82, no. 10, pp. 4763-4771, 1997.

[248] E. Liston, L. Martinu, and M. Wertheimer, "Plasma surface modification of polymers for improved adhesion: a critical review," *Journal of adhesion science and technology,* vol. 7, no. 10, pp. 1091-1127, 1993.
[249] J. Tavares, A. Shahryari, J. Harvey, S. Coulombe, and S. Omanovic, "Corrosion behavior and fibrinogen adsorptive interaction of SS316L surfaces covered with ethylene glycol plasma polymer-coated Ti nanoparticles," *Surface and Coatings Technology,* vol. 203, no. 16, pp. 2278-2287, 2009.
[250] C. A. Dorval Dion, W. Raphael, E. Tong, and J. R. Tavares, "Photo-initiated chemical vapor deposition of thin films using syngas for the functionalization of surfaces at room temperature and near-atmospheric pressure," *Surface and Coatings Technology,* vol. 244, pp. 98-108, 2014.
[251] J. V. Armstrong, A. A. Burk, J. M. D. Coey, and K. Moorjani, "Wavelength control of iron/nickel composition in laser induced chemical vapor deposited films," *Appl. Phys. Lett. Applied Physics Letters,* vol. 50, no. 18, pp. 1231-1233, 1987.
[252] M. Hanabusa and M. Ikeda, "Wavelength dependence in photochemical vapor deposition of aluminum film using dimethylaluminum hydride," *AOC Applied Organometallic Chemistry,* vol. 5, no. 4, pp. 289-293, 1991.
[253] C. Wu, F. Chen, and D. Judge, "Measurements of temperature-dependent absorption cross sections of C2H2 in the VUV-UV region," *Journal of Geophysical Research: Planets,* vol. 106, no. E4, pp. 7629-7636, 2001.
[254] M. Nobre *et al.*, "The VUV electronic spectroscopy of acetone studied by synchrotron radiation," *Physical Chemistry Chemical Physics,* vol. 10, no. 4, pp. 550-560, 2008.
[255] A. U. Corporation. (2015). *STER-L-RAY Germicidal Ultraviolet Lamps*. Available: https://d163axztg8am2h.cloudfront.net/static/doc/7e/4c/84c923fee3d73f7ddbc95af748d6.pdf
[256] C. D. Wagner, L. E. Davis, M. V. Zeller, J. A. Taylor, R. H. Raymond, and L. H. Gale, "Empirical atomic sensitivity factors for quantitative analysis by electron spectroscopy for chemical analysis," *Surface and Interface Analysis,* vol. 3, no. 5, pp. 211-225, 1981.
[257] W. Xi, T. F. Scott, C. J. Kloxin, and C. N. Bowman, "Click chemistry in materials science," *Advanced Functional Materials,* vol. 24, no. 18, pp. 2572-2590, 2014.
[258] M. Van Dijk, D. T. Rijkers, R. M. Liskamp, C. F. van Nostrum, and W. E. Hennink, "Synthesis and applications of biomedical and pharmaceutical polymers via click chemistry methodologies," *Bioconjugate chemistry,* vol. 20, no. 11, pp. 2001-2016, 2009.
[259] M. Danno and M. Hanabusa, "Amorphous-carbon films prepared by photo-CVD from acetylene," *Materials Letters,* vol. 4, no. 5-7, pp. 261-264, 1986.
[260] D. Halwidl, *Development of an effusive molecular beam apparatus*. Springer, 2016.
[261] S. Sivaram, *Chemical vapor deposition: thermal and plasma deposition of electronic materials*. Springer Science & Business Media, 2013.
[262] S. Matteucci, Y. Yampolskii, B. D. Freeman, and I. Pinnau, "Transport of gases and vapors in glassy and rubbery polymers," *Materials science of membranes for gas and vapor separation,* vol. 1, pp. 1-2, 2006.
[263] E. Kasparek, D. Thiry, J. R. Tavares, M. R. Wertheimer, R. Snyders, and P. L. Girard-Lauriault, "Growth mechanisms of sulfur-rich plasma polymers: Binary

gas mixtures versus single precursor," *Plasma Processes and Polymers,* pp. 1800036-1-1800036-11, 2018.
[264] O. Kylian, A. Choukourov, and H. Biederman, "Nanostructured plasma polymers," *Thin Solid Films,* vol. 548, pp. 1-17, 2013.
[265] E. Grimoldi, S. Zanini, R. A. Siliprandi, and C. Riccardi, "AFM and contact angle investigation of growth and structure of pp-HMDSO thin films," *The European Physical Journal D,* vol. 54, no. 2, pp. 165-172, 2009.